

SEMI ACTIVE CONTROL SYSTEM DESIGN OF AIR SPRINGS FOR MOTORCYCLE USAGE

Authors: Benincasa Edoardo
Bertozzi Davide
Reali Luca



Abstract

Motorcycles have been improved consistently in the last few years. Innovation of technologies allows to enrich them with bleeding edge equipment such as low emission high power engines, highly aerodynamic structures that simultaneously provide high performance and low fuel consumption, but mainly electronic systems for improving control and rider safety. One of the main contributions in terms of driveability and handling is given by the suspension system. To achieve the best driving experience at the lowest cost, semi-active suspensions have been introduced. They allow to dynamically adjust one at a time damping and stiffness of the suspension to achieve brilliant results in terms of dynamic behavior or comfort maximization according to the requests.

In this report it will be analysed how to design a control system for a super sport bike equipped with semi active air spring suspensions, on both front and rear end. The mathematical model will be based on the half-car approach and different scenarios will be considered, like standard city commuting and race track driving. Both of them will be optimized based on the driver requests. The results will be then analysed to compare the behavior of standard passive suspensions and semi-active controlled one.

Contents

1	Introduction	2
1.1	Motivations	2
1.2	Contributions	5
1.3	State of art and literature comparison	6
1.4	Organisation of the manuscript	10
1.5	List of the symbols	11
2	Main body	12
2.1	Model and Problem Formulation	12
2.2	Model analysis	17
2.2.1	Linearisation	17
2.2.2	Eigenvalues	18
2.2.3	Reachability	22
2.2.4	Observability	24
2.3	Proposed solution	26
3	Application	32
3.1	Simulator description	32
3.1.1	Non-linear plant, Closed Loop	32
3.1.2	Non-linear plant, Open loop	33
3.1.3	Linear Plant	33
3.1.4	Coordinates linearisation	34
3.1.5	Noise generator	34
3.1.6	Disturbance generator	35
3.1.7	Non-linear control implementation	37
3.1.8	Linear Control implementation	38
3.1.9	Observer	39
3.1.10	Cost function block	39
3.2	Simulation results	40
3.2.1	System investigation	40
3.2.2	Effect of individual control components	49
3.2.3	Sweep test	50
3.2.4	Final optimization	55
3.2.5	Analysis results	58
4	Conclusions and further investigations	62

Chapter 1

Introduction

1.1 Motivations

Motorcycle dynamics is heavily influenced by the suspensions behaviour; the suspension system serves multiple purposes, such as keeping the motorcycle ideally always in contact with the ground, isolating the driver from road bumps, roughness and vibrations.

In figure 1.1 a telescopic fork is shown; this document will consider the upside-down fork because it allows a higher performance due to higher structural stiffness that implies better capability of handling extreme stress during hard steering, braking and other strenuous conditions.

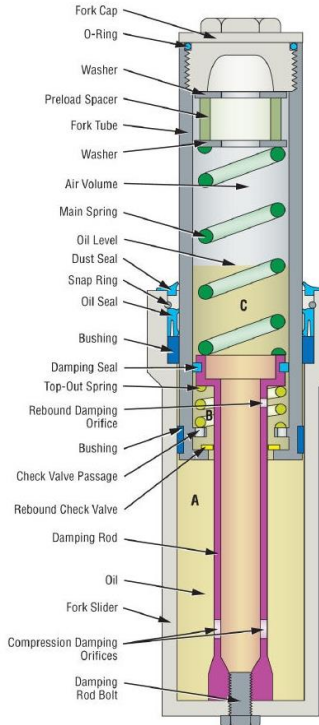


Figure 1.1: Telescopic fork

Suspensions are characterized by two main parameters: stiffness and damping. Both of them can be adjusted manually by the rider using specific tools, in particular by acting on the adjustment screws or gears that are usually placed on the upper part of the suspension.

Motorcycle suspension are designed so that the springs are always under compression, even when fully extended. Preload is used to adjust the initial position of the suspension to the weight of the motorcycle and rider acting on it. Some motorcycles allow adjustment of preload by changing the air pressure inside the forks. Valves at the top of the forks allow air to be added or released from the fork. More air pressure implies more preload and vice-versa.

Basic fork design use a simple *damper-rod* system, in which damping is controlled by the passage of fork oil through an orifice. Though cheap to manufacture, it is hard to tune such forks, as they tend to give too little damping at low slider speeds, yet too much damping at higher slider speeds. Any adjustment setting will always be a compromise, giving both over-mushy and over-stiff damping. Since forks act as hydraulic dampers, changing the weight of the fork oil will alter the damping rate. Some telescopic forks have external adjustments for damping.

It is now evident how much important are suspension on safety and handling, by guaranteeing continuous road contact in the wildest condition and allowing to digest hard braking and strong accelerations manoeuvre.

In this context, semi-active suspensions introduces an innovation on vehicle handling and performances. In particular they allow to change the suspension behavior while riding without the need to stop and manually adjust it. Semi-active suspensions then allow to choose the optimal configuration based on the driving scenario, for example during city commute the suspensions would be mushy and poorly damped, while for high speed highways traveling they would be much stiffer and damped.

The advantage is evident if compared to passive ones, but what is really important is that they can almost instantaneously adjust the controlled parameters to avoid dangerous conditions like a deep pothole taken at high speed. Indeed the damping and stiffness parameters would be adjusted to avoid the driver lift off from the seat.



Figure 1.2: Ohlins top of the line semi-active suspension with controlled damping

The active suspension system enable a further step forward; for instance, in addition to the aforementioned advantages, they enable the possibility to control the suspensions by applying a force on it that modifies the height of the suspensions actively to dynamically adjust the motorcycle set-up.

The disadvantage of an active system is the complexity, which results in higher prices, more components and lower reliability. Another important factor to be considered is the intrinsic energy consumption that active suspensions cause, so they are still a field of research, especially in high performance motorcycles in which there are huge constraints in weight. As a compromise, the semi-active control design typically follows its unconstrained active counterpart when it can, and operates along the passivity envelope when it cannot. [14]

Therefore it is possible to consider that the semi active suspensions represent the optimal trade-off between the 3 main types of suspension seen (passive, semi-active, active). They are easily implementable on high performance bikes without increasing weight significantly. Furthermore depending on which kind of control is actuated on them, price and energy consumption may vary.

Semi-active suspension have received a lot of attention since they seem to provide the best compromise between the performance and cost, which is related to energy consumption, actuators and sensors price. The concept of semi-active suspensions can be applied over a wide rage of application domains, such as road vehicles, rail and agricultural vehicles, bio-mechanical structures (e.g. artificial legs) and more.

However, numerical and experimental results stated that, compared to passive and semi-active suspension systems, active ones offer improved riding ease and level of comfort for both the rider and the

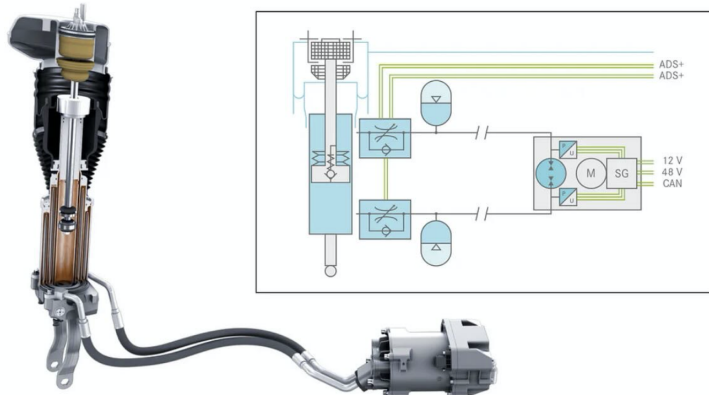


Figure 1.3: Fully active suspension with 48 Volt wheel-individual force control

passenger. The mechanism of active suspension is set among sprung and unsprung masses based on the passive suspension. A pneumatic actuator produces the active control force due to a feedback generated by the sensor in order to measure the reaction interval of the displacement, acceleration and velocity of the vehicle.

The core of the active suspension system is its control strategy used to build the active behavior of the suspension. There are two states to be considered: the first one is the acceleration, the second one is the displacement sensors which can be employed to screen the vehicle's continuous status. The latter parameter is exploited to improve the system performance [8].

1.2 Contributions

It all started from the discussion on how may a motorbike benefit from an active control on the suspensions parameters, then proceeding to the possible means and methods to realize such active or semi-active control. The latter type of suspension may be found especially in high-tier bikes and it represents the state-of-art of shock absorbers.

Semi-active suspensions investigation allows to enrich mechanical suspension and electronic control system knowledge both on the theoretical and practice side.

The choice of investigating further semi-active air suspension system is the result of the analysis of various paper, market analysis and research of optimal components.

The problem may be approached in various ways; in order to find a path to follow, to develop an exhaustive solution some constraints have been chosen to the possible alternatives. Researches have been carried out in order to find an innovative solution to motorbike suspension control and air suspension came out to be the most interesting technology.

Most of the semi-active suspension available on the market relies on the variable damping approach; that was the first approach to the solution of the problem. However, after some calculation, the solution of that kind of system through the Riccati equation couldn't guarantee neither stability nor performance. In particular, the optimal solution for the problem could only be obtained through the MPC (Multi Predictive Control), but that would have fall outside the purpose of this project.

As an alternative, the air suspension solution has been adopted, which implies that the control is not applied on damping, but on a pressure that generates a variable equivalent stiffness. Moreover air suspension is still a technology under development for motorcycle purposes and it may be interesting for future employment. Figure 1.4 shows an example of air suspension.



Figure 1.4: Example of air suspension

After the project initial set-up, the first step was the optimization of the system through the tuning of its components in order to achieve different goals such as Optimal Comfort and Maximum Performance. These two very different features represent the potential of semi-active suspension system. In order to investigate those performances some indexes have been defined based on: acceleration, pitch, pitch rate, suspension stroke and some other parameters resulting from cost functions.

Approach to the issue

After an initial theoretical investigation of the control problem and of the suspension technology, the drafting of the Matlab and Simulink code has been conducted. The most important mathematical tools exploited are: *State Feedback*, *Integral Action* and *Observer*.

The problem has been represented in a schematic way by applying the half car model and by solving all the equilibrium equations. Figure 1.5 depict the basic idea of the simplified problem.

All the theoretical part has been exploited to fully understand which were the control goals and the final results we wanted to achieve to create a robust system with great performances. After deciding the control components, the analysis of the system's equation has been conducted using the half car model. After that the air suspension system has been analyzed in order to write equations capable of

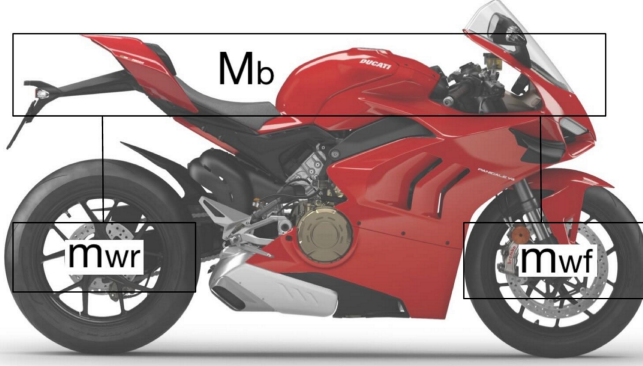


Figure 1.5: Model simplification

representing its influence on the model. Then a first open loop test has been performed in order to verify if the results were consistent when compared to a real motorbike.

Some minor adjustment has been introduced on the values of the suspension system characteristic due to the fact that the leverage on the rear suspension modifies the behaviour of the suspension if compared to a perfectly vertical one [2]. The same operation has been conducted for the front suspension to resemble the real case scenario. All the control components have been added one by one, and their performances have been evaluated to verify the effectiveness of all the subsystems that were being introduced.

Once the control system was completed, all the parameters were set to their first approximated value or the first attempt one. With the goal of creating an effective system, a rough tuning phase was necessary at the beginning, followed by a fine tuning one later on in the process.

A final performance evaluation has been done to verify the optimization process, comparing the optimized system to other conditions and verifying that the tuned one works better in any scenario, even if subjected to very different external disturbances.

1.3 State of art and literature comparison

The main objectives of semi active air suspension are the following:

- Maintain the contact between the tire and the road;
- Maximize the adherence;
- Increase the motorbike safety;
- Provide comfort to the rider;
- Increase the performance by reducing excessive suspension stroke due to hard braking or fast accelerations.

State of art semi active control systems suspensions-oriented are characterised by very complex architectures able to track and analyse in real time all the performance indexes that describe how the system is working and consequently adjusting its control parameters to maximise the performance based on the driver requests. For example, in an off-road usage the needs could be different from a high speed highway scenario, indeed, to be able to meet the various requests that can be made from the driver, various performance indexes has been developed:

- *Performance index for riding comfort*: it is based on the RMS value of vertical acceleration of the sprung masses, typically measured or projected at the rider seat location. It is to note that the maximum human sensitivity to vertical vibration lies between 4 to 8 Hz. To account for the frequency dependency of human sensitivity to vibrations and the length of time of human exposure, a standard has been developed by the International Organization for Standardization as ISO 2631.
- *Performance index for suspension displacement constraint*: because the available suspension displacement - or so-called rattle space - is limited, it's possible to include this constraint by adding the suspension displacement in the performance index.

- *Performance index for road holding:* it is conceivable that a very large variation of tyre deflection may even lead to a loss of contact with the ground. Therefore, the RMS value of tyre deflection variation can be explicit metric for handling characteristics. The most widely used performance index for active suspension study is the combination of the three previously discussed RMS values. That is, using a weighted combination of RMS acceleration of sprung mass, RMS suspension displacement and RMS tyre deflection variation to represent the performance index for optimisation.

Even though semi active suspensions guarantee a much lower energy consumption, the cost is a lack of performance that has been evaluated to a 20% more or less. This may result in 20% lower performance in ride comfort when compared to its active suspension counterpart. [14]

However performance loss with respect to the active counterpart strongly depends on the driven scenario. Further investigation showed that in order to control the semi-active suspension system at the best of its possibilities, then Hybrid MPC has been confirmed analytically the optimal controller, especially if the road disturbance profile is it not known in advance. [3]

Although not always explicitly mentioned, most of the studies with traditional simple ride models (e.g. quarter-car, half-car, and full-car) focus on road roughness disturbances only, neglecting external (inertia) forces and loads due to, for example, braking and turning. The control damping for inertia load-induced excitation can be included later in a separate and independent design procedure. In practice, this is accomplished using longitudinal and lateral acceleration measurements as feed-forward signals indicating braking or turning actions. This typically leads to appropriate ‘stiffening’ of the active or semi-active suspension to prevent or counteract excessive pitch or roll. This stiffening action may reduce the riding quality, but in practice this may be of secondary importance, especially during hard braking and/or handling manoeuvres. [6]

After all the possible control systems implementations , a state of art semi active suspension system can have different features based on it's kind:

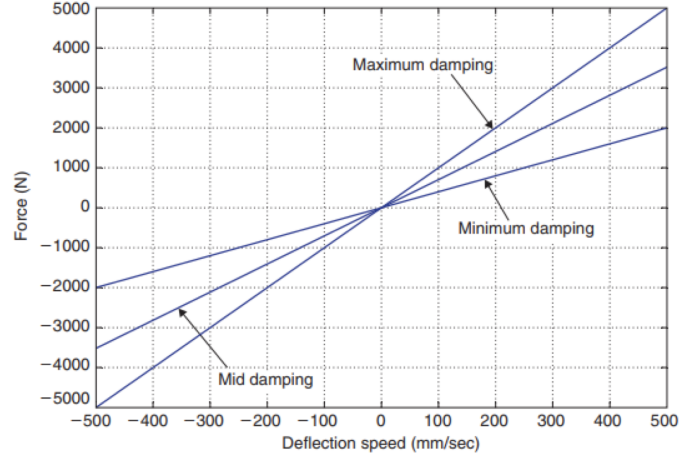
- *Semi active electromechanical* suspension has the capability to vary the damping, which allows them to vary the damping coefficient of the suspensions based on the scenario. They are generally constructed using an adjustable damper in parallel with the primary suspension spring. These are typically constructed from pneumatic and/or hydraulic piston/cylinder combinations with electromechanical control of an orifice. Actuator bandwidth is primarily determined by the reaction time of the controlling valve and associated pressure/force production dynamics. Another implementation of adjustable damping is through magnetorheological (MR) fluids. MR fluid characteristics can be changed electronically, allowing the force across the actuator to change quickly. This method benefits from faster response time, although limited fluid life can contribute to service concerns. It is composed of suspended iron particles in a base fluid of synthetic hydrocarbon. The variable damping is adjusted in milliseconds. The fast response time of the MR damper enables closed-loop vehicle stability control through the control of lateral and longitudinal load transfer characteristics of the suspension during transient movements.
- *Semi active air spring* suspension is an air-worked, microchip controlled suspension framework. This framework substitutes the traditional curl spring suspension and enables programmed front and back load-leveling. It assists in restoring the vehicle load at the front and rear wheels. This innovation permits vehicle producers to accomplish a more prominent level of ride quality and motorcycle handling. An air suspension system for motorcycles comprises a sealed chamber inside the handlebars and a fluid line that interconnects the chamber with the vehicle's pneumatic shock absorber, typically part of the forks. Preferably, the system includes a control valve in fluid communication with the chamber and disposed at or between the handlebars or at the forks. In the preferred embodiment, the control valve is connected to a port located near the center of the handlebars. The preferred embodiment also includes a manual pressure release valve in communication with the chamber and an oil/air separator and/or check valve configured to generally prevent oil from entering the chamber. The pressure release valve and/or the separator or check valve can be made integral with or separate from the control valve.

Technically speaking the air suspension system comprises:

- a vulcanized rubber air spring at each wheel;
- an air compressor;
- a compressed air storage tank may be included for rapid ‘kneel’, storing air at 770 kPa;



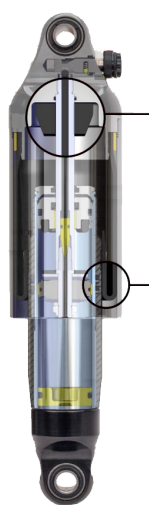
(a) Audi R8 electronically controlled gas spring suspension with load-leveling capabilities and semi-active damper



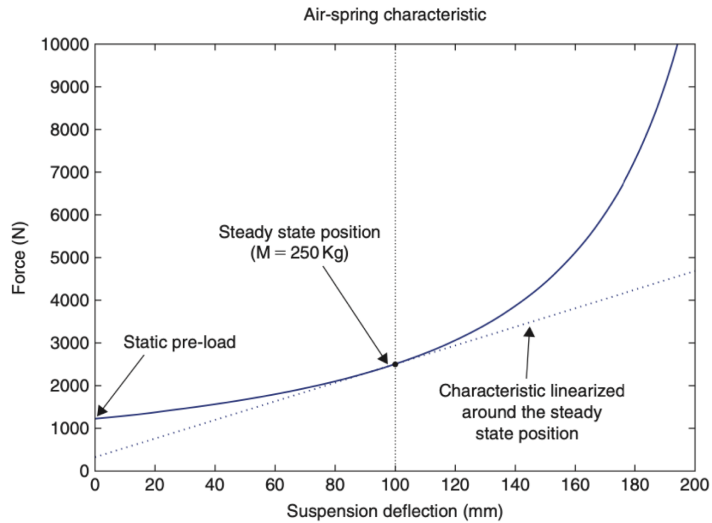
(b) Ideal damping characteristics of an electrohydraulic shock absorber

Figure 1.6: State of the art semi active suspension characteristic

- a valve block which routes air from the storage tank to the air springs via a series of solenoids, valves and many o-rings;
- an ECAS (Electronically Controlled Air Suspension) computer which communicates with the vehicle main computer and decides where to route air pressure;
- an air drier canister because humidity would change the characteristics of the gas inside the camber;
- potentiometers to continuously track the motorcycle suspension displacement.



(a) Air suspension section view with highlighted bump-stop and sealed chamber



(b) Typical force-deflection characteristic of an automotive air spring

Figure 1.7: State of the art gas spring characteristic

Recently a patent has been deposited regarding a new concept of air suspension for motorcycles. Patent No.: US 7,559,396 B2

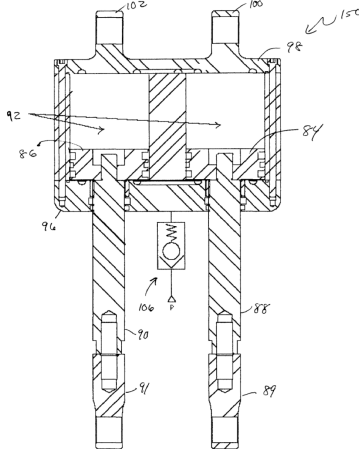
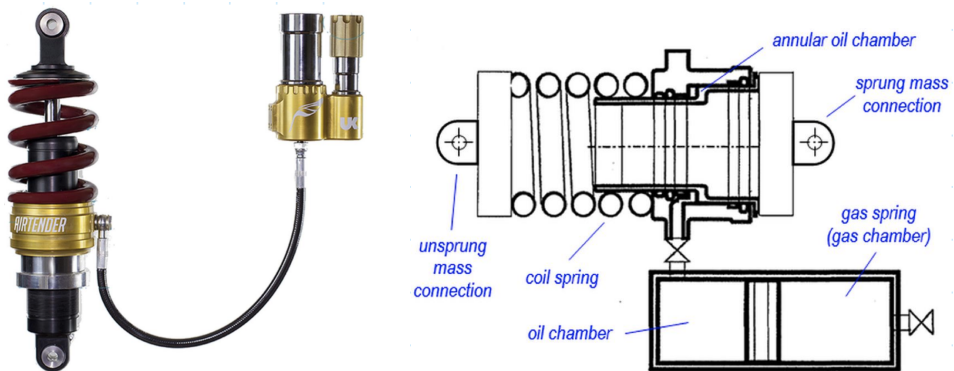


Figure 1.8: Patented double air chamber suspension

The patent refers to a suspension system having double-acting air cylinders. In one illustrative embodiment, a control mechanism allows the ride height to be adjusted independently of the ride firmness. In such an embodiment, the operator may set the firmness of the system and ride quality via two adjustments. A first adjustment, via a main regulator, can address the weight of the motorcycle, rider(s) and load. A second adjustment, via a bias regulator, can provide the rebound control. The system is charged via an air compressor and may be applied to either or both of the rear and front motorcycle suspension. The present invention may also use a biasing pilot-operated high-relief regulator. Such a bias regulator could automatically respond to, proportionally, the main regulator (pressure) setting, therefore, once the system is calibrated, only one adjustment is necessary. The bias regulator controls the dampening of the suspension action. In another embodiment, the bias of the double-acting air cylinder is not adjustable, but rather is set to a pre-selected pressure, or is configured to utilize ambient air pressure. Due to the compact size of the cylinders described herein, longer suspension strokes or travel is possible and allows travel of the full stroke of the suspension. The system also allows the motorcycle frame to be lowered to the ground. Further, the system disclosed herein could be applied to other vehicles or Suspension systems, such as those found in autos and trailers.

In future this system could be coupled to a semi active suspension system to automatically adjust the regulation based on the driving conditions.

The last type of suspension that will be considered is the 'hybrid' configuration based on a suspension with both spring and air chamber/spring and oil chamber. It could further reduce the energy consumption and the pump dimension, allowing a faster response and smaller exercise pressures, that consists in a weight reduction. The control system should also take into account the high non linearity of the hybrid spring system and the hysteresis cycle that is intrinsic of this kind of system due energy dissipation.



(a) AIRTENDER™ hybrid air suspension system (b) Hybrid air suspension section technical view

Figure 1.9: Hybrid air suspension architecture

The system proposed in this report will consider a semi-active suspension system based on an air spring

in which the control system varies the pressure inside the suspension in order to change the equivalent stiffness. The model is simplified respect to the reality:

- an infinitely fast pump dynamics is assumed, meaning that it's able to satisfy the controller request in any circumstance;
- an unlimited outlet air pressure can be provided;
- no thermodynamic effects of the gas, so the influence of temperature due to the compression has no influence on air density.

These assumptions are accepted for educational reasons. In fact, the purpose of the project is to analyse the control architecture and behaviour and not to perfectly adhere to a real case and simulate the hardware limitation that the control itself would face in an on board application.

1.4 Organisation of the manuscript

Chapter 1 was an introductory section to describe how the system - topic of this project - works in practice. The components of a suspension have been discussed, as for the possible control implementations on the vehicle. Advantages and disadvantages were pointed out, providing an overview useful on taking decisions on which system should be the one to prefer based on the need.

In Chapter 2, the mathematical problem formulation will be deeply analysed. A schematic system architecture and the equations used to describe the plant will be seen. Then, the full analysis of the proposed solution will be done to investigate the mathematical solution adopted, and finally its implementation in the Matlab environment.

In Chapter 3, all the components of the simulator and their importance for the good functioning will be investigated. Then, the system tuning will be described and the results will be shown in order to check the correctness of the procedure and all the hypothesis are verified. A final performance evaluation will be done to compare different state conditions and different disturbances on the system.

In Chapter 4, conclusions about the system performance and limitations will be presented. Then the future possible implementations will be listed. Finally a particular hybrid suspension system will be shown as possible alternative to accomplish optimal performance level.

1.5 List of the symbols

Symbol	Meaning	Symbol	Meaning
θ	Pitch of the motorbike	e_1	Front suspension controlled output
\tilde{x}_0	Initial condition vector	e_2	Rear suspension controlled output
c_f	Front suspension damping	\tilde{x}	Linearised state vector
c_r	Rear suspension damping	\tilde{u}	Linearised control vector
d	Disturbances	\tilde{w}	Linearized exogenous vector
g	Gravity	x^*	State equilibrium vector
k_{sf}	Front suspension stiffness	u^*	Control equilibrium vector
k_{sr}	Rear suspension stiffness	w^*	Exogenous equilibrium vector
l_{sf}	Length of the front suspension	\mathbf{D}	Sensor matrix
l_{sr}	Length of the rear suspension	$\tilde{\epsilon}$	Linearised controlled output vector
m_b	Mass of the body	\mathbf{J}	Jordan Matrix
m_f	Mass of the front unsprung mass	\mathbf{V}	Matrix of the chain of generalised eigenvectors associated to \mathbf{A}
m_r	Mass of the rear unsprung mass	λ	Eigenvalue of \mathbf{A}
u	Control vector	\mathcal{R}	Reachability subspace
u^*	Equilibrium control	\mathbf{R}	Reachability matrix
u_{lin}	Linearised control vector	z_R	Reachable dynamics
x	State vector	z_{NR}	Non-reachable dynamics
y_1	Vertical acceleration of the body measurement	\mathbf{K}_S	State feedback matrix
y_2	Pitch rate measurement	\mathbf{K}_I	Integral action matrix
y_3	Front suspension length measurement	\mathbf{K}_O	Control matrix associated to the state observer
y_4	Rear suspension length measurement	\mathbf{O}	Observability matrix
z_{gr}	Height of the ground	u_{FF}	Feed Forward control
z_b	Vertical displacement of the body	u_{FB}	Feedback control
z_f	Vertical displacement of the front end of the motorbike	J	Cost function
z_r	Vertical displacement of the rear end of the motorbike	ε	Linear function of both the plant and the control that has to be penalised
ν	Noise	Q	weight of ε inside the cost function
w	Exogenous vector	\mathbf{S}	Matrices solution of the optimal control problem that minimises the cost function
\mathcal{E}	Unobservability subspace		

Table 1.1: List of the Symbols

Chapter 2

Main body

2.1 Model and Problem Formulation

The control problem goes through the formalisation of a physical model able to mimic as better as possible the behaviour of the real system. A motorcycle can be modelled by means of the half car model. Originally, it was meant to be used in car applications, but it can be successfully implemented even in case like the one under investigation. The motorcycle is supposed to be standing still from a lateral view and considered as a multi mass-damper-spring system as shown in figure 2.1.

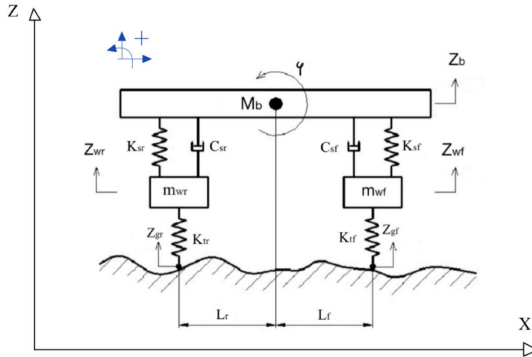


Figure 2.1: Half car model applied to a motorcycle

From figure 2.1 it is possible to see a physical analogy between the mechanical elements and its model.

Front and rear tires are considered as masses linked to the ground by means of springs which simulates their own stiffness (k_{tr} and k_{tf}). The front m_f and rear m_r masses are called unsprung masses because they are not supported by the vehicle suspensions. Their values take into account the respective wheel, tyre and brake assembly and 1/3 of the suspension weight. The mass m_b is the body mass and regards 2/3 of the suspension weight, the vehicle and the rider weights. Suspensions are modelled as mass-damper-spring systems, in particular they connect the sprung and unsprung masses through springs (k_{sf} and k_{sr}) and dampers (c_{sf} and c_{sr}). Due to the much higher value of damping of a suspension with respect to the typical one of a tyre, the latter has been neglected since it doesn't affect as much the accuracy of the model.

Each mass can freely move along the z-axis which is meant to be the vertical one. The DoF (Degrees of Freedom) are z_b , z_f and z_r and they are explicit in the figure. The sprung mass is free to rotate as well around the y-axis, thus it has a further DoF θ . This rotational motion is called *pitch*. The inertia of the body I_{by} against rotation around the y-axis has been considered as well.

The geometry of the motorbike is taken into account through the wheelbase and the position of the CoG (Centre of Gravity). The CoG position along the x-axis and z-axis is given by the static bias of the motorbike when the rider seats onto it.

The dynamics of the system is finally described in the following equations of motion.

$$\begin{cases} \ddot{z}_b m_b = -m_b g + (k_{sf} + u_f)[l_{sf} - (z_b - z_f - L_f \theta)] - c_f(\dot{z}_b - \dot{z}_f + L_f \dot{\theta}) + \\ \quad + (k_{sr} + u_r)[l_{sr} - (z_b - z_r - L_r \theta)] - c_r(\dot{z}_b - \dot{z}_r + L_r \dot{\theta}) \\ \ddot{z}_f m_f = -m_b g - (k_{sf} + u_f)[l_{sf} - (z_b - z_f - L_f \theta)] + c_f(\dot{z}_b - \dot{z}_f + L_f \dot{\theta}) + k_{tf}[l_{tf} - (z_f - z_{gf})] \\ \ddot{z}_r m_r = -m_b g - (k_{sr} - u_r)[l_{sr} - (z_b - z_r - L_r \theta)] + c_r(\dot{z}_b - \dot{z}_r - L_r \dot{\theta}) + k_{tr}[l_{tr} - (z_r - z_{gr})] \\ \ddot{\theta} I_{by} = (k_{sf} + u_f)L_f[l_{sf} - (z_b - z_f + L_f \theta)] - c_f L_f(\dot{z}_b - \dot{z}_f + L_f \dot{\theta}) + \\ \quad - (k_{sr} + u_r)L_r[l_{sr} - (z_b - z_r - L_r \theta)] + c_r L_r(\dot{z}_b - \dot{z}_r - L_r \dot{\theta}) \end{cases} \quad (2.1)$$

It is to note that in order to explicitly write θ , we assume $\theta \approx \sin(\theta)$ which it's true for small angles ($<11^\circ$), otherwise the error would be higher than 5%. This would be an acceptable assumption in the case of a car, but in the one of a motorcycle, it's pretty strong because of its inherently emphasized pitch motion. Rotational oscillation of the sprung mass has to be controlled in the simulation to not produce misleading results.

The equations embed the control through the air spring (u_f, u_r) and the disturbances through the road profile (z_{gf}, z_{gr}). The latter are given by the silhouette of the ground, so the change in altitude of the ground with respect to a horizontal plane. They're defined for both front and rear tyre. As long as the system which controls the motorcycle behaviour is an air spring, the control will be a stiffness which works in accordance to the stiffness of the suspensions. As earlier mentioned, on a practical point of view this variable stiffness is made by the pressurised air inside the volume of the suspension.

All the values of the quantities contained in the equations of motion are summarised in the table below and they're taken referring to the Ducati Panigale V4S available data. Suspensions stiffness are reduced according to V. Cossalter [2] and the tires considered are the *Pirelli Diablo Corsa* model.

Variable name	Value	Meaning	Unit
ksf	1000	Front spring stiffness	[N/m]
ksr	1000	Rear spring stiffness	[N/m]
ktf	195000	Front wheel stiffness	[N/m]
ktr	270000	Rear wheel stiffness	[N/m]
cf	1850	Front suspension damping	[Ns/m]
cr	2300	Rear suspension damping	[Ns/m]
mb	244.96	Mass of motorcycle + rider	[kg]
Lf	0.74919	Front portion of the wheelbase	[m]
Lr	0.71981	Rear portion of the wheelbase	[m]
mf	18.8	Unsprung masses of the front wheel	[kg]
mr	16.4	Unsprung masses of the rear wheel	[kg]
Ib	34.078	Moment of inertia	[kg · m ²]
g	9.81	Gravity	[m/s ²]
lsf	0.59	Free length of the front suspension	[m]
lsr	0.565	Free length of the rear suspension	[m]
susp_travel_f	0.13	Front suspension stroke	[m]
susp_travel_r	0.11	Rear suspension stroke	[m]
ltf	0.2995	Height of front wheel pivot	[m]
ltr	0.3355	Height of rear wheel pivot	[m]

Table 2.1: Parameters of the motorcycle

This model is the most suitable one for a control purpose. It has some limitations regarding the real motorcycle dynamics and it works as long as the vehicle speed is kept constant. In such conditions, it usually underestimates the body acceleration of about 15% with respect to the experimental data that it's still considered an acceptable result.

The goal of the control system is to modify the natural behaviour of the motorbike, in particular the one of this case which is meant to be used on track and it doesn't guarantee good riding experience on daily road usage. What mainly interest is so to control the vertical acceleration of the body and the overall setup of the bike. The set of sensors employed and their purpose is:

- Accelerometer: it is installed at the CoG of the bike and it measures the vertical acceleration of the sprung mass which the rider joins with its weight;

- Gyroscope: it is installed at the CoG of the bike as well and it gives information on the rate of change of the pitch motion;
- Potentiometers: there are two of them, one for each suspension, and they measure the travel distance of the suspensions themselves. The measurement ranges from zero to the maximum stroke.

The accelerometer model is Metrolog 4203. It's a high performance sensor designed for racing application and it is quite expensive (nearly 500\$). This is acceptable because of the type of motorcycle which belongs to the high price market region. It features a low-pass filter to ensure no high frequency engine noise will leak into the passband. A heavy-duty shielded cable and an EMI/RFI module protects the accelerometer from the harsh operating environment. Available in ranges from $\pm 6g$ to $\pm 50g$, the model 4203 will provide reliable measurements from -40°C to $+125^{\circ}\text{C}$.

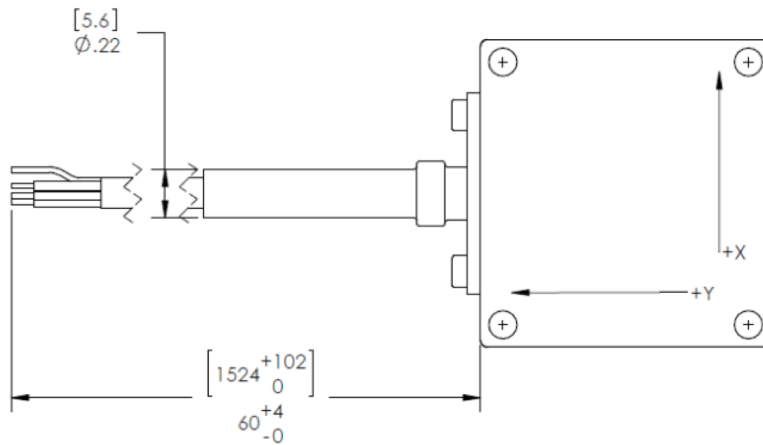


Figure 2.2: Metrolog 4203 accelerometer blueprint

The gyroscope is a Microelectronics A3G4250D 3-axis digital output gyroscope. It's a low-power 3-axis angular rate sensor able to provide high stability at zero rate level and sensitivity over temperature and time. The two potentiometers belong to the same family powered by I2M electronics. They ranges

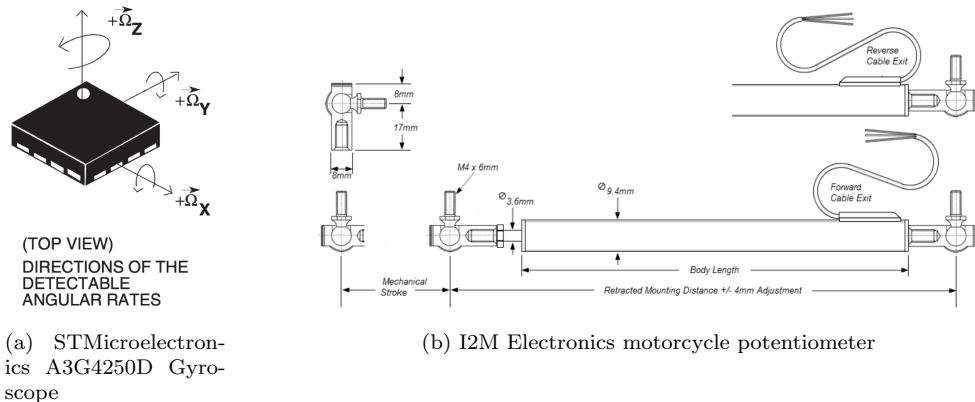


Figure 2.3: Gyroscope and potentiometer

from 75mm to 150mm and its particularly suggested for motorbikes application thanks to it's durability, reliability and high precision. Numerical calculation for the performance estimation in terms of noise and standard deviation are performed in Section 3.1.5.

The system of equations of the sensors (2.2) are described in the same reference system of the motorcycle physical model and they turn to be:

$$\begin{cases} y_1 = \ddot{z}_b \\ y_2 = \dot{\theta} \\ y_3 = z_b - z_f + L_f \theta \\ y_4 = z_b - z_r - L_r \theta \end{cases} \quad (2.2)$$

Unfortunately, the non-linear system of equations couldn't be directly implemented in a control architecture. In control engineering is usually used the *state space representation*, a mathematical model of a physical system seen as a set of input, output and state variables. The state variables are in the smallest possible number able to describe the entire system at any given time. The dynamics of the system is described by a set of Ordinary Differential Equations (ODEs) of the first order:

$$\begin{cases} \dot{x} = f(x, u, d, r) & x(t_0) = x_0 \\ y = h(x, u, \nu) \\ e = h_e(x, u, d, r) \end{cases} \quad (2.3)$$

where:

- $\dot{x} \in \mathbb{R}^{n \times 1}$ represents the state dynamics of the system;
- $x \in \mathbb{R}^{n \times 1}$ is the state vector of the system. It depends on both the current inputs and the past inputs as memory;
- $x_0 \in \mathbb{R}^{n \times 1}$ is the vector of initial conditions of each state variable. It's needed in order to solve the Cauchy problem associated to the set of ODE;
- $u \in \mathbb{R}^{m \times 1}$ is the input vector. It's the controlled variable and in the example of this dissertation is the variable stiffness of the air spring;
- $y \in \mathbb{R}^{p \times 1}$ is the output vector and it depends on the sensors;
- d is the disturbance, in this case given by the road profile;
- r is the reference which the controlled system has to follow. It's generated at will;
- $\nu \in \mathbb{R}^{p \times 1}$ is the noise contribution of the sensors;
- $w = col(d, \nu, r)$, $w \in \mathbb{R}^{r \times 1}$ is called exogenous. Its characteristic is to be not observable, so it can't be reconstructed from the available data (output);
- $e \in \mathbb{R}^{q \times 1}$ is the error associated to the shift among the current state and the reference.

Note that $n, m, p, q, r \in \mathbb{N}$.

In order to properly set the control problem, it is needed to make some assumptions:

1. w is bounded, i.e. $\exists \bar{w} > 0 : \|w(t)\| \leq \bar{w} \quad \forall t \geq 0$. This means that at any time a physical phenomenon is bounded, \bar{w} is a number. For example, the wind, like any other natural phenomenon, is bounded, not infinite. However, w is **not observable**, which means that it is not possible to reconstruct and observe it from the data available;
2. $m \geq q$, which means that the number of inputs is larger or equal to the errors. In physical sense, a number of DoFs larger or equal to the outputs is needed. This relates inputs and outputs.
3. e is readable from y , i.e. $\exists E : \mathbb{R}^p \rightarrow \mathbb{R}^q : e = E(y)$. E is a non-linear transformation.

The goals of the system are the following:

- **G1 Goal:** $\exists x_0 \in \mathbb{R}^n$ and thus $\|u(t)\|, \|x(t)\|, \|e(t)\|$ are bounded.

x_0 is a subset of the space \mathbb{R}^n and x_0 (initial conditions) are stored in the subset. The physical meaning of this concept is that the position, the velocity and the relative error are bounded. This problem is linked to the stability and robustness. The latter two concepts mean:

- *Stability*: the system state does not tend to ∞ ;
- *Robustness*: is the capability to work in opposition to an indefinite exogenous w .

- **G2 goal:** if $d(t) \equiv const.$ and $\nu(t) = 0$, then:

$$\limsup_{t \rightarrow \infty} \|e(t)\| = 0 \quad (2.4)$$

In this particular condition, the controller is able to reach asymptotically the goal. If this is not verified, only goal **G1** is achievable.

The state space representation of the half-car model is based on the change of coordinate described in table 2.2.

$z_b \rightarrow x_1$	$z_f \rightarrow x_3$	$z_r \rightarrow x_5$	$\theta \rightarrow x_7$	$u_f \rightarrow u_1$	$z_{gf} \rightarrow d_1$
$\dot{z}_b \rightarrow x_2$	$\dot{z}_f \rightarrow x_4$	$\dot{z}_r \rightarrow x_6$	$\dot{\theta} \rightarrow x_8$	$u_r \rightarrow u_2$	$z_{gr} \rightarrow d_2$

Table 2.2: State space change of coordinates

The physical model of the motorcycle is defined in the state space by the following system of equations:

$$\begin{cases} \dot{x}_1 = x_2 \\ \dot{x}_2 = \{-m_bg + (k_{sf} + u_1)[l_{sf} - (x_1 - x_3 + L_fx_7)] - c_f(x_2 - x_4 + L_fx_8) + \\ \quad + (k_{sr} + u_2)[l_{sr} - (x_1 - x_5 - L_rx_7)] - c_r(x_2 - x_6 - L_rx_8)\}/m_b \\ \dot{x}_3 = x_4 \\ \dot{x}_4 = \{-m_fg - (k_{sf} + u_1)[l_{sf} - (x_1 - x_3 - L_fx_7)] - c_f(x_2 - x_4 + L_fx_8) + \\ \quad + k_{tf}[l_{tf} - (x_3 - d_1)]\}/m_f \\ \dot{x}_5 = x_6 \\ \dot{x}_6 = \{-m_rg - (k_{sr} + u_2)[l_{sr} - (x_1 - x_3 - L_rx_7)] + c_r(x_2 - x_6 - L_rx_8) + \\ \quad + k_{tr}[l_{tr} - (x_5 - d_2)]\}/m_r \\ \dot{x}_7 = x_8 \\ \dot{x}_8 = \{(k_{sf} + u_1)[l_{sf} - (x_1 - x_3 + L_fx_7)] - c_f(x_2 - x_4 + L_fx_8)L_f + \\ \quad + \{-(k_{sr} + u_2)[l_{sr} - (x_1 - x_5 - L_rx_7)] + c_r(x_2 - x_6 - L_rx_8)\}L_r\}/I_{by} \end{cases} \quad (2.5)$$

It is necessary to underline that the quantities are not forces anymore, but accelerations. This is made in order to write the system according to the mathematical formalism aforementioned. The initial conditions will be defined later in Section 2.2. Considering the previous assumptions, from the available state space model it is possible to check that the problem is well posed.

The same change of variables is applied to the sensors equations (2.6) in order to represent them in the state space too and obtain an output from the plant.

$$\begin{cases} y_1 = \{-m_bg + (k_{sf} - u_1)[l_{sf} - (x_1 - x_3 + L_fx_7)] - c_f(x_2 - x_4 + L_fx_8) + \\ \quad + (k_{sr} - u_2)[l_{sr} - (x_1 - x_5 - L_rx_7)] - c_r(x_2 - x_6 - L_rx_8)\}/m_b + \nu_1 \\ y_2 = x_8 + \nu_2 \\ y_3 = x_1 - x_3 + L_fx_7 + \nu_3 \\ y_4 = x_1 - x_5 - L_rx_7 + \nu_4 \end{cases} \quad (2.6)$$

Given the vector dimension, we classify the plants as Multi-Input Multi-Output (MIMO) because it shows $p, m > 1$. The vector of controlled output is defined as in equation 2.7.

$$\begin{cases} e_1 = x_1 - x_3 + L_fx_7 - r_1 \\ e_2 = x_1 - x_5 - L_rx_7 - r_2 \end{cases} \quad (2.7)$$

On a physical point of view, the designer request is to maintain the suspension travel position as close as possible to a value set in the vector r . The dimensions of the vectors can be now defined:

- $n = 8$;
- $m = 2$;
- $p = 4$;

- $q = 2$;
- $r = 8$.

The state-space representation is finally formalised and the model analysis can be performed.

2.2 Model analysis

2.2.1 Linearisation

The model analysis has to be previously preceded by the linearisation of the system. Linearisation can be used to give important information about how the system behaves in the neighbourhood of equilibrium points. Typically, it is possible to understand whether the point is stable or unstable, as well as how the system approaches (or moves away from) the equilibrium point.

The basic idea is that, in most circumstances, one can approximate the non-linear differential equations that govern the behaviour of the system by linear differential equations. The resulting set of linear ODEs can be solved, whereas it couldn't be possible to solve the initial set of non-linear differential equations.

An equation can be linearised if in the chosen linearisation point it is continuous up to the first grade derivative. In accordance to the formalism of Eq. 2.3, the plant system of equations could be written exploiting the Taylor expansion as:

$$\begin{aligned} \dot{x} = f(x, u, w) &= f(x^*, u^*, w^*) + \frac{\partial f}{\partial x} \Big|_{\substack{x=x^* \\ u=u^* \\ w=w^*}} (x - x^*) + \frac{\partial f}{\partial u} \Big|_{\substack{x=x^* \\ u=u^* \\ w=w^*}} (u - u^*) + \\ &+ \frac{\partial f}{\partial w} \Big|_{\substack{x=x^* \\ u=u^* \\ w=w^*}} (w - w^*) + \sigma(||(x - x^*), (u - u^*), (w - w^*)||^2) \end{aligned} \quad (2.8)$$

where x^* , u^* and w^* are the equilibrium points respectively for the state vector, input and exogeneous. The set of linearised coordinates is defined as:

$$\begin{aligned} \tilde{x} &= x - x^* & \tilde{u} &= u - u^* \\ \tilde{y} &= y - y^* & \tilde{w} &= w - w^* \end{aligned} \quad (2.9)$$

The dynamics of the error \tilde{x} are given by:

$$\dot{\tilde{x}} = \dot{x} - \dot{x}^* = f(x, u, w) - f(x^*, u^*, w^*) \quad (2.10)$$

Including the Taylor expansion of the state-space in equation 2.10, the linearised coordinates can be written as:

$$\dot{\tilde{x}} = \frac{\partial f}{\partial x} \Big|_{\substack{x=x^* \\ u=u^* \\ w=w^*}} \tilde{x} + \frac{\partial f}{\partial u} \Big|_{\substack{x=x^* \\ u=u^* \\ w=w^*}} \tilde{u} + \frac{\partial f}{\partial w} \Big|_{\substack{x=x^* \\ u=u^* \\ w=w^*}} \tilde{w} + \sigma(||(\tilde{x}, \tilde{u}, \tilde{w})||^2) \quad (2.11)$$

Finally, if the linearised system in the state-space representation is linear, time-invariant (usually abbreviated as LTI) and finite-dimensional, then the differential equations can be written in the following matrix form:

$$\dot{\tilde{x}} = \underbrace{\mathbf{A}(x^*, u^*, w^*)}_{\frac{\partial f}{\partial x} \Big|_{\substack{x=x^* \\ u=u^* \\ w=w^*}}} \tilde{x} + \underbrace{\mathbf{B}_1(x^*, u^*, w^*)}_{\frac{\partial f}{\partial u} \Big|_{\substack{x=x^* \\ u=u^* \\ w=w^*}}} \tilde{u} + \underbrace{\mathbf{B}_2(x^*, u^*, w^*)}_{\frac{\partial f}{\partial w} \Big|_{\substack{x=x^* \\ u=u^* \\ w=w^*}}} \tilde{w} \quad (2.12)$$

The system is time invariant as long as it exists a triplet of $[x^*, u^*, w^*]$ such that all the matrices are time invariant. This statement lies even for the subsequent linearisation of the outputs equations.

Reconsidering the general expression, it is possible to do the same for the sensors equations:

$$y = h(x, u, w) \quad y^* = h(x^*, u^*, w^*) \quad (2.13)$$

$$\tilde{y} = y - y^* = \mathbf{C}(x^*, u^*, w^*) \tilde{x} + \mathbf{D}_1(x^*, u^*, w^*) \tilde{u} + \mathbf{D}_2(x^*, u^*, w^*) \tilde{w} \quad (2.14)$$

and for the error e :

$$e = h_e(x, u, w) \quad e^* = h_e(x^*, u^*, w^*) \quad (2.15)$$

$$\tilde{e} = e - e^* = \mathbf{C}_e(x^*, u^*, w^*)\tilde{x} + \mathbf{D}_{1e}(x^*, u^*, w^*)\tilde{u} + \mathbf{D}_{2e}(x^*, u^*, w^*)\tilde{w} \quad (2.16)$$

In this problem, the triplet coincides with the equilibrium of the system. The physical system is considered in equilibrium if subjected to gravity only and standing-still on a perfectly horizontal flat plane. The suspensions stiffness benefits from two contributions given by the passive spring characterised by a constant stiffness and the variable stiffness of the air spring. Even in rest conditions, the overall suspensions stiffness is given by this two contributions, where the control is set in order to maintain the CoG and the pitch in a comfortable position for the rider. The equilibrium triplet values are summarised below:

$$x^* = \begin{pmatrix} 0.8414 \\ 0 \\ 0.2925 \\ 0 \\ 0.3304 \\ 0 \\ -0.02 \\ 0 \end{pmatrix} \quad u^* = \begin{pmatrix} 20000 \\ 30000 \end{pmatrix} \quad w^* = \begin{pmatrix} d^* \\ \nu^* \\ r^* \end{pmatrix} = \begin{pmatrix} 0 \\ 0 \\ 0 \\ 0 \\ 0 \\ 0 \\ 0.5339 \\ 0.5255 \end{pmatrix} \quad (2.17)$$

From the initial definition of w , it can be seen that the reference that the control has to follow coincides with the equilibrium position of the suspensions. This means that the goal is to make the bike stabilising at its equilibrium setup whenever subjected to an external perturbation.

The control via linearisation is limited by its structure. In fact, it can be tuned and optimised in the neighbourhood of the linearisation point whereas its performance may deteriorate a lot far from this condition. Because of this, the subsequent model analysis is meant to be true at the linearisation point and its neighborhood.

2.2.2 Eigenvalues

The analysis of the system dynamics goes through a further change of coordinates. This new set is meant to describe the whole system dynamics through the composition of independent sub-dynamics. The goal is to state if the system is BIBS (Bounded Input Bounded State), that is a criteria for the stability of the system. Hereinafter such concept is formalised.

Let $\dot{x} = \mathbf{Ax} + \mathbf{Bu}$ and $x(0) = x_0$ be the system. Then if:

$$\forall \varepsilon > 0 \exists \bar{\delta}_u(\varepsilon) > 0 : \forall \delta u : \|\delta u\| < \bar{\delta}_u$$

thus:

$$\begin{aligned} \chi_u(x_0, t) &:= x_0 \exp(\mathbf{At}) + \int_0^t \exp(\mathbf{A}(t-\tau)) \mathbf{Bu}(\tau) d\tau \\ \chi_{u+\delta u}(x_0, t) &:= x_0 \exp(\mathbf{At}) + \int_0^t \exp(\mathbf{A}(t-\tau)) \mathbf{B}[u(\tau) + \delta u(\tau)] d\tau \end{aligned}$$

This means that the system is BIBS.

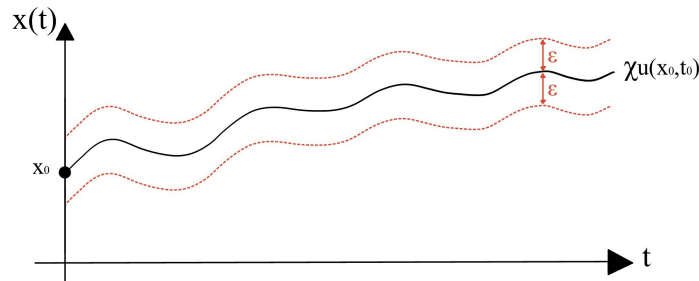


Figure 2.4: Bounded trajectory of the state

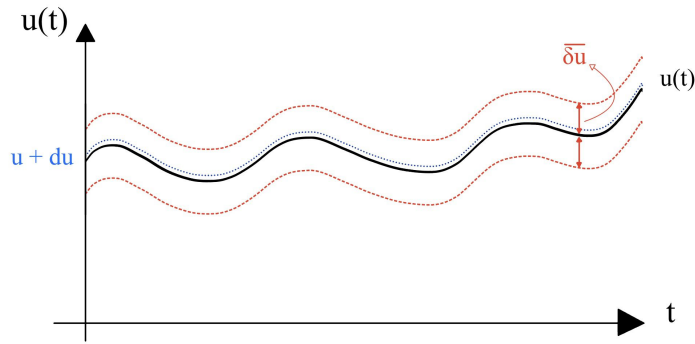


Figure 2.5: Bounded trajectory of the input

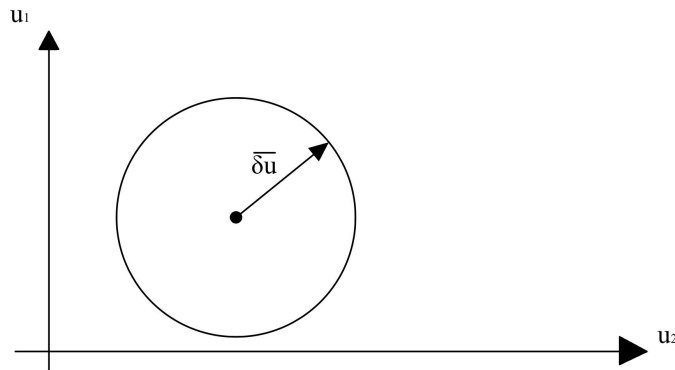


Figure 2.6: Field of existence of the bounded input

Finally, if any sufficiently small perturbation of the input gives a small perturbation on the system, the system is robust, otherwise no.

$$\delta u = \begin{bmatrix} u_1 \\ u_2 \end{bmatrix}$$

In order to achieve the results and properly analyse the system, three elements are needed:

1. Jordan transformation;
2. Knowledge of the generalised eigenvectors;
3. Knowledge of the eigenvalues.

The Jordan transformation is the mathematical tool which allows to pass to the new set of coordinates. The transformation relies on the computation of the chain of generalised eigenvectors, which are a chain of linearly independent eigenvectors, such that:

$$\mathbf{J} = \mathbf{V}^{-1} \mathbf{A} \mathbf{V} \quad (2.18)$$

where:

- $\mathbf{A} \in \mathbb{R}^{n \times n}$ is actually the matrix defined in equation 2.12.
- $\mathbf{J} \in \mathbb{C}^{n \times n}$ is the matrix in Jordan form;
- $\mathbf{V} \in \mathbb{C}^{n \times n}$ is the matrix made by the chain of generalised eigenvectors associated to the matrix \mathbf{A} . On a physical point of view, they're associated to the modes shape of the system in free evolution.

By defining a new transformation $\mathbf{T} = \mathbf{V}^{-1}$, the new set of coordinates is obtained:

$$z = \mathbf{T}x \quad (2.19)$$

The dynamics of z can therefore be obtained as follows:

$$\dot{z} = \bar{\mathbf{A}}z + \bar{\mathbf{B}}u \quad z(t_0) = \mathbf{T}x_0 \quad (2.20)$$

where $\bar{\mathbf{A}} := \mathbf{TAT}^{-1}$ and $\bar{\mathbf{B}} = \mathbf{TB}$. The vector z represents the modes of the system. The linear independence of the chain of generalised eigenvectors guarantees that the dynamics of the z components is decoupled one from each other.

The last step is to define the eigenvalues associated to the eigenvectors. This is possible by properly setting up the eigenvalue problem. What it is obtained is the vector $\lambda \in \mathbb{C}^{1 \times n}$. The real and imaginary part of λ will be analysed later.

Now that all the elements are known, it is possible to proceed by analysing the modes which can reveal the nature of the system (free oscillating case). The modes are defined as follows:

$$\begin{aligned} z_{ig}(t) &= \exp(\mathbf{J}_{ij}t)z_{i,j0} \\ &= \exp(\lambda_i t) \begin{bmatrix} 1 & t & t^2/2 & \dots \\ 0 & \ddots & \ddots & \ddots \\ 0 & 0 & \ddots & t \\ 0 & 0 & 0 & 1 \end{bmatrix} \begin{bmatrix} z_{i,j0} \\ \vdots \\ z_{i,j,q_j-10} \end{bmatrix} \end{aligned} \quad (2.21)$$

where \mathbf{J}_{ij} is the Jordan block associated to the i, g mode of the system and λ_i is the eigenvalues associated to the i^{th} eigenvector.

It is possible to appreciate the magnitude of the eigenvalues to define the behaviour of the i^{th} sub-dynamic. In particular, the real part is the one which tells the quickness to reach the equilibrium, following the trend depicted in figure 2.7.

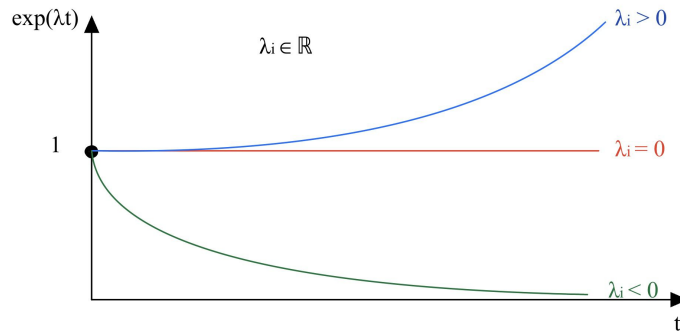


Figure 2.7: Eigenvalues response

There are three possible λ values:

- $\lambda = 0 \Rightarrow \exp(\lambda t) = 1$. From Eq. 2.21, for a single term states:

$$z_{ijq_{ij}-1}(t) = \exp(\lambda t) \cdot z_{ijq_{ij}-1}(0) \quad (2.22)$$

this means that the system remains constant.

- $\lambda > 0 \Rightarrow \exp \rightarrow \infty$ the system exponentially increases.
- $\lambda < 0 \Rightarrow \exp \rightarrow 0$; this means that the system goes to zero in infinite time.

Then it must be studied the behaviour of the complete term.

From Fig. 2.8 it is possible to see how if and only if all the eigenvalues have negative real part, the system is BIBS. In such case, it is possible to state that all the roots are Hurwitz, or that the \mathbf{A} matrix is Hurwitz. The imaginary part of the eigenvalues is associated to the oscillation of the mode.

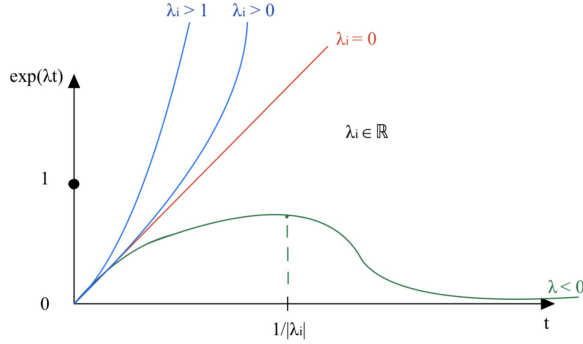


Figure 2.8: Full dynamics response in time

Eigenvalues	
-62.5455	+96.1710i
-62.5455	+96.1710i
-1.0556e+02	+0.0000e+00i
-29.2996	+71.2134i
-29.2996	-71.2134i
-7.7082	-12.3905i
-16.3855	+0.0000i

Table 2.3: Free oscillation eigenvalues

In table 2.3, the eigenvalues associated to the free oscillation of the system are listed. It is possible to state that the system is BIBS. The free evolution of each mode can be seen in Fig. 2.9. In order to get the influence of each independent dynamics z on the plant behaviour represented by the state vector x , it is possible to consider a weight given by the associated generalised eigenvector. For the sake of clarity, considering $x \in \mathbb{R}^{n \times 1}$, $z \in \mathbb{C}^{n \times 1}$ and $\mathbb{V} \in \mathbb{C}^{n \times n}$, for the i^{th} element of x :

$$x_i(t) = \sum_{j=1}^n v_{ij} z_j(t) \quad (2.23)$$

$$v_i = [v_{i1} \dots v_{in}] \quad (2.24)$$

$$\|v_i\| = \sqrt{\sum_{j=1}^n v_{ij}^2} \quad (2.25)$$

$$x_i(t) = \|v_i\| \underbrace{\sum_{j=1}^n \frac{v_{ij}}{\|v_i\|} z_j(t)}_{\in [0,1]} \quad (2.26)$$

The best way to visualize the weight of the modes z on each x , a spider plot is generated in figure 2.10. The further analysis of the linear system concerns the study of its properties directly associated to the achievement of the control goals **G1** and **G2**. The overall architecture of the system has to be defined as follows.

Let $e_x := x_O - \tilde{x}$ and $\chi := \text{col}(\tilde{x}, \eta, e_x, x_{FF})$. Then by considering $x_O = e_x + \tilde{x}$ it is possible to compute the closed loop dynamics:

$$\begin{aligned} \dot{\chi} &= \mathbf{A}_\chi \chi + \mathbf{B}_{\chi\omega} + \sum_{i=0}^{r_{max}} \mathbf{B}_{\chi_i} \frac{d^i}{dt^i} r \\ \tilde{u} &= \mathbf{C}_\chi \chi + \sum_{i=0}^{r_{max}} \mathbf{D}_{FFi} \frac{d^i}{dt^i} r \end{aligned} \quad (2.27)$$

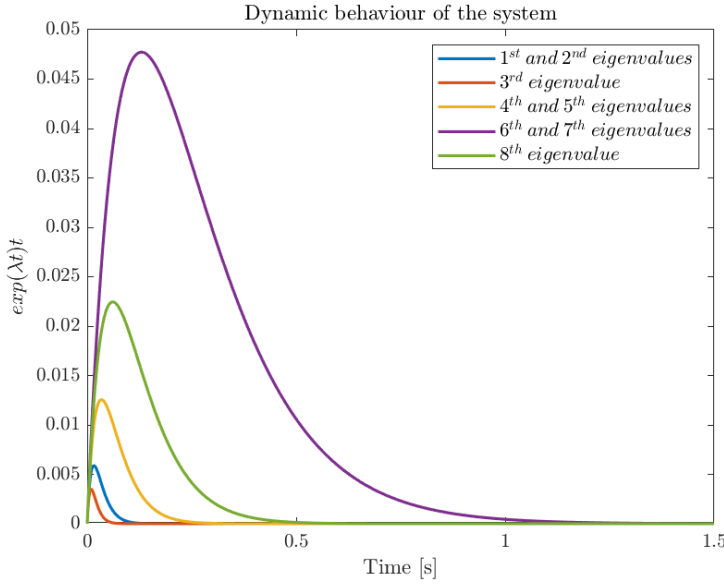


Figure 2.9: Dynamic behaviour of the system

where

$$\mathbf{A}_x = \begin{bmatrix} \mathbf{A} + \mathbf{B}_1 \mathbf{K}_S & \mathbf{B}_1 \mathbf{K}_I & \mathbf{B}_1 \mathbf{K}_S & \mathbf{B}_1 \mathbf{C}_{FF} \\ \mathbf{C}_e + \mathbf{D}_{e1} \mathbf{K}_S & \mathbf{D}_{e1} \mathbf{K}_I & \mathbf{D}_{e1} \mathbf{K}_S & \mathbf{D}_{e1} \mathbf{C}_{FF} \\ \mathbf{A}_O + \mathbf{K}_O \mathbf{C} - \mathbf{A} + \mathbf{M} \mathbf{K}_S & \mathbf{M} \mathbf{K}_I & \mathbf{A}_0 + \mathbf{M} \mathbf{K}_S & \mathbf{M} \mathbf{C}_{FF} \\ 0 & 0 & 0 & \mathbf{A}_{FF} \end{bmatrix} \quad (2.28)$$

The final goal is actually to make a \mathbf{A}_x Hurwitz, which means to make Hurwitz step-by-step the 1×1 , 2×2 and 3×3 matrices on the main diagonal. Reachability and observability analysis are provided.

2.2.3 Reachability

The aim of the reachability analysis is to understand if the plant ‘can be modified through the control input \tilde{u} and which are the assumption that the plant must verify to let the existence of \mathbf{K}_S such that $\mathbf{A} + \mathbf{B}_1 \mathbf{K}_S$ is Hurwitz. These results are obtained through the called *Reachability Kalman Decomposition*, which allows to define a reachability subset \mathcal{R} . If a state belongs to the reachability subset, there exists a control law which brings the state to another one arbitrary. This means that we can modify the behaviour of the system. In practice, this is performed by defining the reachability matrix:

$$\mathbf{R} := [\mathbf{B}_1 \ \mathbf{A}\mathbf{B}_1 \ \mathbf{A}^2\mathbf{B}_1 \ \dots \ \mathbf{A}^{n-1}\mathbf{B}_1] \quad (2.29)$$

and

$$Im(\mathbf{R}) = \mathcal{R} \quad (2.30)$$

If $Im(\mathbf{R})$ and $ker(\mathbf{R}^T)$ span the whole vectorial space, so they can entirely describe it, the system is fully reachable. The implication is that it exist a control law that makes $\mathbf{A} + \mathbf{B}_1 \mathbf{K}_S$ Hurwitz, moreover it can modify (and then stabilise) the whole system dynamics. The system is fully reachable if $rank(\mathbf{R}) = n$. By definition, the rank of \mathbf{R} is the dimension of its image, so of the reachability subset. If \mathbf{R} has the same dimension of \mathbf{A} , it means that it can completely describe the state-space.

In general, in order to know which is the reachable and non-reachable dynamics of the system, and its dimension, it is possible to define a transformation:

$$\mathbf{T}_R^{-1} := [Im(R) \ ker(R^T)] \quad (2.31)$$

Therefore:

$$\begin{aligned} z &= \mathbf{T}_R x & x &= \mathbf{T}_R^{-1} z \\ z &= \mathbf{T}_R x = \mathbf{T}_R \mathbf{A} x + \mathbf{T}_R \mathbf{B}_1 u & = \mathbf{T}_R \mathbf{A} \mathbf{T}_R^{-1} z + \mathbf{T}_R \mathbf{B}_1 u = \bar{\mathbf{A}} z + \bar{\mathbf{B}} u \end{aligned} \quad (2.32)$$

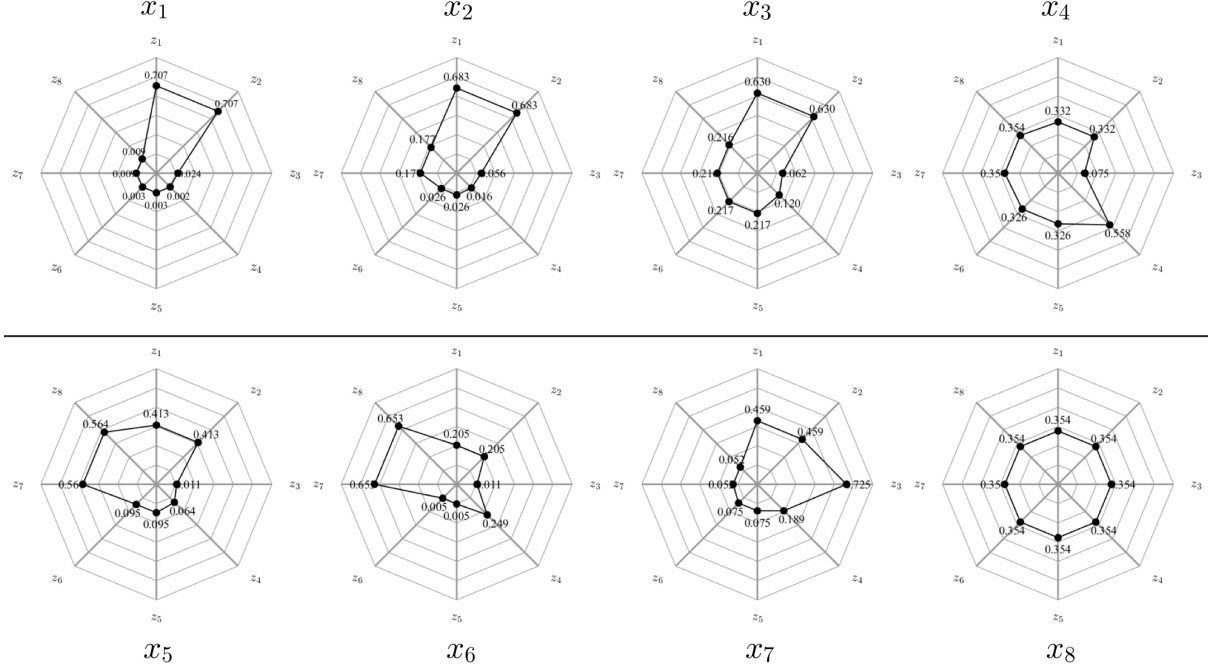


Figure 2.10: Influence of the decoupled dynamics on the state

$$z = \begin{bmatrix} z_R \\ z_{NR} \end{bmatrix} \quad (2.33)$$

In particular $z_R \rightarrow \mathbb{R}^{n_R}$ and $z_{NR} \rightarrow \mathbb{R}^{n_{nR}}$ where $n_R = \text{rank}(\mathbf{R})$ is the dimension of the reachability subspace and $n_{nR} = \dim(\ker(R^T))$ is the dimension of the non-reachable part. In general, $n = n_R + n_{nR}$. It is possible to write:

$$\begin{bmatrix} \dot{z}_R \\ \dot{z}_{NR} \end{bmatrix} = \underbrace{\begin{bmatrix} \mathbf{A}_{11} & \mathbf{A}_{12} \\ 0 & \mathbf{A}_{22} \end{bmatrix}}_A \begin{bmatrix} z_R \\ z_{NR} \end{bmatrix} + \underbrace{\begin{bmatrix} \bar{B}_1 \\ 0 \end{bmatrix}}_B u \quad (2.34)$$

The first row of \bar{A} represents the reachable dynamics of the system, while the second one represents the non-reachable dynamics. The non-reachable part of \bar{A} can be modified by z_{NR} , but not by z_R . The reachable dynamics can be affected by z_{NR} .

As long as the non-reachable dynamic has a convergent behaviour, so the eigenvalues associated to its part have negative real part, the system is stabilisable. This means that it is not possible to directly control the whole state-space at will, but the stability of the system after a perturbation is guaranteed. Conversely, the non-reachable dynamics would diverge and the system couldn't be stabilised in any way and the control goal **G1** wouldn't be satisfied.

The reachable analysis can be extended even to the system error. Let:

$$\begin{cases} \dot{x} = \mathbf{A}x + \mathbf{B}_1u + \mathbf{B}_2d \\ e = \mathbf{C}_e x + \mathbf{D}_{1e}u + \mathbf{D}_{2e}w \end{cases} \quad (2.35)$$

By considering $\dot{\eta} = e$, equation 2.35 can be written in matrix form as follows:

$$\begin{bmatrix} \dot{x} \\ \dot{\eta} \end{bmatrix} = \underbrace{\begin{bmatrix} \mathbf{A} & 0 \\ \mathbf{C}_2 & 0 \end{bmatrix}}_{\bar{A}} \begin{bmatrix} x \\ \eta \end{bmatrix} + \underbrace{\begin{bmatrix} \mathbf{B}_1 \\ \mathbf{D}_{1e} \end{bmatrix}}_{\bar{B}_1} u + \underbrace{\begin{bmatrix} \mathbf{B}_2 \\ \mathbf{D}_{2e} \end{bmatrix}}_{\bar{B}_2} d \quad (2.36)$$

By implementing information about the error, a new control law will be defined:

$$u = \mathbf{K}_S x + \mathbf{K}_I \eta \quad (2.37)$$

where:

- $\mathbf{K}_s x$ is the contribution of the state feedback;
- $\mathbf{K}_I \eta$ is the contribution of the integral action.

The explanation of these two contributions will be given in Section 3.1. The system described by Eq. 2.36 is called *extended plant* because it embeds information even about the error associated to the reference. The previous considerations about the reachability of the original plant can be performed even for the extended one, noting that even its meaning is extended to the capability of the control to stabilise (steer to zero) the error. The reachability matrix will be defined as:

$$\mathbf{R} := [\bar{\mathbf{B}}_1 \bar{\mathbf{A}}\bar{\mathbf{B}}_1 \bar{\mathbf{A}}^2\bar{\mathbf{B}}_1 \dots \bar{\mathbf{A}}^{n-1}\bar{\mathbf{B}}_1] \quad (2.38)$$

If the system is stabilisable, it means that there exist a couple of \mathbf{K}_s and \mathbf{K}_i such that the 2×2 matrix on the main diagonal of \mathbf{A}_X is Hurwitz. In such case, the system has proved to be fully reachable, so it is stabilisable by definition.

The part of *Matlab* code in charge of checking the reachability of the system is listed below.

```
R = ctrb(Ae,Be);
rankR = rank(R,1e-10);

ImR = orth(R);
kerR = null(R');
invTr = [ImR, kerR];
A_bar_R = (invTr^-1)*Ae*invTr;
B_bar = (invTr^-1)*Be;

if rankR == length(Ae)
    disp('The extended system is Fully Reachable, hence stabilisable')
    A_11R = A_bar_R;
    A_12R = [];
    A_22R = [];
    B1_bar = B_bar;
else
    B1_bar = B_bar(1:rankR,:);
    A_11R = A_bar_R(1:rankR,1:rankR);
    A_12R = A_bar_R(1:rankR,rankR+1:end);
    A_22R = A_bar_R(rankR+1:end,rankR+1:end);
    A_22R_eig = eig(A_22R);
    anseig = real(A_22R_eig)≥0;
    if anseig==0
        disp('The extended system is NOT Fully Reachable, but stabilisable')
    else
        disp('The extended system is NOT Fully Reachable and NOT stabilisable')
    end
end
```

A more in-depth analysis was performed in order to study a different configuration of air springs. The reachability analysis is performed assuming the only presence of the front gas spring. The system turns to be fully reachable, so the system is completely stabilisable. However, on a real application, performance would be much worse due to a limited capability of changing the motorcycle set up.

2.2.4 Observability

The last step to perform in order to reach the goals is to make the 3×3 matrix on the main diagonal of matrix 2.28 Hurwitz too. This goes through the observability analysis. The question that drives it is if it's possible to estimate the state of the system. This is needed because the state vector is given time-by-time by the physical model in Fig. 2.1 that is an approximation of the reality. In fact, the only information available are the input and the output of the system from which we've to estimate the state. The observability answers if this estimation is possible and in which extent, in a deep analogy with the reachability analysis. Given a simplified plant not affected by any control nor external disturbances:

$$\begin{aligned} \dot{x} &= \mathbf{Ax} \\ y &= \mathbf{Cx} \end{aligned} \quad (2.39)$$

The goal is to find a \mathbf{K}_o such that $\mathbf{A} - \mathbf{K}_o\mathbf{C}$ is Hurwitz. By using the "Observability Kalman Decomposition", it's possible to define an unobservability subset \mathcal{E} and to verify if the state belongs to it. Let:

$$\mathbf{O} := \begin{bmatrix} \mathbf{C} \\ \mathbf{CA} \\ \vdots \\ \mathbf{CA}^{n-1} \end{bmatrix} \quad (2.40)$$

being the observability matrix. The basis for \mathcal{E} is defined by the kernel:

$$\mathcal{E} = \ker(\mathbf{O})$$

The unobservability subset includes all the initial states belonging to \mathbb{R}^n such that the output is null at each time. Because the origin is always zero by definition, the unobservable states can't be distinguished from the origin. If a vector state component has a projection on a direction different from \mathcal{E} it means that it doesn't belong to it and it can be observed. If no one of the state vector components belongs to \mathcal{E} then the system is fully observable. The requirement is that $\text{rank}(\mathbf{O})=n$, in analogy with the reachability analysis. In order to state which is the observable and unobservable dynamics, a transformation is defined:

$$\begin{aligned} z &= \mathbf{T}_o x \\ \mathbf{T}_o^{-1} &:= [\ker(\mathbf{O}) \quad \text{Im}(\mathbf{O}^T)] \end{aligned} \quad (2.41)$$

$\ker(\mathbf{O})$ is the unobservable part, $\text{Im}(\mathbf{O}^T)$ is the observable part.

We can apply a change of coordinates and we can rewrite the system as observable and unobservable.

$$z = \begin{bmatrix} z_{NO} \\ z_O \end{bmatrix} \quad (2.42)$$

$$\begin{aligned} \dot{z} &= \mathbf{T}_o \dot{x} = \mathbf{T}_o \mathbf{A} x = \mathbf{T}_o \mathbf{A} \mathbf{T}_o^{-1} z = \bar{\mathbf{A}} z \\ y &= \mathbf{C} \mathbf{T}_o^{-1} z = \bar{\mathbf{C}} z \end{aligned} \quad (2.43)$$

By applying it to Eq. (2.39):

$$\begin{bmatrix} \dot{z}_{NO} \\ \dot{z}_O \end{bmatrix} = \underbrace{\begin{bmatrix} \bar{\mathbf{A}}_{11} & \bar{\mathbf{A}}_{12} \\ 0 & \bar{\mathbf{A}}_{22} \end{bmatrix}}_A \begin{bmatrix} z_{NO} \\ z_O \end{bmatrix} \quad (2.44)$$

$$y = \underbrace{\begin{bmatrix} \mathbf{0} & \bar{\mathbf{C}}_1 \end{bmatrix}}_{\bar{\mathbf{C}}} \begin{bmatrix} z_{NO} \\ z_O \end{bmatrix} \quad (2.45)$$

The system is fully observable if and only if $\bar{\mathbf{A}} \equiv \bar{\mathbf{A}}_{22}$. The system is detectable if the matrix $\bar{\mathbf{A}}_{11}$ associated to the non observable dynamics is Hurwitz, so the system is bounded and stabilisable. Finally, it can be demonstrated that the implementable control law $u = \mathbf{K}_s \hat{x}$ that takes advantage of the estimated state vector \hat{x} makes the below matrix Hurwitz:

$$\begin{bmatrix} \mathbf{A} + \mathbf{B}_1 \mathbf{K}_s & \mathbf{B}_1 \mathbf{K}_I & \mathbf{B}_1 \mathbf{K}_S \\ \mathbf{C}_e + \mathbf{D}_{e1} \mathbf{K}_s & \mathbf{D}_{e1} \mathbf{K}_I & \mathbf{D}_{e1} \mathbf{K}_S \\ \mathbf{A}_O + \mathbf{K}_o \mathbf{C} - \mathbf{A} + \mathbf{M} \mathbf{K}_S & \mathbf{M} \mathbf{K}_I & \mathbf{A}_O + \mathbf{M} \mathbf{K}_S \end{bmatrix} \quad (2.46)$$

Where :

- $\mathbf{A}_O = \mathbf{A} - \mathbf{K}_O \mathbf{C}$
- $\mathbf{B}_O = \mathbf{B} - \mathbf{K}_O \mathbf{D}_1$

In our case, the system has proved to be fully observable too, then detectable by definition by means of the set of sensors previously chosen (Section 2.1).

The part of *Matlab* code in charge of checking the observability of the system is attached below.

```

O = obsv(A,C);
rankO = rank(O);

ImO = orth(O');
kerO = null(O);
invTo = [kerO, ImO];
A_bar_O = (invTo^-1)*A*invTo;
C_bar = C*invTo;
z = (invTo^-1)*x;

if rankO == length(A)
    disp('The system is Fully Observable')
    A_11O = [];
    A_12O = [];
    A_22O = A_bar_O;
    C2_bar = C_bar;
else
    C2_bar = C_bar((length(z)-rankO+1):end,:);
    A_11O = A_bar_O(1:(length(z)-rankO),1:(length(z)-rankO));
    A_12O = A_bar_O(1:(length(z)-rankO),(length(z)-rankO+1):end);
    A_22O = A_bar_O((length(z)-rankO+1):end,(length(z)-rankO+1):end);
    A_11O_eig = eig(A_11O);
    anseig = real(A_11O_eig)≥0;
    if anseig==0
        disp('The system is NOT Fully Observable, but detectable')
    else
        disp('The system is NOT Fully Observable and NOT detectable')
    end
end

```

A further analysis was performed in order to study a different set of sensors. Actually, the system without the data provided by neither the accelerometer nor the gyroscope turns to be still fully observable. By removing one of the two potentiometers too, it's not fully observable anymore, but still detectable. Obviously, the consequence would be a worsening in the performance of the state estimation.

However, the result provided by the observability analysis makes BIBS stable the closed loop Plant of Eq. 2.5, so it guarantees the achievement of the goal **G1** and **G2** and it's possible to proceed with the actual design of the control itself.

2.3 Proposed solution

The half car model equipped with two air spring actuators for the suspensions and four sensors on the vehicle has proved to be fully reachable and fully observable. On a control design point of view, this let the possibility to set the eigenvalues of the closed loop system at will by means of a proper design of the matrices \mathbf{K}_s , \mathbf{K}_I and \mathbf{K}_o . Calling our LTI system controlled by a state feedback stabiliser and an integral action:

$$\begin{aligned}
\dot{x} &= \mathbf{A}x + \mathbf{B}_1u + \mathbf{B}_2d \\
\dot{\hat{x}} &= (\mathbf{A} - \mathbf{K}_o \mathbf{C})\hat{x} + (\mathbf{B}_1 - \mathbf{K}_o \mathbf{D}_1)u + \mathbf{K}_o y \\
\dot{\eta} &= \mathbf{D}_e x + \mathbf{D}_{e_1} u + \mathbf{E}\nu \\
u &= \mathbf{K}_s \hat{x} + \mathbf{K}_I \eta \\
y &= \mathbf{C}x + \mathbf{D}_1 u + \nu
\end{aligned} \tag{2.47}$$

Define the estimation error as $e_x = \hat{x} - x$, let:

$$\mathbf{A}_{cl} = \begin{bmatrix} \mathbf{A} + \mathbf{B}_1 \mathbf{K}_s & \mathbf{B}_1 \mathbf{K}_I \\ \mathbf{C}_e + \mathbf{D}_{e_1} \mathbf{K}_s & \mathbf{D}_{e_1} \mathbf{K}_I \end{bmatrix} \quad (2.48)$$

The final result will be the wanted behaviour of the controlled plant affected by an unknown disturbance. Unfortunately, the presence of sensors noise affects the actual evolution of the plant, corrupting the performance of the control.

The control system architecture implemented is depicted in Fig. 2.11.

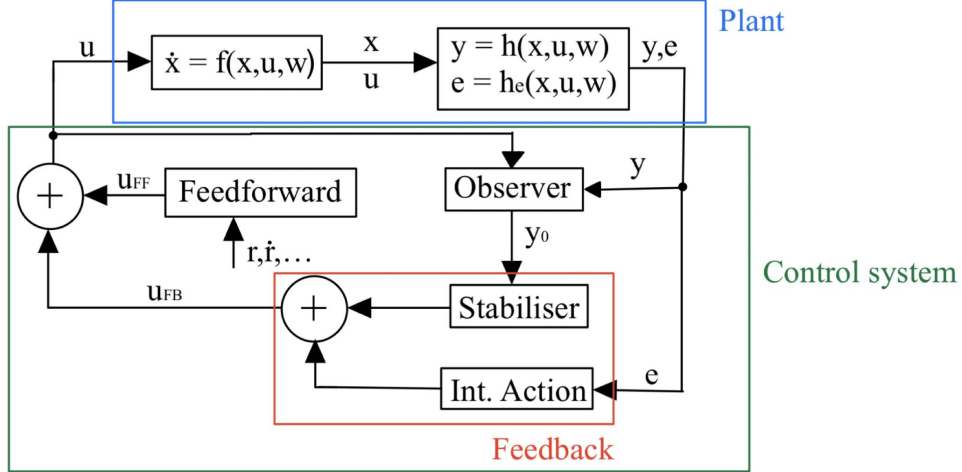


Figure 2.11: Control system architecture block scheme

The control takes advantage of both the feedback stabiliser and the integral action. In addition to their mathematical definition, it's worth specifying their role and why they're both needed:

- *Feedback stabiliser*: it's in charge of providing a control proportional to the state vector coordinates. Actually, they're the estimated ones by the observer. It has a very fast response on a 'macroscopic' scale, meaning that its action is higher the higher the shift from the equilibrium conditions, preventing limit cycles. It's not able to steer the error to zero after a perturbation on the plant;
- *Integral action*: it is in charge of steering the error to zero after a disturbance kicked in. Conversely to the feedback stabiliser, its action is much slower because proportional to the integral of the error. This means that it relies on the time history of error, so it needs the error to endure in time in order to provide a significant contribution.

The above explanation is purely qualitative: the actual behaviour depends on the design of the matrices. The design criteria which allows to obtain the best control is called "*Robust Stationary Optimal Control*". It's applied to the extended linear plant in order to design at the same time the matrices \mathbf{K}_s and \mathbf{K}_I for the mathematical reasons explained in Section 2.2. The robust optimal criteria takes advantage of altering the stability of the system and introducing a cost function. Let:

$$\begin{aligned} \dot{x} &= (\mathbf{A} + \alpha \mathbf{I})x + \mathbf{B}u \\ \varepsilon &= \mathbf{C}_\varepsilon x + \mathbf{D}_\varepsilon u \end{aligned} \quad (2.49)$$

A cost function J is defined:

$$J = \int_{t_0}^{\infty} \varepsilon^T \mathbf{Q} \varepsilon + u^T \mathbf{R} u dt \quad (2.50)$$

Where:

- α is a design parameter which allows to make the eigenvalues of the extended plant less negative, then more unstable;

- ε is a linear function of both the plant and the control that has to be penalised, so to keep under control. It's bounded by definition. The matrices C and D are not the one associated to the output y .
- J is the cost function that accumulates the value of the terms inside the integral. The aim of the optimal control is to minimise the cost for the given problem;
- Q is the weight of ε inside the cost function. It's associated to how much the designer cares about the state. The meaning of a higher Q is that we'd want the state to be as closer as possible to the origin, so to its linearisation point. $Q \geq 0$ semidefinite positive. If $Q < 0$, it would mean that the more the state is far from the origin, the less the cost, which it doesn't make sense on a control point of view;
- R is associated to the cost of the control u . The higher R , the higher the cost of u , which means that the control law will be more restrictive on actuating a large control. However, it doesn't define a boundary on the maximum value the control can apply. $R > 0$ definite positive. If $R < 0$, it would mean that the higher the control applied, the less the cost, leading to the control to diverge to infinite. Analogue condition for $R = 0$, because it would mean that it doesn't care at all the values it assumes and it will tend to diverge as well.

Q and R are defined as it follows. Let:

$$\varepsilon := \begin{bmatrix} \varepsilon_1 \\ \vdots \\ \varepsilon_m \end{bmatrix}, \quad u := \begin{bmatrix} u_1 \\ \vdots \\ u_p \end{bmatrix} \quad (2.51)$$

and define $\varepsilon_{i_{max}}, u_{j_{max}} > 0$ for $i = 1, \dots, m$ and $j = 1, \dots, p$. Let:

- $|\varepsilon_i(t)| \leq \varepsilon_{i_{max}} \in \mathbb{R}_{>0}$ for $i = 1, \dots, m$;
- $|u_i(t)| \leq u_{i_{max}} \in \mathbb{R}_{>0}$ for $i = 1, \dots, p$;

$$Q^{-1} = q \begin{bmatrix} \varepsilon_{1_{max}}^2 & 0 & \dots & 0 \\ 0 & \varepsilon_{2_{max}}^2 & \dots & 0 \\ \vdots & \vdots & \ddots & \vdots \\ 0 & 0 & \dots & \varepsilon_{p_{max}}^2 \end{bmatrix} \quad (2.52)$$

$$R^{-1} = p \begin{bmatrix} u_{1_{max}}^2 & 0 & \dots & 0 \\ 0 & u_{2_{max}}^2 & \dots & 0 \\ \vdots & \vdots & \ddots & \vdots \\ 0 & 0 & \dots & u_{p_{max}}^2 \end{bmatrix} \quad (2.53)$$

The terms q and p are the normalization weights which makes the matrices Q and R independent on the dimensions of the vectors ε and u .

The numerical solution of the problem is provided by the mathematical tool represented by the *Algebraic Riccati Equation* (ARE) presented below:

$$S B \bar{R}^{-1} B^T S - S(A + \alpha I - B \bar{R}^{-1} D^T Q C) - (A + \alpha I - B \bar{R}^{-1} D^T Q C)^T S - C^T Q [I - D \bar{R}^{-1} D^T Q] C = 0 \quad (2.54)$$

Where:

- S is the matrix solution of the optimal control problem that minimises the cost function. Because the expression is non-linear, what it's actually provided is the solution of ARE stationary, so at infinite time. It's demonstrated that if the extended plant is stabilisable and detectable, S makes the control BIBS in closed loop;
- $\bar{R} = D^T Q D + R$
- C and D are the matrices of the expression of ε .

The subsequent assumption are proposed:

- $\mathbf{D} = 0$, so that x and u are decoupled;
- $\mathbf{E} = \mathbf{I}$ (identity matrix);
- $\mathbf{G} = 0$.

Partial Matlab code implemented to obtain the solution is listed hereafter.

```

epsilon = [
    eta(1);
    eta(2);
    (-mb*g+(ksf-u(1))*(lsf-(x(1)-x(3)+Lf*x(7)))-cf*(x(2)-x(4)+Lf*x(8)) ...
    +(ksr-u(2))*(lsr-(x(1)-x(5)-Lr*x(7)))-cr*(x(2)-x(6)-Lr*x(8)))/mb+nu(1);
    x(8)+nu(2);
    x(1)-x(3)+Lf*x(7)+nu(3);
    x(1)-x(5)-Lr*x(7)+nu(4)
];

xe = [
    x;
    eta
];

C_eps = jacobian(epsilon,xe);
...
D_eps = jacobian(epsilon,u);
...

epsmax = zeros(length(epsilon),1);
str = upper(str);
switch str
    case 'COMFORT'
        epsmax(1) = 0.5;
        epsmax(2) = 0.5;
        epsmax(3) = 1*g;
        epsmax(4) = 1.75*1.49;
        epsmax(5) = lsf-(x_star(1)-x_star(3)+Lf*x_star(7));
        epsmax(6) = lsr-(x_star(1)-x_star(5)-Lr*x_star(7));
    case 'RACE'
        ...
end

Q = inv(length(epsilon)*diag(epsmax.^2));

umax = zeros(length(u),1);
umax(1) = 35000;
umax(2) = 45000;

R = inv(length(u)*diag(umax.^2));
R_bar = R+D_eps.*'Q*D_eps;

alpha = 12;
Am = Ae+alpha*eye(length(Ae));
Em = eye(length(Ae));
Bm = Be;
Gm = 0;
Qm = C_eps.*'Q*C_eps; %#ok<MINV>
Sm = C_eps.*'Q*D_eps; %#ok<MINV>
Rm = R_bar;

% Reachability optimal control
...
% Observability optimal control
...

[Xm,Km,Lm] = icare(Am,Bm,Qm,Rm,Sm,Em,Gm);
K_bar = -Km;
Ks = K_bar(:,1:length(A));
Ki = K_bar(:,length(A)+1:end);

```

In Fig. 2.11 is proposed an architecture which embeds the state observer that is in charge of estimating the state of the plant basing on the available data of input and output. It's not hard to get that a precise estimation promotes the proper functioning of the optimal controller with the subsequent benefit of the performance achieved. In order to design the best \mathbf{K}_O , it's possible to take advantage of the same design criterion of Robust Stationary Optimal Control, but applied to a modified plant and exploiting the duality with the optimal control problem. Let:

$$\begin{aligned}\dot{x} &= \mathbf{Ax} + \mathbf{Bu} & x(t_0) &\equiv x_0 \\ y &= \mathbf{Cx} + \mathbf{Du}\end{aligned}\tag{2.55}$$

Be an LTI system with $x \in \mathbb{R}^n, u \in \mathbb{R}^p$, then the dual system associated to the primary system 2.55 is defined as:

$$\begin{aligned}\dot{\chi} &= \mathbf{A}^T \chi + \mathbf{C}^T \nu, & \chi(t_f) &= \chi_f \\ \mu &= \mathbf{B}^T \chi + \mathbf{D}^T \nu\end{aligned}\tag{2.56}$$

with $\chi \in \mathbb{R}^n, \nu \in \mathbb{R}^q$ and $\mu \in \mathbb{R}^p$.

The primary and the dual systems are two equivalent representation of the same mathematical model, thus any property of one plant belongs to its dual:

- (\mathbf{A}, \mathbf{B}) fully reachable $\iff (\mathbf{A}^T, \mathbf{B}^T)$ fully observable
 $\mathbf{R}_{primary} = [\mathbf{BAB} \dots \mathbf{A}^{n-1}\mathbf{B}]$
 $\mathbf{O}_{dual} = [\mathbf{B}^T \mathbf{B}^T \mathbf{A}^T \dots \mathbf{B}^T [\mathbf{A}^T]^{n-a}]^T$
 $\mathbf{R}_p = \mathbf{O}_d^T \implies$ observability and reachability are the same thing;
- (\mathbf{A}, \mathbf{C}) fully observable $\iff (\mathbf{A}^T, \mathbf{C}^T)$ fully reachable;
- $\text{eig}(\mathbf{A}) = \text{eig}(\mathbf{A}^T)$, \mathbf{A} is Hurwitz $\iff \mathbf{A}^T$ is Hurwitz \implies the solution in closed loop for the primary space is solution even for the dual space.

They are called '*duality properties*'.

Let the observer of the primary plant being:

$$\begin{cases} \dot{\hat{x}} = \mathbf{Ax} + \mathbf{Bu} + \mathbf{K}_o(y - \hat{y}) \\ \hat{y} = \mathbf{Cx} + \mathbf{Du} \end{cases}\tag{2.57}$$

and the error defined as $e_x = \hat{x} - x$, then its dynamics can be described as:

$$\dot{e}_x = (\mathbf{A} - \mathbf{K}_o \mathbf{C}) e_x\tag{2.58}$$

The analogue for the dual plant is:

$$\dot{\chi} = (\mathbf{A}^T + \mathbf{C}^T \mathbf{K}_{sd}) \chi \quad \text{where } \nu = \mathbf{K}_{sd} \chi\tag{2.59}$$

This means that the optimal control solution of the dual plant is the solution for the optimal observer of the primary plant:

$$\mathbf{K}_{op} = -\mathbf{K}_{sd}^T\tag{2.60}$$

The cost function is defined as:

$$\mathbf{J}_d = \int_0^\infty \mu \mathbf{Q}_d + \nu^T \mathbf{R}_d \nu dt\tag{2.61}$$

Where:

- $\mathbf{Q}_d \geq 0$. It's associated to the uncertainty on the predictor model. If the state is perfectly defined, we're sure that the copied plant is perfect and $\mathbf{Q}_d = 0$. The solution of such case would be the identity observer (even called Luenberger observer). This would be possible if and only if we knew the exogenous w that it's unlikely and at which we associate an uncertainty. \mathbf{Q}_d is usually designed by trial and error;

- $\mathbf{R}_d > 0$ It's associated to the uncertainty given by the sensors. The uncertainty is strongly related to the standard deviation provided in datasheets by the OEM of the sensor. Because of this, it's usually designed as a covariance matrix. If $\mathbf{R}_d = 0$, it would mean that the measurement provided by the sensors is perfect, so they're ideal and we can fully trust them whereas the uncertainty on the plant would be infinitely larger. This is obviously not a real condition. The higher \mathbf{R}_d , the higher the uncertainty associated to the sensors, the lower we trust them. The uncertainty is linked to the sensor noise: if we adopted low quality sensors, the controller will be less prone to feed back their signals due to the high presence of noise.

The assumptions on the other matrices are in analogy with the optimal control solution for the primary plant. The Matlab code implemented to obtain the solution for the optimal observer is listed hereafter.

```

Ad = A.';
Bd = C.';
Cd = [B2, zeros(length(B1), 6)].';
Dd = [D2 D3 zeros(length(D1), 2)].';

mu = zeros(size(Cd,1),1);
mu(1) = 0.01;
mu(2) = 0.01;
mu(3) = 0.0004905;
mu(4) = 0.0003702;
mu(5) = 0.000013484;
mu(6) = 0.000013484;
mu(7) = 0.0001;
mu(8) = 0.0001;

Qd = inv(diag(mu.^2));

std = ones(size(Dd,2),1);
std(1) = 0.0001*g;
std(2) = 0.00047787;
std(3) = 0.00001;
std(4) = 0.00001;

Rd = inv(diag(std.^2));
Rd_bar = Rd+Dd.*Qd*Dd;

alphad = 7;
Adm = Ad+alphad*eye(length(Ad));
Edm = eye(length(Ad));
Bdm = Bd;
Gdm = 0;
Qdm = Cd.*Qd*Cd;
Sdm = Cd.*Qd*Dd;
Rdm = Rd_bar;

[Xd, Kd, Ld] = icare(Adm, Bdm, Qdm, Rdm, Sdm, Edm, Gdm);
Ko = Kd.';

Ao = A-Ko*C;
Bo = B1-Ko*D1;

```

Chapter 3

Application

3.1 Simulator description

The next step of the project is based on Simulink. It was chosen to design and perform simulations on the system analysed up to now. The simulator description is provided in Section 3.1.1 in order to make the logic of its functioning more clear. The analysis of all the simulations performed in order to study the system and validate our hypothesis is presented in Section 3.2.

3.1.1 Non-linear plant, Closed Loop

Figure 3.1 represents the non-linear plant in closed loop implemented in the Simulink environment through a Matlab function - called *Plant* - where the state vector x , the input u and the exogenous w are introduced. The latter is handled in its singular three components: disturbance, noise and reference. Noise can be activated via a switch to be null or real in order to evaluate the performance of the system after the signal corruption.

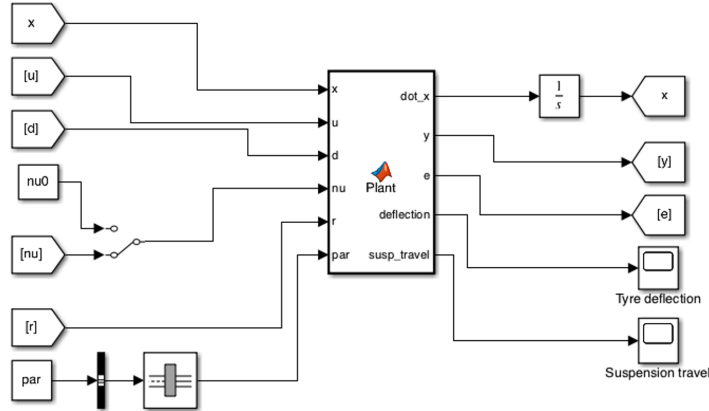


Figure 3.1: Non-linear plant, closed loop

A bus block is employed in order to drive a Matlab structure - which contains all the vehicle parameters listed in Table 2.1 - inside the function.

The simulated Plant gives as outputs:

- state dynamics \dot{x} which is integrated in order to obtain x and feed the model for the next time step;
- the updated output from the sensors y ;
- the error e among the reference and the current actual position of the motorcycle.

The last two functions "Tyre deflection" and "Suspension travel" are useful to evaluate a possible detachment of the tyre that would cause an unstable condition for the control system.

3.1.2 Non-linear plant, Open loop

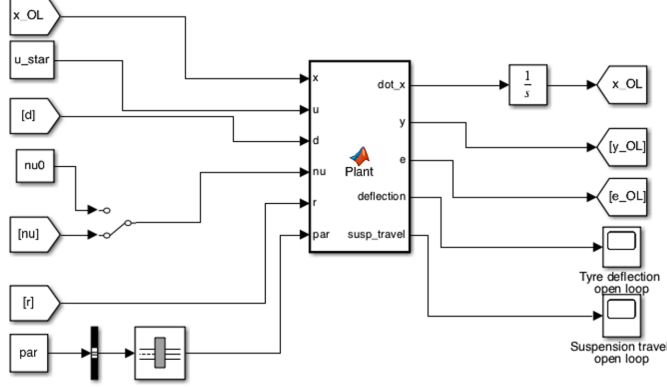


Figure 3.2: Non-linear plant, Open loop

The non-linear plant in open loop configuration works in the same way of the system described in the previous subsection 3.1.1. The only exception is the control which is equal to its equilibrium (i.e. $u(t) \equiv u^* \forall t$). Conceptually the function u^* only mimic the correct stiffness for the suspension of a motorcycle as the one under investigation.

3.1.3 Linear Plant

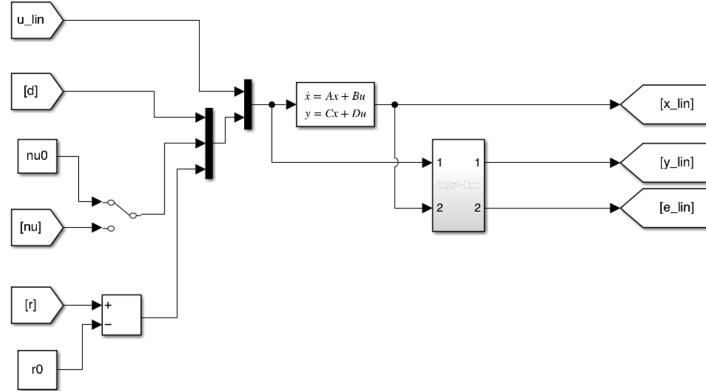


Figure 3.3: Linear plant

The implementation of the linear plant is shown in Figure 3.3. It takes advantage of the Simulink block "State space". By definition, all the input coordinates are linearised. The block needs to receive all the coordinates in input and it output the sensors signal. The input is considered to be a columnar vector of both the control and the exogenous. The output was preferred to be the state space vector x by properly setting the matrices then obtain the real one y by performing the matrix product in the external subsystem in figure.

To better understand how the state space block works, it is useful to mention the system of equation employed for describing the Plant:

$$\begin{aligned} \dot{\tilde{x}} &= \mathbf{A}\tilde{x} + \mathbf{B}\tilde{u} & \tilde{x}(t_0) &= \tilde{x}_0 \\ \tilde{y} &= \mathbf{C}\tilde{x} + \mathbf{D}\tilde{u} \end{aligned} \quad (3.1)$$

The matrices are defined according to the block definition and their dimensions refer to Eq. 2.3:

- $\mathbf{A} \in \mathbb{R}^{n \times n}$, which coincides with the one mentioned up to now;
- \mathbf{B} , built as unification of the \mathbf{B}_1 and \mathbf{B}_2 matrices. It turns to be $\mathbf{B} \in \mathbb{R}^{n \times (m+r)}$;

- \mathbf{C} matrix is an identity matrix with the same dimensions of \mathbf{A} ;
- \mathbf{D} matrix is a null matrix with the same dimension of \mathbf{B} ;
- $\tilde{x}_0 \in \mathbb{R}^{n \times 1}$ defines the initial conditions.

By setting \mathbf{C} and \mathbf{D} in this way, the output vector is actually the state vector x . The generalised dimensions of the matrices to be respected are depicted in Fig. 3.4.

	n	m
n	\mathbf{A}	\mathbf{B}
r	\mathbf{C}	\mathbf{D}

Figure 3.4: State space matrices dimensions

Superscripts must not be confused with the one defined above: they're both generic letters.

3.1.4 Coordinates linearisation

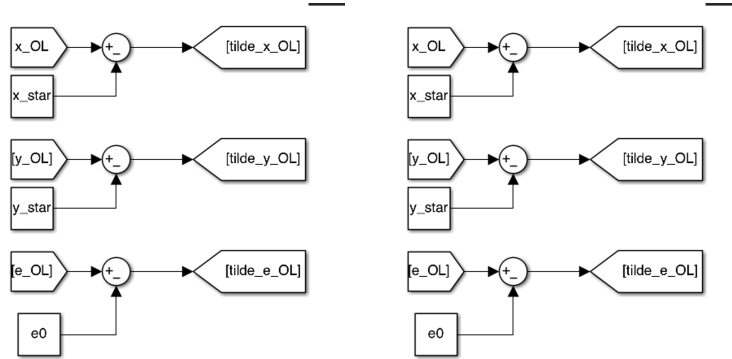


Figure 3.5: Open and closed loop linearisation block

The open and closed loop coordinates linearisation blocks subtract the ‘star’ coordinates from the real ones, thus creating the linearised coordinates ‘tilda’. This operation is performed on the state coordinates, sensors output, error and control in order to use that coordinates to drive the linear system. The same operation is repeated for the open loop coordinates with the only difference that the linearised control \tilde{u}_{OL} is not calculated because null.

3.1.5 Noise generator

The noise generator works with a *band-limited white noise* block with an associated power that is equal to the PSD of the noise relative sensor. Hereafter are listed the calculation performed to obtain the needed value of the height of the PSD inserted in the block.

$$\begin{aligned}
 PSD_{noise} &= \frac{RMS_{noise}^2}{Bandwidth} \left[\frac{\text{unit}^2}{\text{Hz}} \right] \\
 PSD_{noise_{acc}} &= \frac{(4.905 \cdot 10^{-4})^2}{50} = 4.811805 \cdot 10^{-9} \left[\frac{\text{m}^2}{\text{s}^4 \text{Hz}} \right] \\
 PSD_{noise_{gyro}} &= \frac{(3.702 \cdot 10^{-4})^2}{50} = 2.740960 \cdot 10^{-9} \left[\frac{\text{rad}^2}{\text{s}^2 \text{Hz}} \right] \\
 PSD_{noise_{pot}} &= \frac{(1 \cdot 10^{-5})^2}{50} = 2 \cdot 10^{-12} \left[\frac{\text{m}^2}{\text{Hz}} \right]
 \end{aligned} \tag{3.2}$$

Fig. 3.1.5 shows the superposed signals which corrupts the output from the sensors.

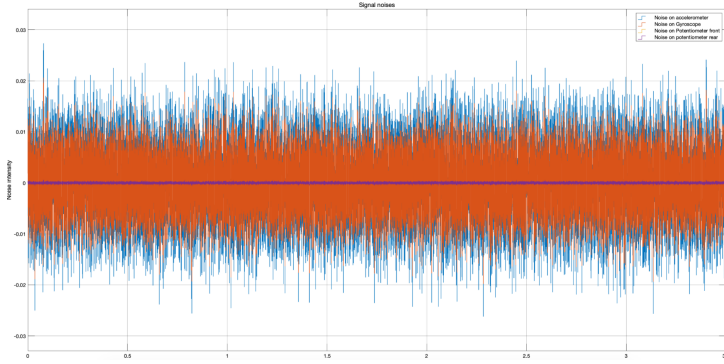


Figure 3.6: Noise signal

3.1.6 Disturbance generator

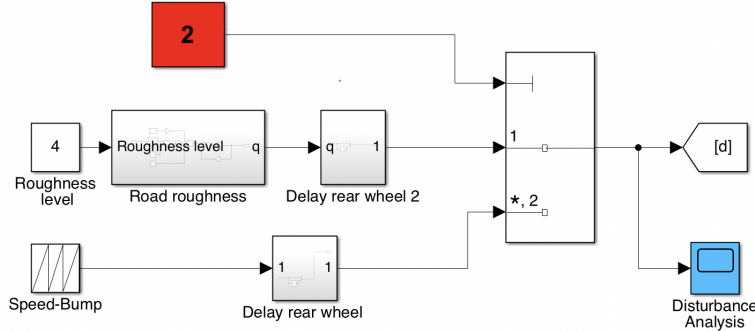


Figure 3.7: Disturbance generator

The disturbance generator simulates two different types of ground floors. An ISO (International Standards Organization) road roughness simulator, based on the ISO 8608 standards, simulates the behaviour of a road depending on its condition. The classification identifies eight road roughness level ranging from class A to H in increasing roughness order, where the first five classes (A, ..., E) are the most usual in a real life application. In the ISO classification, the statistical characteristics of the road can be described by PSD. Level A corresponds to an almost perfectly smooth road and H represents a very rough road. [9]

In order to implement the road roughness in the Simulink project, the below equation has been used:

$$\dot{q}(t) = 2\pi n_0 \sqrt{Gq(n_0)v} \cdot w(t) - \omega_0 q(t) \quad (3.3)$$

where:

- $q(t)$ is the time domain signal of $Gq(\omega)$;
- $Gq(n_0)$ is the road roughness coefficient in m^3 ;
- $w(t)$ is time domain signal of white noise;
- n_0 is spatial reference frequency and it's usually equal to $0.1m^{-1}$;
- v is the vehicle speed in m/s ;
- ω_0 is a cut-off frequency and it's usually equal to $1 rad/s$.

In Fig. 3.8 is shown the block system which simulates Eq. 3.3.

Note that the values of the road roughness coefficient are stored in a look-up table which takes as input the desired level from 1 to 8, corresponding to the levels from A to H. Table 3.1 shows the coefficient values used in the simulation.

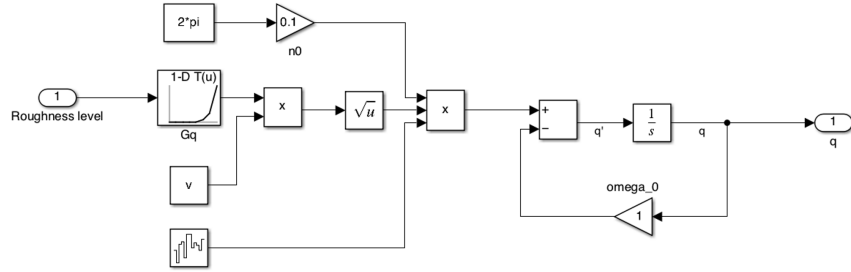


Figure 3.8: Block scheme of the road roughness equation

Road roughness level comparison $G_q(n_0)$ value (m^3), geometric average	
A	16×10^{-6}
B	64×10^{-6}
C	256×10^{-6}
D	1024×10^{-6}
E	4096×10^{-6}
F	16384×10^{-6}
G	65536×10^{-6}
H	262144×10^{-6}

Table 3.1: Road roughness in compact form

Figure 3.9 shows different levels of road roughness, in particular the most usual ones on a daily usage of the motorcycle and so the ones used to evaluate the system's response. The frequency of the asperities is the same for all the roads roughness: what changes is the amplitude only.

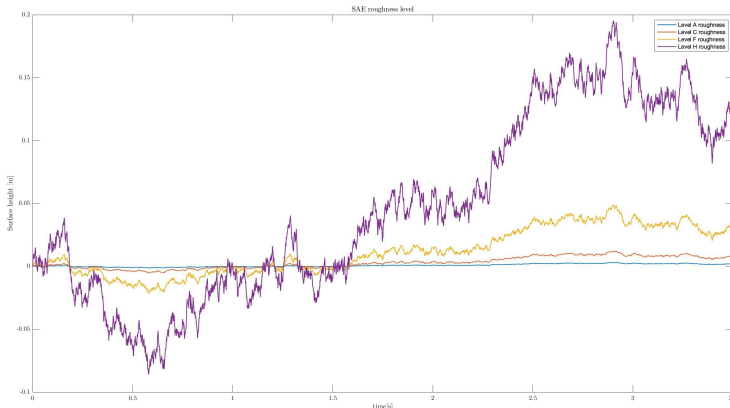


Figure 3.9: Road roughness profiles

The last road disturbance is a speed bump defined through a sinusoidal equation without any discontinuities and which can be parameterised. It's modelled through the following equation:

$$\left(\frac{L^2}{4} + H^2 \right) \cdot x^2 - \frac{L^2}{2} \cdot x + \left(\frac{L^2}{4} - H^2 \right) = 0 \quad (3.4)$$

where:

- H is the bump height;
- L is the bump length;
- $x = \cos\alpha$ where α is the arc length of the bump.

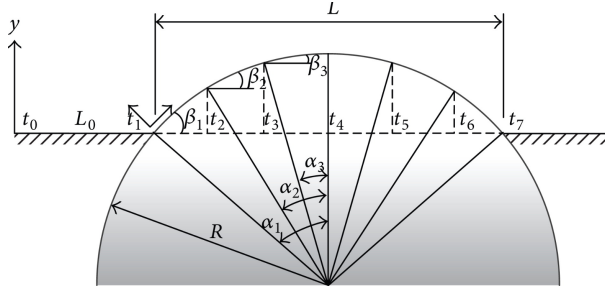


Figure 3.10: Geometry of the bump

The parameters completely defines the bump geometry, as shown in Figure 3.10.

The bump generator function allows to set the time where the bump is met by the front wheel as well. In this regard, it worth noting that, for both disturbances, a delay block is necessary to introduce a delay between the front and the rear wheel, it is defined as the wheelbase divided by the velocity.

3.1.7 Non-linear control implementation

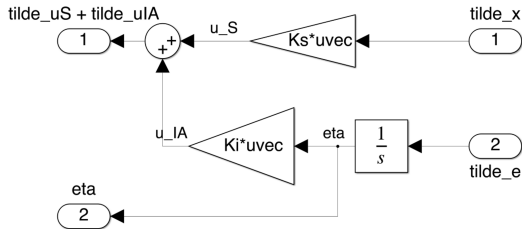


Figure 3.11: Non linear control implementation

In order to obtain the integral action control it is necessary to input to the system the linearised coordinates coming from the non-linear plant. The \tilde{x} variables are multiplied by the \mathbf{K}_s matrix (obtained through the solution of the Riccati equation) and the η variables by the \mathbf{K}_I matrix. In such way it is possible to obtain both the state feedback and the integral action control since the calculation is performed in the extended state. Afterward the contribution are added up to find the linear control \tilde{u} . The latter is summed up with u^* in order to obtain the actual control vector u .

Subsequently, the real control intervenes, which takes as input the ideal control action and outputs a control signal that is based on the condition of the motorcycle. Indeed, the capabilities of the air spring are highly influenced by the available volume inside the suspension (which depends on the suspension stroke) and the maximum pressure allowed by the compressor. The overall stiffness achievable by the system is a function of the suspension stroke. A range of allowed relative pressure is set ($[p_{min}, p_{max}] \in [0, 7.7] \text{ bar}$), a chamber volume for each spring is defined ($V_{cv0} = 0.1 \text{ lt}$). The gas thermodynamic is neglected. What is shown in Figure 3.12 is a subsystem able to limit the controller capabilities.

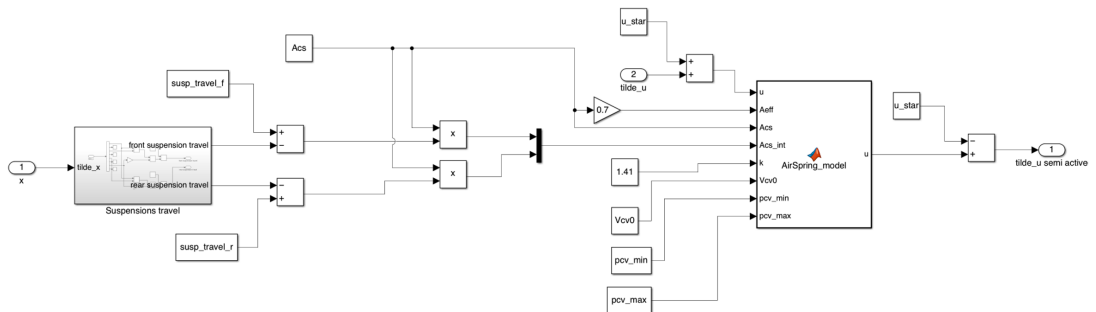


Figure 3.12: Simulator of the air spring stiffness function of pressure and stroke

In order to calculate the available suspension stroke, the actual compression is subtracted by the full travel. Then, by multiplying it with the cross section area of the air spring, the inside volume is obtained. The suspensions diameters are 60 mm for the front one and 70 mm for the shock absorber. Unfortunately, this is just a theoretical volume not fully available to be inflated with air to create sustain to the motorbike, indeed almost 30% of the cross section area needs to be cut off from the equation because of the deflection transient. Indeed, air takes time in order to fill the volume: this ‘virtual reduction’ takes into account the inflation transient. The equation inside the Matlab function block is the following one:

$$k_{eq} = A_{eff} \frac{dp_{cv}}{dz} + (p_{cv} - p_{atm}) \frac{dA_{eff}}{dz} \quad (3.5)$$

where $\frac{dA_{eff}}{dz} = 0$ because the effective area is considered constant during the simulation and:

$$\frac{dp_{cv}}{dz} = -kP_{cv} \frac{A_{cs}}{V_{cv0} + \int_{curr}^{max} A_{cs} dz} \quad (3.6)$$

where p_{cv} is the current pressure level, A_{cs} is the cross sectional area of the air spring, A_{eff} is the effective area, $k = \frac{c_p}{c_v}$ and dz is the suspension stroke travelled in the time step, positive if the volume increases, negative on the contrary.

The logic of the subsystem in Fig. 3.12 is to revert the formula of Eq. 3.5 in order to obtain the pressure that would be needed inside the volume, then compare it with the available pressure range. If the pressure is higher than the maximum one, it’s set to 7.7 bar and then the stiffness is directly calculated through Eq. 3.5. Finally, the realistic control is outputted and it is ready to be sent to the non-linear plant, as shown in Figure 3.13.

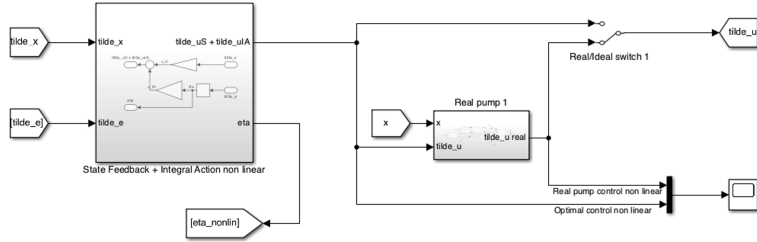


Figure 3.13: Semi-active control block scheme

3.1.8 Linear Control implementation

The linear control implementation is depicted in figure 3.14, which is analogue to the non-linear one, but it outputs the linearised control that is sent to the linear plant.

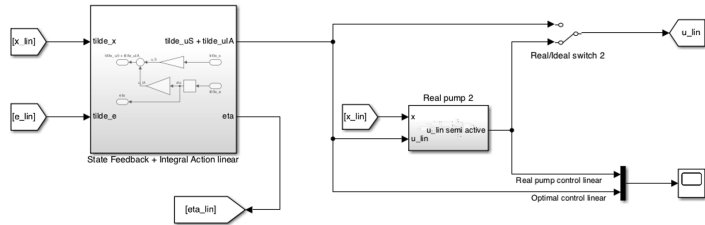


Figure 3.14: Linear Semi-active control block scheme

3.1.9 Observer

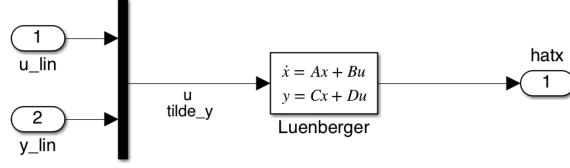


Figure 3.15: Observer

The observer block requires as input the linearised control and the linearised output sensor in order to build the estimated values \hat{x} . It works with a state space block in which:

- $\mathbf{A} \equiv \mathbf{A}_o$;
- $\mathbf{B} \equiv [\mathbf{B}_o \mathbf{K}_o]$ matrix. Both of them has been calculated by previously solving the Riccati equation regarding the dual plant, which gives us the \mathbf{K}_o matrix;
- \mathbf{C} is the identity matrix with the same dimensions as \mathbf{A} ;
- $\mathbf{D} \in \mathbb{R}^{n \times (m+p)}$ is a zero matrix.

\mathbf{C} and \mathbf{D} are set in this way in order to obtain the estimated state as output.

3.1.10 Cost function block

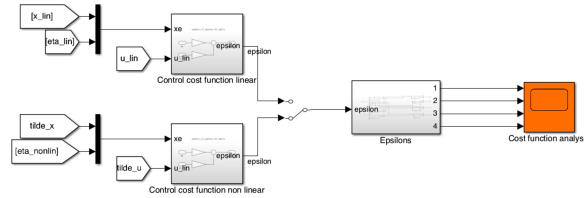


Figure 3.16: ε tracking block

The cost function block is represented in Figure 3.16. It's subdivided in two main subsystems: the upper one is meant to calculate the control cost function error for the linear plant, the bottom one is meant to calculate the cost function for the non-linear plant. This block works by inputting the linearised extended state x_e and control \tilde{u} . The vector ε is obtained by its definition:

$$\varepsilon = \mathbf{C}_\varepsilon x_e + \mathbf{D}_\varepsilon u \quad (3.7)$$

Block scheme in Figure 3.17 tracks ε step by step exploiting Eq. 3.7. It's applied to the coordinates of both linear an non-linear plants.

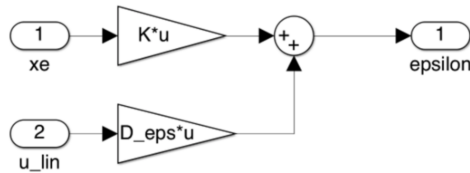


Figure 3.17: ε tracking function

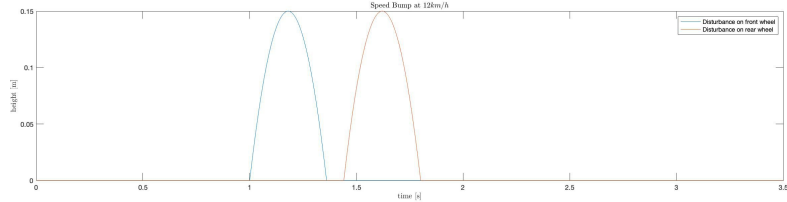
3.2 Simulation results

3.2.1 System investigation

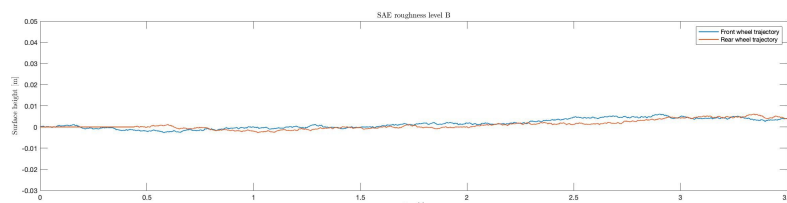
In this section it will be analysed how the system behaves on different conditions. The aim is to quantitatively evaluate the performances of the control system compared to the open loop one. The testing conditions will be equal to the ones described in Section 3.1 and the effect of each disturbance on the system will be analysed separately.

In particular:

- a road roughness level D is chosen, corresponding to a rough peripheral road asphalt. The reason lies in the need to not overcome ground contact and suspension travel conditions boundaries, due to a too aggressive road roughness and to simulate a more probable scenario for this type of motorcycle;
- a sinusoidal speed bump is characterised by a height of 0.15m and a length of 1.2m which corresponds to a quite aggressive speed bump of the type installed in the city centre.



(a) Speed bump



(b) Road roughness level B and H

Figure 3.18: SAE Road model

It is to note that the front and rear wheels are affected by the disturbance in different times. As previously mentioned, the time delay depends on both the motorcycle wheelbase and its forward velocity. Figure 3.18a is a clear example of the effect of the vehicle speed on how the disturbance is perceived.

It is necessary to check that the tyre does not detach from the ground or the suspension does not reach the stop-bump (fully compressed). Those two conditions would be critical for the system, both in terms of mechanical damages, like in the case of suspension, and for the control purpose. For instance, the control wouldn't be able to drive the system to stability if the tyres are not connected to the ground.

The analysis has been carried out by defining a function that instantaneously calculates the tyre deflection by taking advantage of the state space coordinates. Fig. 3.19 shows the front tyre deflection. If this value goes below $0m$, it means that the tyre is detached from the ground, whereas the upper boundary of the tyre compression is set to be $> 0.05m$ for safety reasons. These values are true for the rear tyre as well.

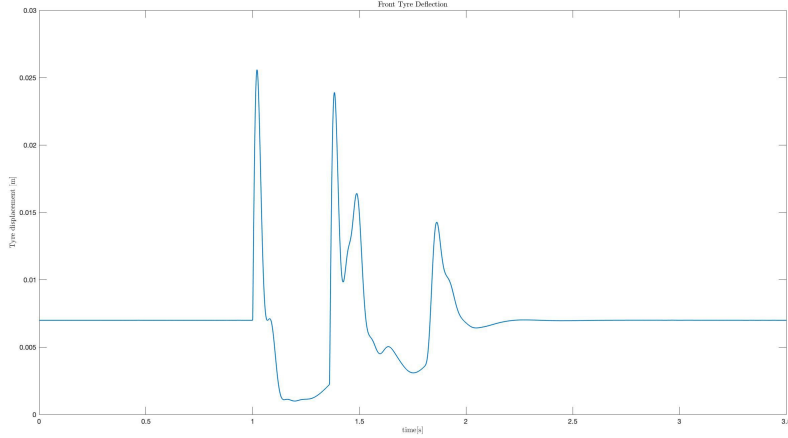


Figure 3.19: Front tyre deflection over a sinusoidal speed-bump at $v = 12\text{km}/\text{h}$

The same analysis has been performed on the suspensions as shown in Figure 3.20. If it reaches values $< 0m$, it means that it's more elongated than the maximum allowed measure; if it reaches values $> 0.13m$ it would mean that the suspension is over its fully compressed capability. They're both unrealistic conditions.

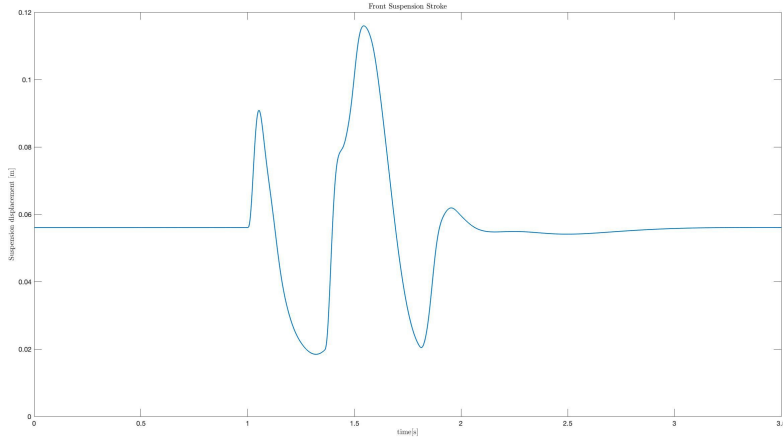


Figure 3.20: Suspension stroke over a sinusoidal speed-bump at $v = 12\text{km}/\text{h}$

Forcing the controller to enforce artificial values due to these four limit conditions has been performed unsuccessfully. The issue relies on the opposite simultaneous needs. If the suspension is close to go beyond its maximum elongation, a support function would increase the suspension stiffness stopping the travel. At the same time, it's likely that the tyre is not in a highly compressed state and a further stiffening of the spring would surely increase the chance to detach it from the ground. After several tests and tuning of the values in order to reach the best compromise, the decision was to take the tyre deflection and the suspension travel under control by not employing too aggressive disturbances.

After having analysed the disturbances, it is possible to proceed checking how the system behaves while crossing the speed bump of Figure 3.18a.

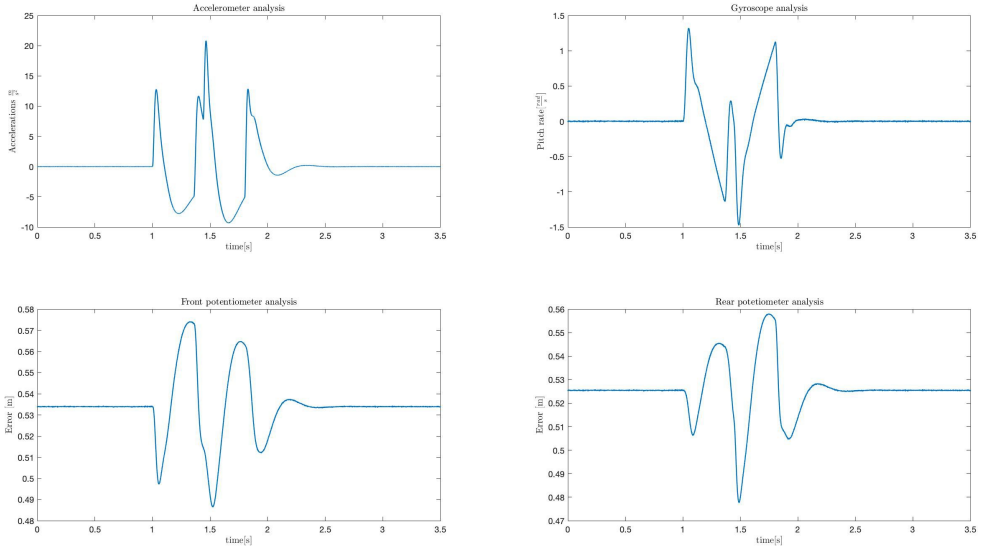


Figure 3.21: Open-Loop speed bump response

Recalling the four sensors with which the motorcycle is equipped, 1 accelerometer, 1 gyroscope and 2 potentiometers - one in the front and one in the rear wheel -, their outputs are shown in Figure 3.21. The test has been registered by using the open loop system, in which the control does not intervene, and starting from initial conditions equal to the equilibrium ones. As shown in section 2.1, the signal coming from the sensors is very smooth due to the high quality of the product installed on the motorbike, which implies very low noise corruption and much more efficient action of the control.

Reminding that the system proposed in this document takes advantage of a compressor that pressurise the air and sends it in the air spring chamber, the performances of the control strongly depend on the specifications of the pump.

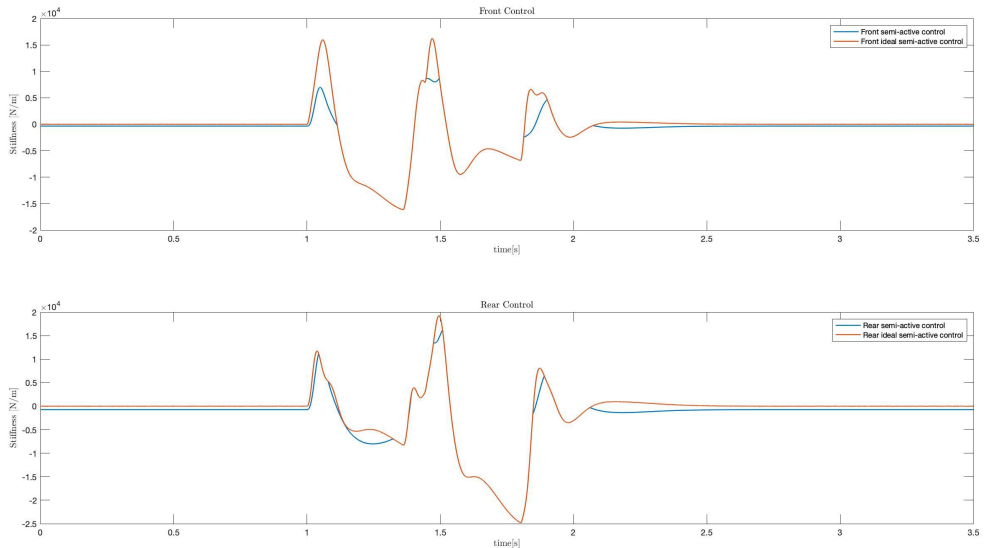


Figure 3.22: Representation of the system control on standard testing condition over a speed-bump

Figure 3.22 clarifies which is the stiffness request from the control system and the one that the real system is able to produce. From this, it is possible to analyse how the ideal and real pump works on keeping the system stable. The request of the control system strongly depends on the kind of disturbance at which the system is subjected to, so Figure 3.23 is proposed in order to have a more complete view of the control system request and response.

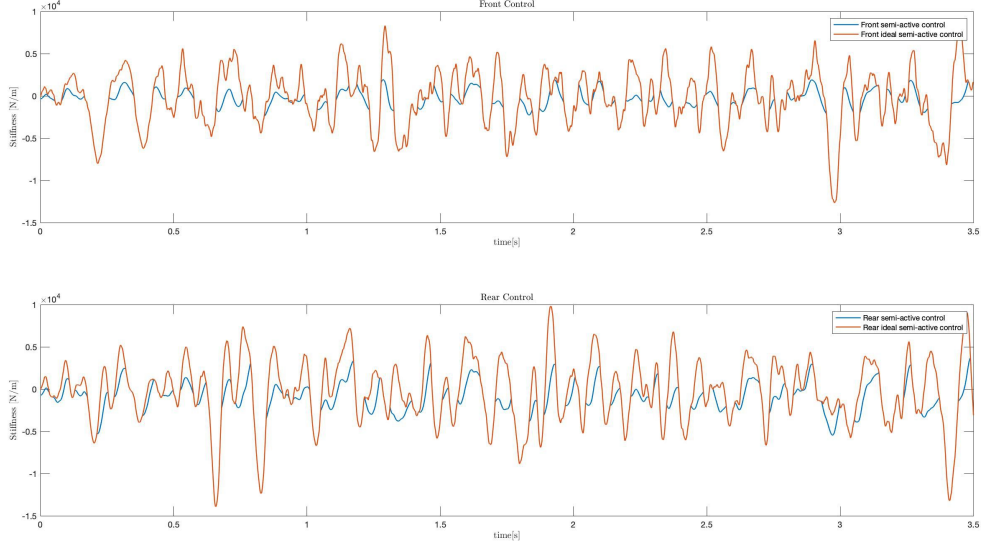


Figure 3.23: Representation of the system control on standard testing condition on level H SAE roughness, speed $v = 12 \text{ km/h}$

Now that the system has been fully defined it is possible to proceed with the tuning.

So far the starting point of the analysis has been defined; the focus will move to the components that will be subjected to tuning. Indeed, in the next section, the reader can find a description of the approach on the optimisation of system's performances. The first step is the analysis of all the parameters that influence the system response in closed loop conditions.

- ε is a vector in which the parameters are meant to apply some ‘virtual’ constraint on the extended system which comprehends x and η . In this application six ε ’s are necessary, two concerning the extended state integrated error and four related to the sensors. In particular has been considered one that limits the theoretical maximum allowed acceleration along vertical axis, one that limits the pitch velocity, and two that limits the suspensions stroke. Those values can be restricted in order to apply a more intense constraint on the system, putting more control effort on them. Furthermore, this values are the components of a very important matrix, \mathbf{Q} , that then gets fed inside the `icare` function to solve the Riccati equation. This is done to obtain as result the \mathbf{K}_{bar} matrix, for state feedback and integral action. The mentioned matrix \mathbf{Q} , composed as a diagonal matrix in which the i -th diagonal term is the inverse of the squared value of the i -th ε . It is immediate to understand that every modification on the ε values directly influences the solution of the Riccati equation. From the ε definition it’s possible to distinct more scenarios, for example, deciding different combination of ε , choosing which should be penalised more. Doing such distinction, it would be possible to create more scenarios. Two are defined: *Race* and *Comfort*. The first one has more restrictive ε on the integrated error and pitch rate, letting the maximum acceleration being higher. The second one has a strong ε penalization on vertical acceleration and a soft penalisation on pitch rate as well as on the error. As already seen, choosing one against the other will generate a different \mathbf{Q} matrix, generating a different control action on the system;
- u_{\max} is the vector that penalise the control and, in a certain extent, limits the values it can assume. It has two components due to the fact that it’s divided between front and rear control, they are indeed separated and can assume two different values based on the geometry of the suspension system and the available volumes of the air suspension chamber, which translates in two different equivalent stiffness values. As for the ε parameter, U_{\max} vector influences one of the most important

matrices of the system, \mathbf{R} , which is the diagonal matrix in which the components are the inverse of the squared values of the control vector. As for \mathbf{Q} it gets fed inside the `icare` function to obtain the \mathbf{K}_{bar} matrix;

- α this is a very important tuning parameter that allows to directly influence the eigenvalues of the \mathbf{A} matrix. It forces the system to apply a stronger control by ‘fooling’ it on believing that the system is actually less stable. As a tuning parameter, it would be subjected to an optimization based on objective data that will be introduced later. Right now it is a sensible parameter, because too high α values will make the system react exaggeratedly to a simple disturbance, making even the noise effect stronger on the signals. Contrarily a too low α value could make the control system ineffective, but this will be deeply analysed later;
- \mathbf{C}_ε and \mathbf{D}_ε are two matrices that derives from the choice of ε parameters, indeed they are obtained as the partial derivatives of the ε equations with respect to extended state and control vector respectively. This means that if the equations have control subjected parameters inside, the matrix won’t be null. In case of null matrix, \mathbf{R}_{bar} matrix (element of the `icare` function) will only depend on \mathbf{R} and not both \mathbf{R} and \mathbf{Q} ;
- μ is a vector composed by all the measurement uncertainties intrinsic of each sensor. It is immediate to understand the importance of the sensor’s set selection for the plant analysis. Sensor’s μ value can be found in the data-sheet of each sensor. Bigger μ values means bigger uncertainties, and as for the ε vector for the extended state, which influences \mathbf{Q} , μ values influences directly the \mathbf{Q}_d matrix of the dual plant, which is the plant necessary to build the observer. Indeed \mathbf{Q}_d matrix is composed as the inverse diagonal matrix whose components are the squared values of the μ vector. The vector is composed of 8 elements, the uncertainties on the 2 disturbances, the ones on the 4 sensors and the ones on the reference value. The effect of μ values on the control will be analysed later;
- ν , similarly to μ vector, represents a physical value, which corresponds to the standard deviation of the sensor’s measurement. It can be found on data-sheet too and as for the U_{\max} vector which influences the \mathbf{R} matrix, ν vector influences the \mathbf{R}_d matrix, component of the `icare` function. \mathbf{R}_d matrix is made as the inverse diagonal matrix of the squared standard deviation values of each sensor. From this definition it is easy to understand that it has 4 components related to accelerometer, gyroscope, front potentiometer and rear potentiometer;
- \mathbf{C}_d and \mathbf{D}_d are two matrices are equivalent to \mathbf{C}_{eps} and \mathbf{D}_{eps} matrix on their usage. Indeed they are summed or multiplied to \mathbf{Q}_d and \mathbf{R}_d matrices to create different matrices that then gets fed inside the `icare` function to solve the Riccati equation for the dual plant, which returns the \mathbf{K}_{o} matrix used to build the Observer;
- α_d is the last parameter that will be subjected to tuning. It is equivalent to α , even though it assumes a different physical meaning for the dual plant. The effect on the system is to modify the eigenvalues of the \mathbf{A}_d matrix generating a ‘virtually’ more stable/unstable observed system based on the value it assumes leading to a different tracking behaviour.

\mathbf{Q} , \mathbf{R} , \mathbf{Q}_d , \mathbf{R}_d matrices are part of the tuning, but being directly influenced by other parameters, it is more efficient to directly tune the values from which those matrices comes from than the matrices itself.

After having defined all the parameters that will be subjected to tuning it is important to understand how their values influences the system response. To do so, tests has been carried on, using the standard speed-bump and the road roughness as disturbances. Testing conditions has already been defined ($v = 12 \text{ km/h}$, speed-bump with 0.15m height and 1.2m length with sinusoidal shape or SAE road roughness) and some effects has already been anticipated in the tuned parameters description. Starting from the parameter α , as already said, it modifies the eigenvalues of the \mathbf{A}_m matrix by tricking the control and making it act in a different way.

Considerations based on the norm of $\bar{\mathbf{K}}$ would be useless because the effect of α on the norm is lost due to the different sign that all the components of the matrices can assume, making the norm analysis almost always ineffective. Then the analysis is carried out on all the components of the matrix. From Fig. 3.24, it’s possible to appreciate how the norm of the matrix \mathbf{K}_s associated to the state feedback tends to increase in magnitude by increasing α . This is coherent with the definition of α that makes the system seems less stable than what it really is. It worth note that the sign of \mathbf{K}_s is opposite for the

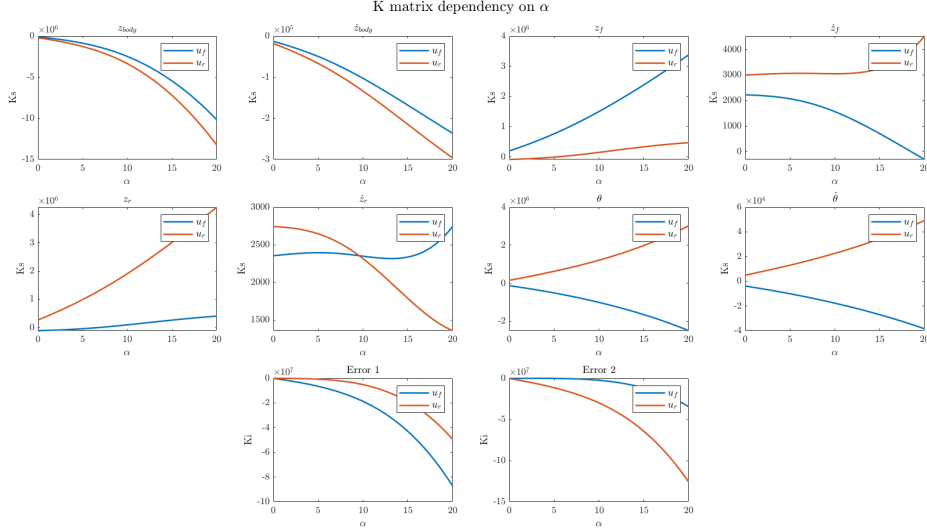


Figure 3.24: Dependency of $\bar{\mathbf{K}}$ on α

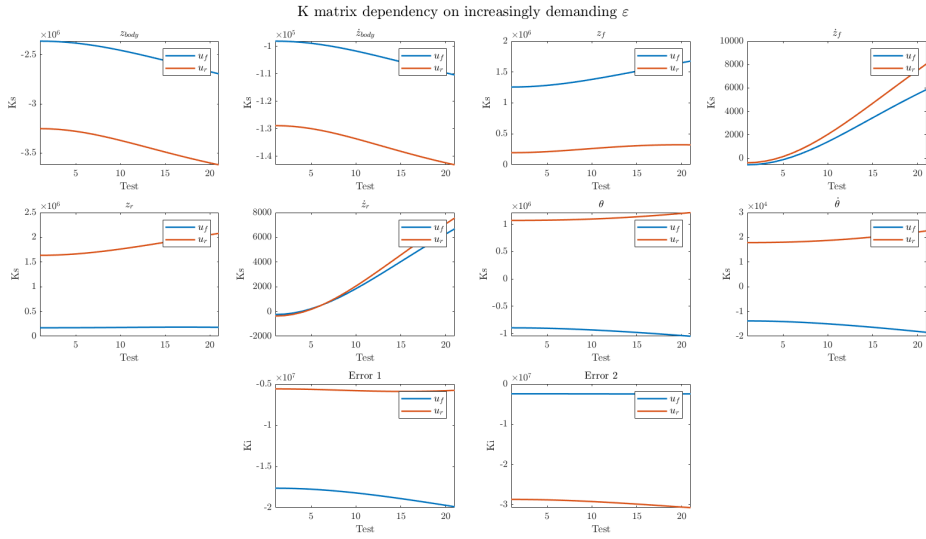


Figure 3.25: Dependency of $\bar{\mathbf{K}}$ on ε

front and rear control associated to some state space coordinates. This makes sense because their action could be opposite on the bike set up, for example on the pitch angle.

Results of an analogue analysis by changing ε is represented in Fig. 3.25.

The effect of continuously more demanding ε is less straightforward than the previous case. The effect of more stringent boundaries on the position of the suspensions that must be as close as possible to the equilibrium - given by a smaller and smaller η - is in opposition to the limitation on the maximum acceleration. Moreover, η is never really demanding, hence the values associated to \mathbf{K}_I don't change a lot.

It makes sense to introduce the effect of μ and ν_d on the system's response. In the case under investigation the sensors are the best ones for automotive application and the values that it is possible to find on the data-sheets are very good.

A further optimization would not be necessary, but it would be useful to analyse how the norm of matrices \mathbf{K}_o , \mathbf{R}_d and \mathbf{Q}_d varies if the sensors' output characteristics changes. Three different tests have been performed to check the plant behavior:

Test 1 Maintain μ constant and let ν_d increases to worsen the standard deviation of the sensors. This test has been performed with the aid of a `for` cycle that continuously increases the standard deviation of the sensors, in particular by adding at each cycle the same starting value of each sensors, bringing at the end of the 100 cycles to a condition in which the ‘final’ sensors have a 100 times higher standard deviation than the one with the initial test. The results are shown in figure 3.26a.

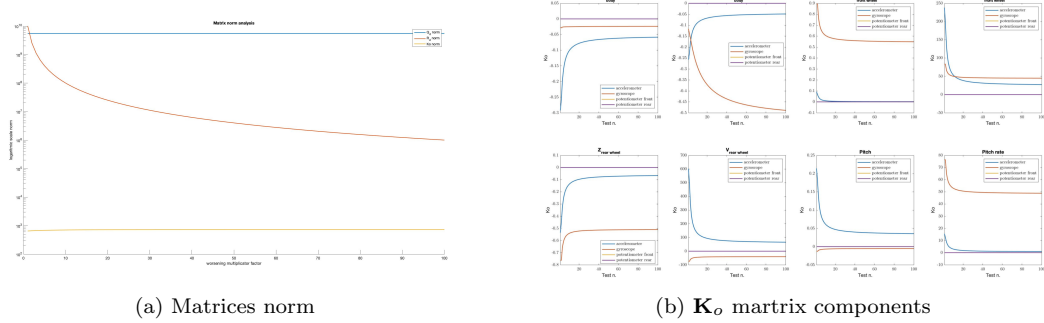


Figure 3.26

It is possible to appreciate that the norm of the \mathbf{Q}_d matrix is remaining constant, and, as the sensors standard deviation worsen, the norm of the \mathbf{R}_d matrix decreases. \mathbf{K}_o matrix norm remains almost constant and even increase slightly around the 50-th test. This simple test shows the trend of the \mathbf{R}_d matrix which is really interesting, considering that the Y axis is in logarithmic scale, indeed the first part of the descending curve is the one with the steepest slope, which means that for a small increase of the standard deviation value, the effect on the system is worse if compared to a condition in which the standard deviation of the sensor is already high (like after the 30-th test). To better understand the motivation of those trends, figure 3.26b is presented, to show the trend of each component of the matrix.

Test 2 Maintain ν_d fixed and let μ increase to increase the uncertainty of the sensors: This test has been performed with the aid of a `for` cycle that continuously increases the uncertainty value of the sensor adding for each cycle the same starting value to each sensor, bringing at the end of the 100 cycles to a condition in which the used sensors has a 100 times higher standard deviation than the ones with the test started with.

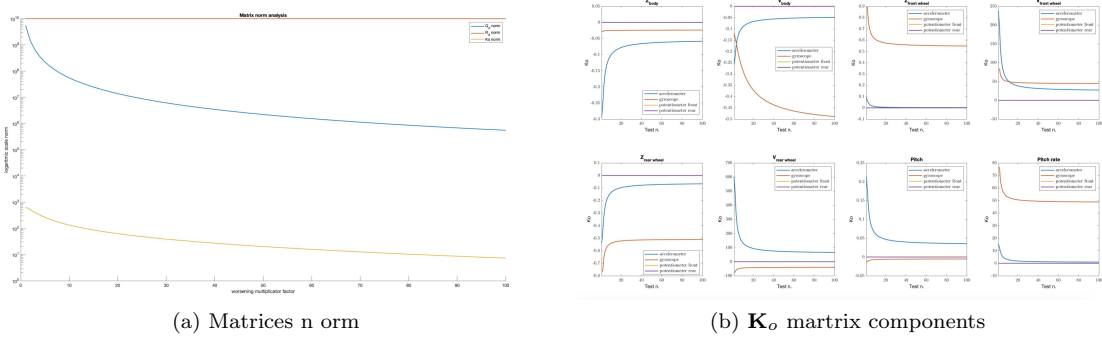


Figure 3.27

Conclusions of this test are perfectly equivalent to the previous one but mirrored, meaning that \mathbf{R}_d norm is constant, \mathbf{Q}_d norm diminishes. In this case \mathbf{K}_o norm diminishes too, with a much higher rate if compared to the previous test. This is due to the fact that each component of the matrix does not saturate to a certain value as seen in the previous results, all terms indeed tends to 0 when the uncertainty increases, even if the standard deviation is pretty good.

Test 3 Let ν_d and μ increase to worsen standard deviation and uncertainty simultaneously:

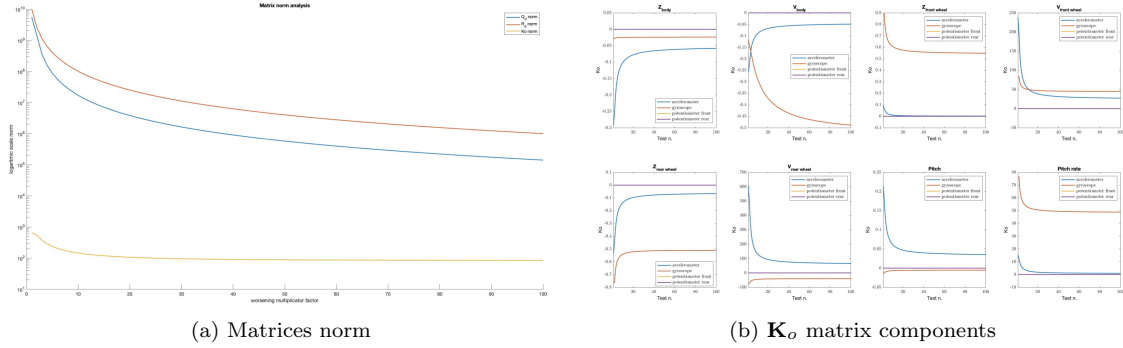


Figure 3.28: Test 3 results

The result is perfectly aligned to the expectations, indeed increasing the value of uncertainty and standard deviation brings to a worsening of the \mathbf{K}_o matrix, making the observer less effective. This will be analysed more in details later on.

Other parameters to be analysed are ε and U_{max} . They have an ‘almost physical’ response on the system, meaning that they act as boundaries. In particular, increasing too much the value of ε vector components, it happens that the control almost does not acts, because for what it can sense, all parameters are kept way inside their maximum boundaries. The admissible value of the ε boundaries is never reached, the system cannot even reach a condition that is close to the imposed boundary. This lets the control to remain almost inactive despite all. The same thing is valid in the opposite condition, meaning that if the ε values are too restrictive, the control would overreact to any kind of excitation. This can cause a worsening behavior if compared to the open loop one, bringing even to instability of the system if the noise can affect it. Is it then necessary to tune correctly the ε vector components by analysing the individual boundaries and evaluating which should be an appropriate value for each one. As previously anticipated, they will be distinguished two different scenarios (Comfort and Race) by building two vectors characterised by different values depending on the needs. The values are listed in Table 3.2.

	Comfort	Race	[Measurement Unit]
ε_1	0.5	0.01	[\cdot]
ε_2	0.5	0.01	[\cdot]
ε_3	1·g	4·g	[$\frac{m}{s^2}$]
ε_4	$1.49 \cdot 1.75$	$1.49 \div 4$	[$\frac{rad}{s}$]
ε_5	0.00561	0.00561	[m]
ε_6	0.00395	0.00395	[m]

Table 3.2: ε vector individual component’s values

Setting the race scenario, it has a much more stringent penalisation on the suspension stroke and a much more relaxed acceleration penalisation, in order to achieve a motorbike with a very good stability during hard braking and acceleration phases. Setting the Comfort scenario, the vertical accelerations and pitch velocity are penalised in order to have the smoothest ride possible.

Figure 3.29 represents the boundaries for race application regarding the η values. In comfort application the boundary is so large that it is no more possible to perceive an η variation, making the system behave freely with respect to that “constraint”, trying to keep the more restricted ones bounded. The other ε ’s boundaries and values are represented in figure 3.30 while being disturbed by a SAE road roughness level E:

It’s performed an analysis of the system behaviour when introducing three different factors that gets multiplied to the ε vector, which modifies the value of the \mathbf{Q} matrix. To do so a multiplier p has been introduced. It assumes values = 1, 10, 100 and it gets multiplied to \mathbf{Q} using the expression: $\mathbf{Q} = \text{inv}(p(i) * \text{diag}(\text{epsmax}.^2))$ By doing this it’s possible to obtain three very different solutions of

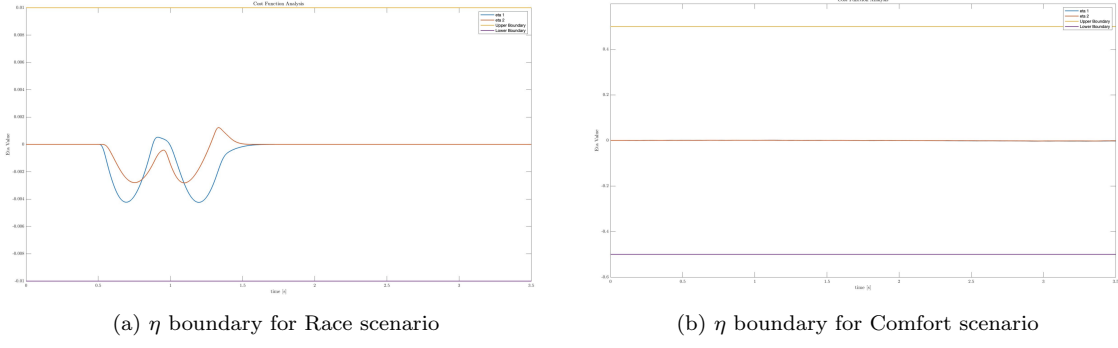


Figure 3.29: Eta analysis for different scenarios

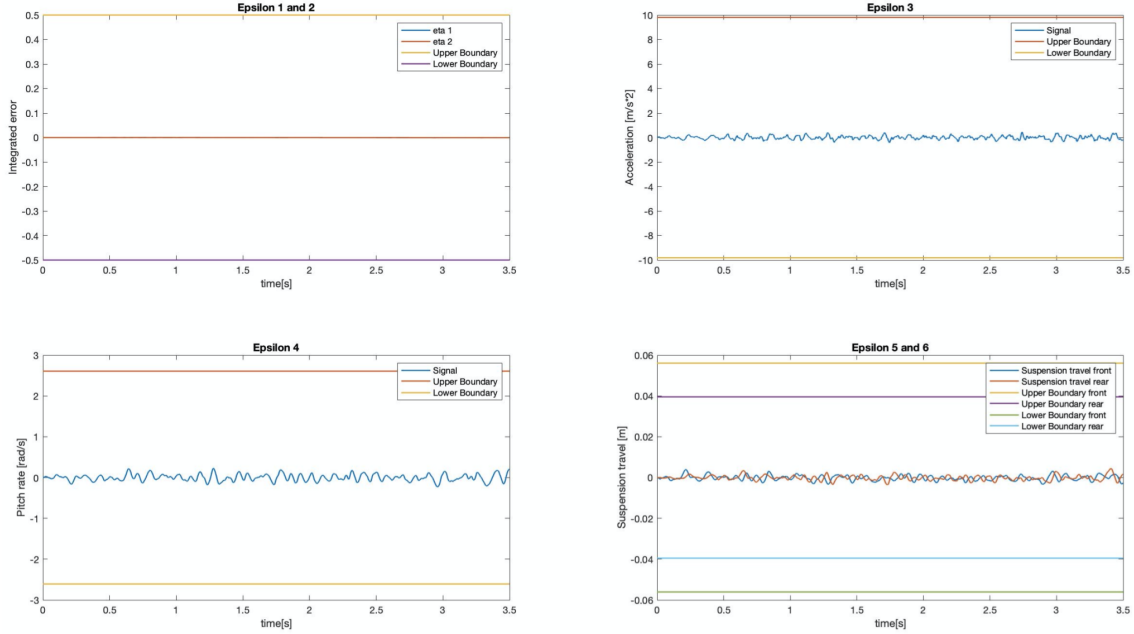


Figure 3.30: ε individual components

the Riccati equation and those ones will be compared over the speed-bump disturbance at $v = 12\text{km/h}$. Results are presented in figure 3.31.

u_{max} defines which is the maximum stiffness that the control can apply. Increasing too much this value creates a condition in which the control acts to stabilise the system, but the high value of equivalent stiffness applied makes the acceleration increase critically. This increase makes again the displacement vary rapidly, that causes a strong response of the system. In such way the system becomes unstable and highly uncomfortable. On the other hand, decreasing too much that value makes the system unable to go back as soon as possible to the equilibrium position. The control becomes then ineffective, working almost as an open loop one.

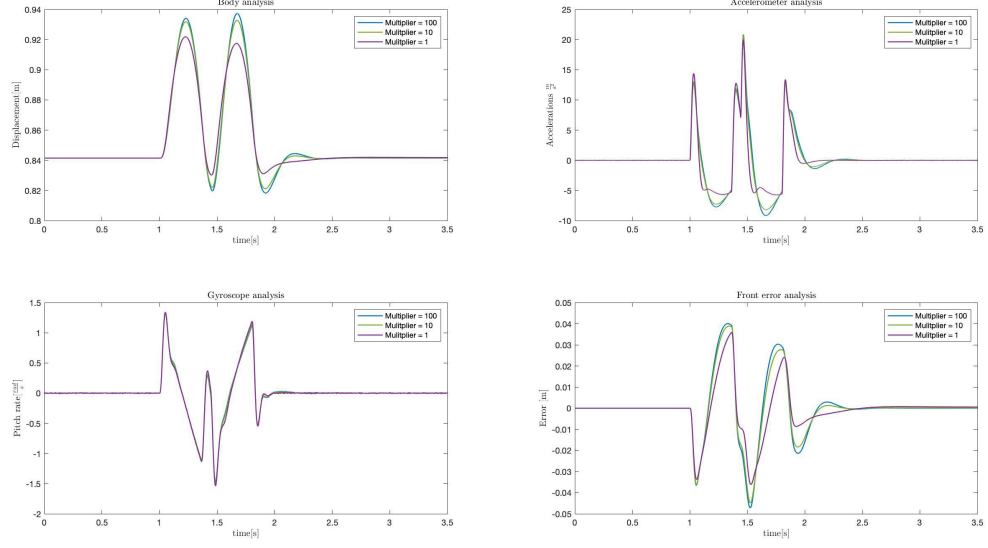


Figure 3.31: System's response with three different \mathbf{Q} matrices

3.2.2 Effect of individual control components

Let's now analyse how each component of the control influences the performances of the closed loop system by comparing it with the open loop one. The test will be performed using as disturbance both the speed-bump and the SAE road roughness level D, the considered scenario will be the 'Comfort' one and $\alpha = 1$.

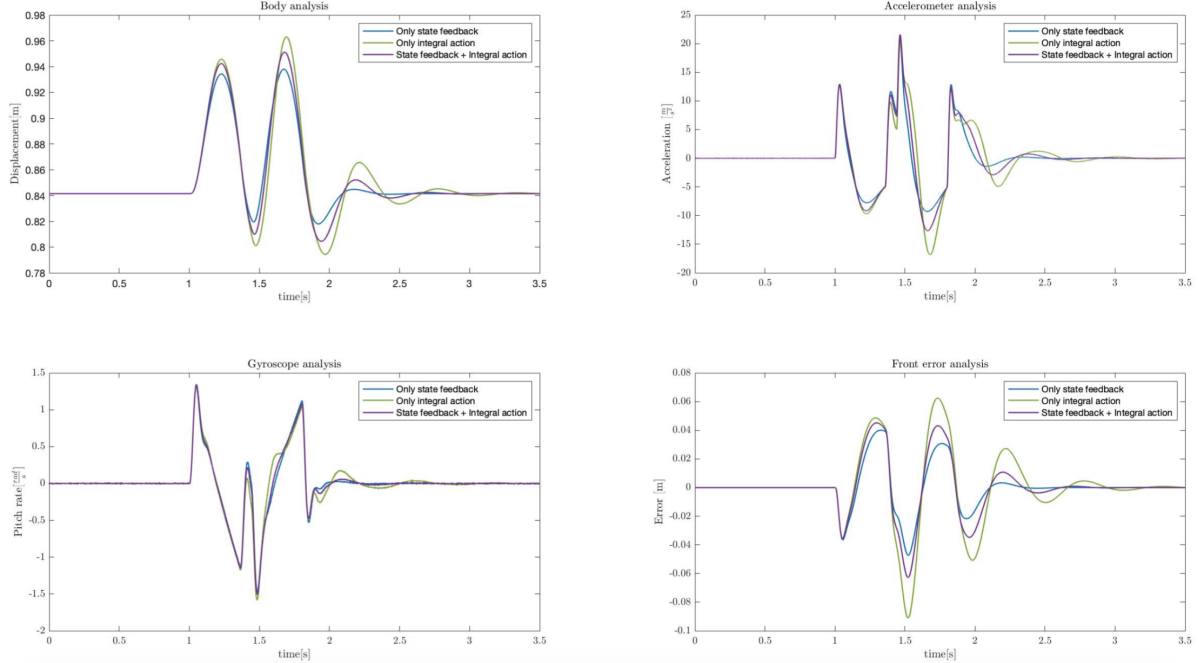


Figure 3.32: Sensor's analysis over speed-bump at $v = 12\text{km}/\text{h}$

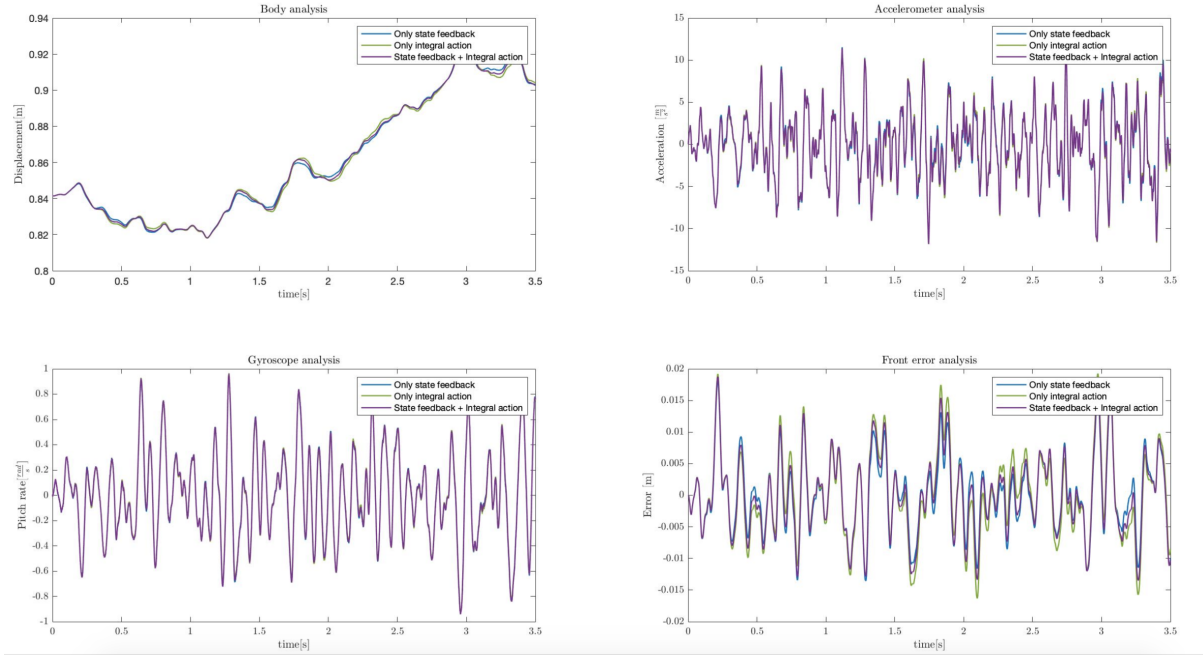


Figure 3.33: Sensor's analysis over ground roughness H at $v = 12\text{km}/\text{h}$

From the speed-bump test in figure 3.32, is evident the increase of performance given by the state feedback, indeed it allows the system to stabilize the body displacement and reduce the vertical acceleration oscillation. It slightly reduces the pitch rate and obtain huge improvements on controlling the error of the suspension. From the road roughness test the same conclusions emerges, while from the system's coordinate analysis body has a great improvement, the other coordinates improves slightly. Especially is evident how important is the combination of that two controllers on bringing the system back to stability, indeed using only state feedback the system would react too aggressively and using only integral action it would be too slow in guaranteeing stability. The optimal configuration is the one that takes advantage on both to keep the system stable in the minimum possible time, while guaranteeing smoothness during control intervention.

3.2.3 Sweep test

To better analyse the system's behavior based on α variability, a sweep test is performed. From this would be possible to evaluate the effect of different α values on the plant behavior and then to select the most appropriate one. The same can be done for α_d parameter to find the optimal couple $[\alpha, \alpha_d]$ that makes the system works at it's best. To do so it's necessary to introduce some indices to evaluate system's performances during the α and α_d individual sweep test.

The first index that allows to evaluate performances it's the RMS value of the accelerations along the z-axis (vertical) at which the rider is subjected to. Indeed it's very important to not expose the rider at certain frequencies for long time in order to avoid injuries, in figure 3.34 are highlighted the frequencies and the maximum time exposures defined in the ISO 2631:2014:

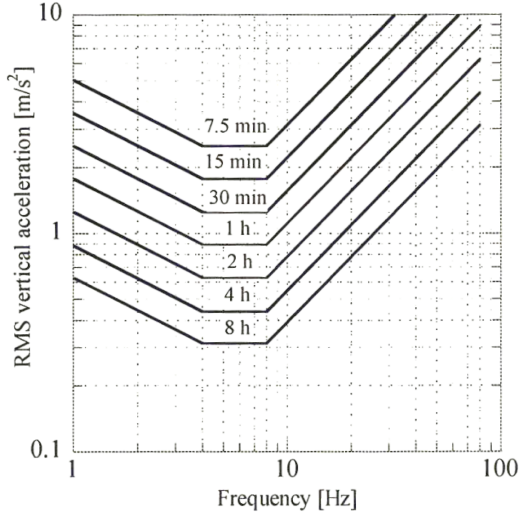


Figure 3.34: Maximum rider exposure time to vertical acceleration

Frequencies around 8 Hz are indeed the resonant frequencies of human spine, it is then of paramount importance to keep those frequencies away from the rider. Of course acceleration limits are related to time of exposure: really high accelerations are tolerated for a short time only.

To evaluate the acceleration during the test run over a speed-bump it is not sufficient to directly consider the acceleration value, indeed, it is more effective to evaluate a statistical metric related to the energy associated to the vertical motion:

$$a_w = \sqrt{\frac{1}{\tau} \int_0^\tau a_w^2(t) dt} \quad (3.8)$$

Then it is possible to do a step further and even consider the contribution of the pitch motion for the acceleration by considering the derivative of the signal coming from the gyroscope and the arm among the CoG and the center of the wheelbase (center of rotation). The metric in Eq. 3.8 is employed for the contribution of the acceleration of the pitch too. Finally, an overall index that comprises both the terms is obtained and shown in Eq. 3.9.

$$a_v = \sqrt{a_{W_t}^2 + (k_y a_{W_r})^2} \quad (3.9)$$

where:

- a_{W_t} is the acceleration associated to the vertical motion;
- a_{W_r} is the acceleration associated to the pitch motion;
- k_y is a weight parameter equal to 0.4.

To do so it is necessary to consider the arm of the pitch motion which basically is half of the wheelbase minus the distance between COM and rear boundary. In such way it has been unified the acceleration contribution in just one term, allowing to reduce the tuning complexity having one less parameter to consider. Another advantage is that it is now possible to relate the **aV** index value of the accelerations to a table that objectively evaluates the system's performances quantifying any improvement. Referring to ISO 2631-1 is it possible to quantify system's performances by means of figure 3.35.

To obtain an *optimization function* from this, it is possible to simply subtract the integral of the acceleration of the open loop plant to the closed loop one, obtaining a goodness parameter that simply evaluates the delta between the two plants. The best possible α value (with respect to the acceleration) is the one that maximises the optimization function:

$$M_{acc} = a_{v_{OL}} - a_{v_{CL}} \quad (3.10)$$

It is now time to introduce the other 2 parameters to objectify the performances, which are the front suspension error and the rear suspension error. It's applied the expression in Eq. 3.8 for them too.

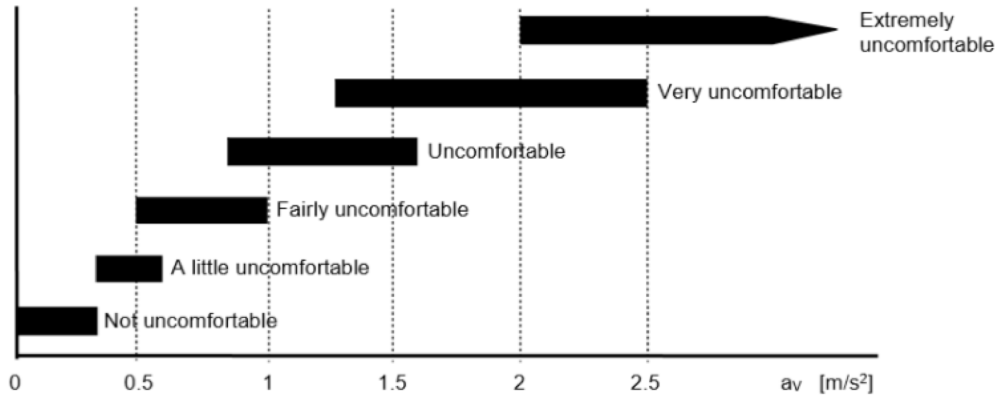


Figure 3.35: Objective assessment on comfort depending on the vibration total value

To obtain an optimization function from them, the integral value of the closed loop test needs to get subtracted by the same parameter of the open loop plant. As for the acceleration optimization, the suspension function finds it's optimal α value on the one that maximises:

$$M_{err_{front}} = e_{v_{OL_f}} - e_{v_{CL_f}} \quad M_{err_{rear}} = e_{v_{OL_r}} - e_{v_{CL_r}} \quad (3.11)$$

Right now is it has been found 3 optimization functions that needs to be maximised. In order to correctly apply the sweep test is it necessary to create a unique weighted optimization function that is made by only one parameter, so that the output is a curve, which maximum will be the optimal α value (trade-off between the individual optimal α of each component, and the global one). To correctly build the unique optimization function it is important to pass the equations into percentage values and then correct them by applying a weight based on the scenario considered.

The passage to percentage values is necessary to sum the different components without discrepancies on the measurement unit. In such way it is possible to have an optimization function that is the sum of components with 'fair' values (indeed it does not consider that the accelerations are in value always bigger than the few millimeters of error that the suspension could have). The weights chosen will then be useful to acknowledge how much the optimal α value will fit the requests, based on the value that it reaches in correspondence of the optimal one.

The chosen weights are:

- `weight_race = [5 40 45]`
- `weight_comfort = [85 5 10]`

To explain why those weights has been chosen let us consider that for race application the most important objective is to keep the motorcycle horizontal in any condition, so the error of the suspension will be highly emphasized, making it having more weight on the overall computation. On the other hand in comfort application, acceleration reduction (both along z -axis and the one derived from pitch motion) needs to be kept under control. Having a total of 100% to distribute, it has been decided to subdivide it as shown in the two vectors.

Setting $\alpha_d = 1$ to exclude any kind of dependency influence and limiting α to 40 (to avoid too high values inside K_{bar}), what it gets from the α sweep test is:

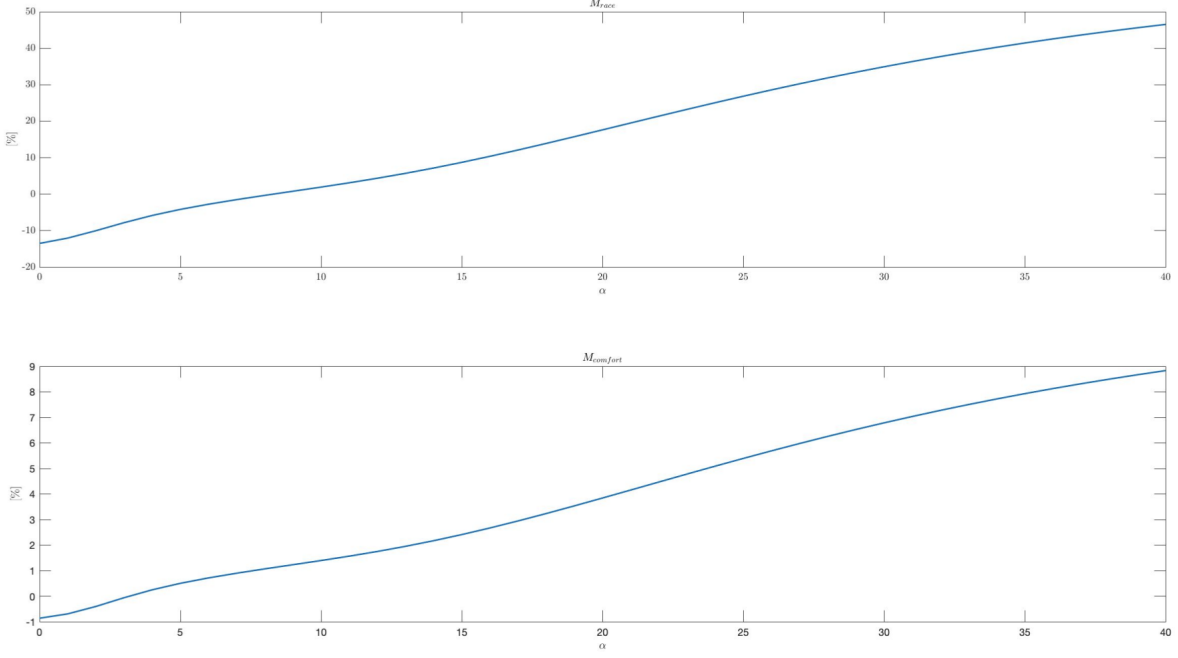


Figure 3.36: Overall performance optimization function trend

What emerges from image 3.36 is that both the curves obtain their optimal value near $\alpha = 40$ (which has been set as maximum value) with different percentage fit, indeed the optimal α for race scenario has a fit of 48.53% while comfort scenario has only a 8.95% fit. This can be explained by studying how the components of the optimization function behaves:

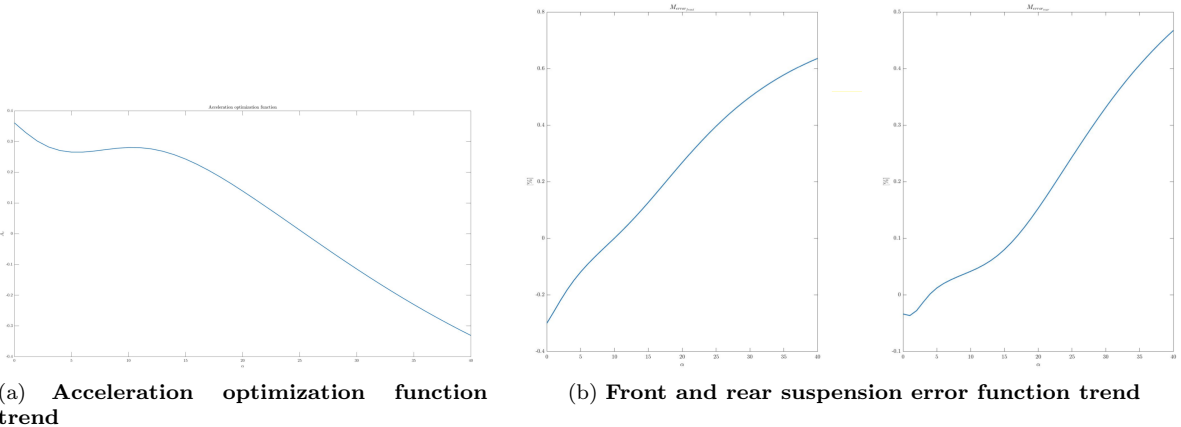


Figure 3.37: Function trend analysis on varying α

The compromise value obtained in the global function can be explained by means of figure 3.37, indeed the components have opposite trend. The function meant to optimize the accelerations on the rider becomes better with decreasing α values. The function that aims to minimize the error of the suspension increases with increasing α . Before choosing the optimal α value let's do one more consideration on the overall function computation. The error given by the suspension counts as double, being calculated for both front and rear suspension, while the weighted contribution given by the pitch acceleration only gets considered by 40% (either way its value is almost negligible). All this explains why for the comfort case scenario it would be better to use the α that minimizes the acceleration only and not the compromise value obtained in the unique function.

To further enhance this, it is useful to consider another element, the PSD of the acceleration. Indeed if the spectrum of the accelerations reveals to be optimal for a low value of α , then is it possible to consider this process validated. Results can be appreciated in figure 3.38

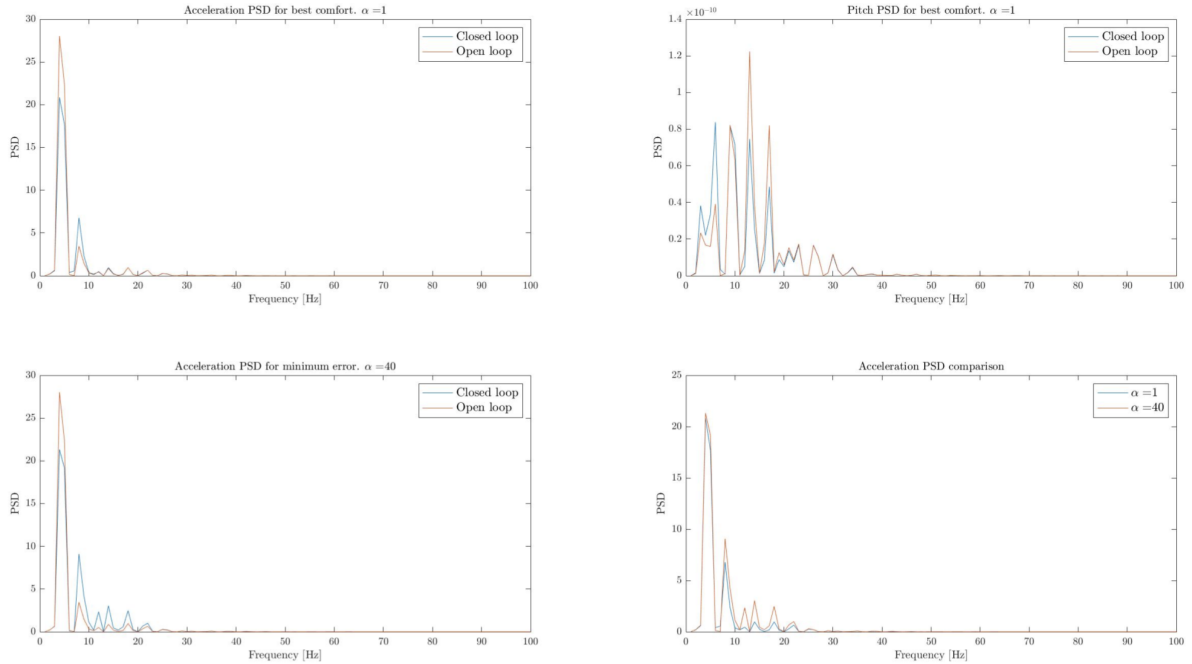


Figure 3.38: Power spectrum density analysis

Having exposed all of that data, it is possible to choose the optimal α value for the two scenarios:

- α optimal for Race application = 40
- α optimal for Comfort application = 0.1

Given those results the α sweep test can be considered concluded.

Having deeply analysed all the optimization function elements and the optimal α value, it is now possible to apply the same procedure for α_d , but with a slightly different approach. Indeed, in order to evaluate the performances of α_d , it's necessary to refer to the observer's estimated coordinates. In particular it gets 4 optimization function to be minimised, each one referring to a different coordinate of the system. They are x_1, x_3, x_5, x_7 which correspond to body displacement, front wheel displacement, rear wheel displacement and pitch angle respectively.

$$E_x = \sqrt{\frac{1}{\tau} \int_0^\tau \hat{x} - \tilde{x}^2(t) dt} \quad (3.12)$$

The optimization function is simply described as the cumulative error during the test.

$$E_{x_{global}} = \frac{E_{x_1} + E_{x_3} + E_{x_5} + E_{x_7}}{4} \quad (3.13)$$

Performing the simulation in the same exact environment and using $\alpha = 1$ to avoid any cross dependency, the result obtained can be seen in figure 3.39. Indeed, it represents the final optimization function to be *minimised* and the minimal cumulative error is reached around $\alpha_d = 1.5$. A further investigation will better define its actual optimal value and the components of the function can be seen in figure 3.40. It worth highlight that in such optimization function, the unique function has been obtained as the exact average of the other four, so that each one has the same weight on the final one.

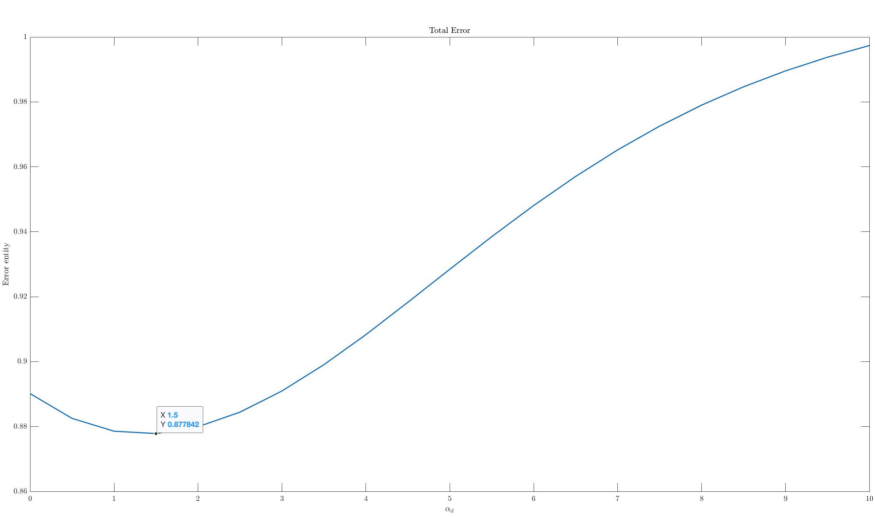


Figure 3.39: Error optimization function to be minimized for optimal value

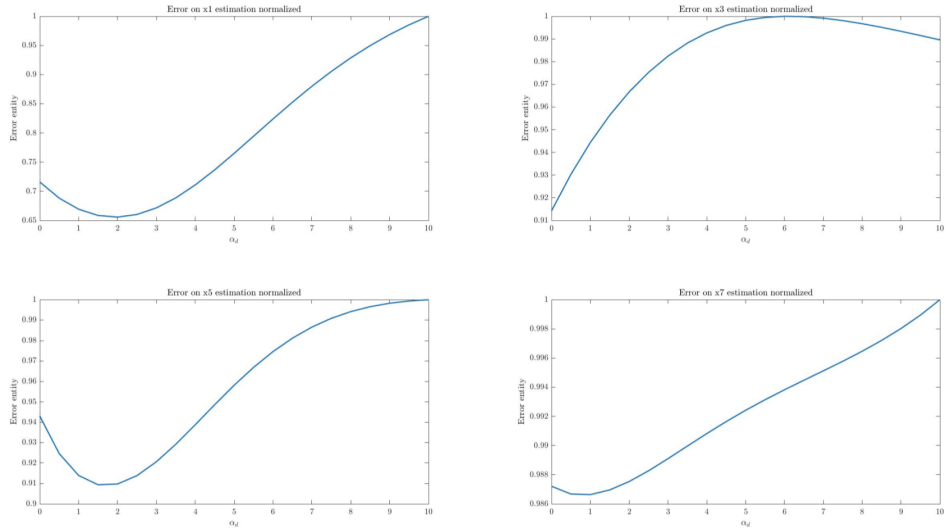


Figure 3.40: Components of the error optimization function

3.2.4 Final optimization

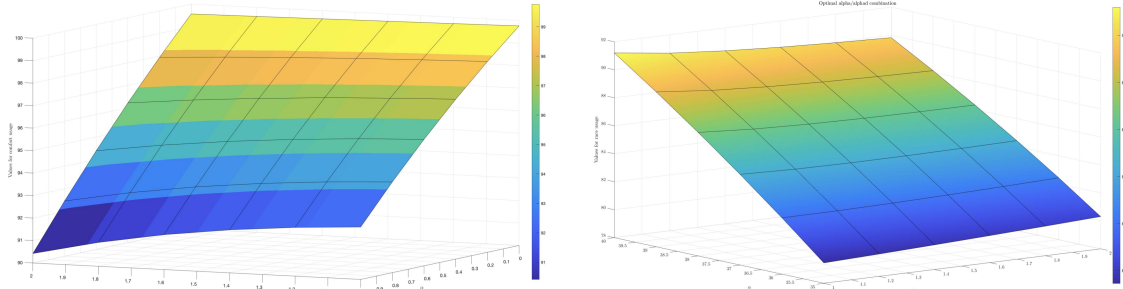
After having completed both the α and α_d sweep tests the system should be optimized, but in order to verify the performances, a further step can be done. It would be possible to create again a *global unique optimization function* composed by both the previous ones. The function is built as follows

$$Fun_{optimal} = M_{global} - E_{x_{global}} \quad (3.14)$$

and it has to be maximised in order to find the overall optimal value, this completely exploits any possible dependency between α and α_d values. In order to do it correctly it would be useful to take advantage of surface plots. They indeed allow to find any combination of values that guarantees maximum performances as an absolute maximum of the function.

Defining a range of variability for α and α_d that is near their closest optimal values (in order to avoid too high computational effort), it is possible to obtain 2 surfaces, one for the optimal couple for race use and one for the optimal couple for comfort use. Results are presented in figure 3.41.

The Optimal comfort usage couple is composed by $\alpha = 0.1$ and $\alpha_d = 1.5$. The Optimal race usage couple is composed by $\alpha = 40$ and $\alpha_d = 0.1$. The previous result has been obtained testing the system on the standard speed-bump disturbance ($h=0.15m$ $l=1.2m$ at $v = 12km/h$). From a brief analysis what



(a) Surface plot trend analysis for comfort scenario

(b) Surface plot trend analysis for race scenario

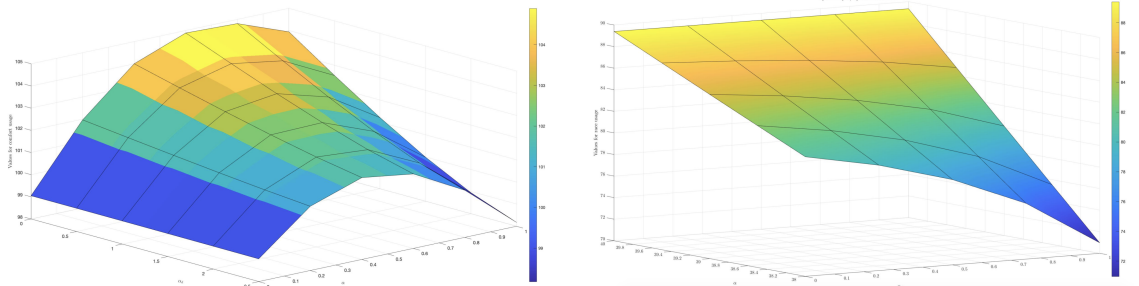
Figure 3.41: Global optimization function analysis

emerges is that a dependence correlation exists between the two values and the optimization performed allows to let it be fully exploited, indeed the surface has curvatures along all the axis.

The surface plots shows clearly the optimal combination of the two values but this condition is specific for only one disturbance. To understand if that optimal couple of values is applicable in various case, is it possible to study some different bump conditions and verify the dispersion of that couple based on the different conditions. To do so, two variants of the bump disturbance are considered at two different speeds:

- **First test:** Speed-bump $l=1.2m$, $h=0.15m$, velocity= $12km/h$;
- **Second test:** Speed-bump $l=1.2m$, $h=0.15m$, velocity= $20km/h$;
- **Third test:** Speed-bump $l=1m$, $h=0.10m$, velocity = $12km/h$;
- **Fourth test:** Speed-bump $l=1m$, $h=0.10m$, velocity = $20km/h$.

Repeating now the just seen analysis for all the tests what it gets is:



(a) Optimal couple for comfort scenario [$\alpha = 0.1$, $\alpha_d = 0.4$]

(b) Optimal couple for race scenario [$\alpha = 40$, $\alpha_d = 0.1$]

Figure 3.42: Second test's optimization function results

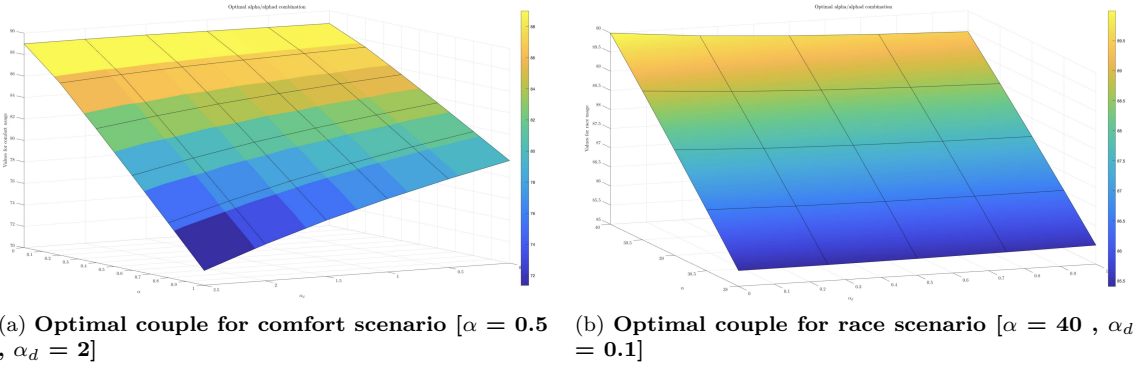


Figure 3.43: Third test's optimization function results

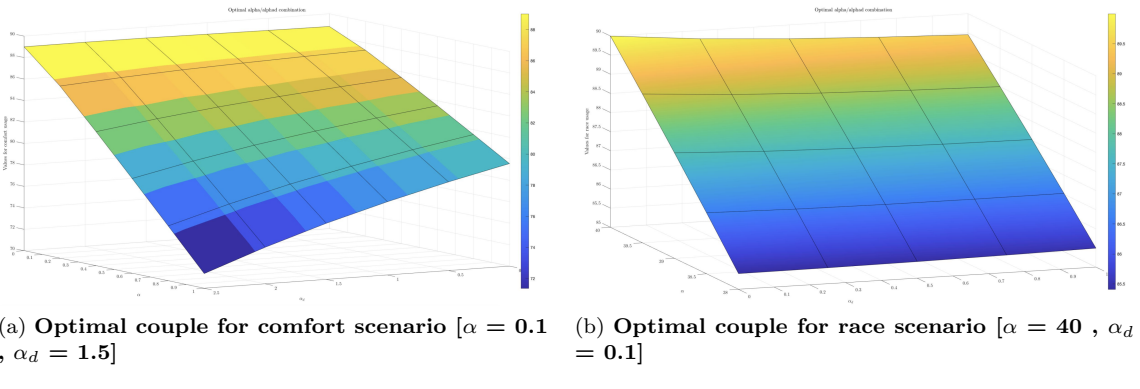


Figure 3.44: Fourth test's optimization function results

Let us now recap all the results and collect them in a table to better visualize the results:

COMFORT	α	α_d
Test 1	0.1	1.5
Test 2	0.1	0.4
Test 3	0.5	2
Test 4	0.1	1.5

Table 3.3: Results collected for **comfort** scenario

RACE	α	α_d
Test 1	40	0.1
Test 2	40	0.1
Test 3	40	0.1
Test 4	40	0.1

Table 3.4: Results collected for **race** scenario

Tables 3.3 and 3.4 highlights how the system modifies the couple α/α_d depending on the condition. Results are consistent, which means that the *optimization function is well posed* and fully exploited, optimal performances has been reached. 3.35

3.2.5 Analysis results

The last thing to be done to consider the tuning procedure complete and effective would be the plant response analysis based on the results obtained using the optimization algorithms already implemented. To analyse the performances, there different signal will be considered:

- Open loop plant response;
- Closed loop plant response with α and α_d with middle values ($\alpha = 20$, $\alpha_d = 1$);
- Closed loop plant response with the optimal α and α_d couple.

Test 1 Standard speed-bump disturbance at 12km/h.

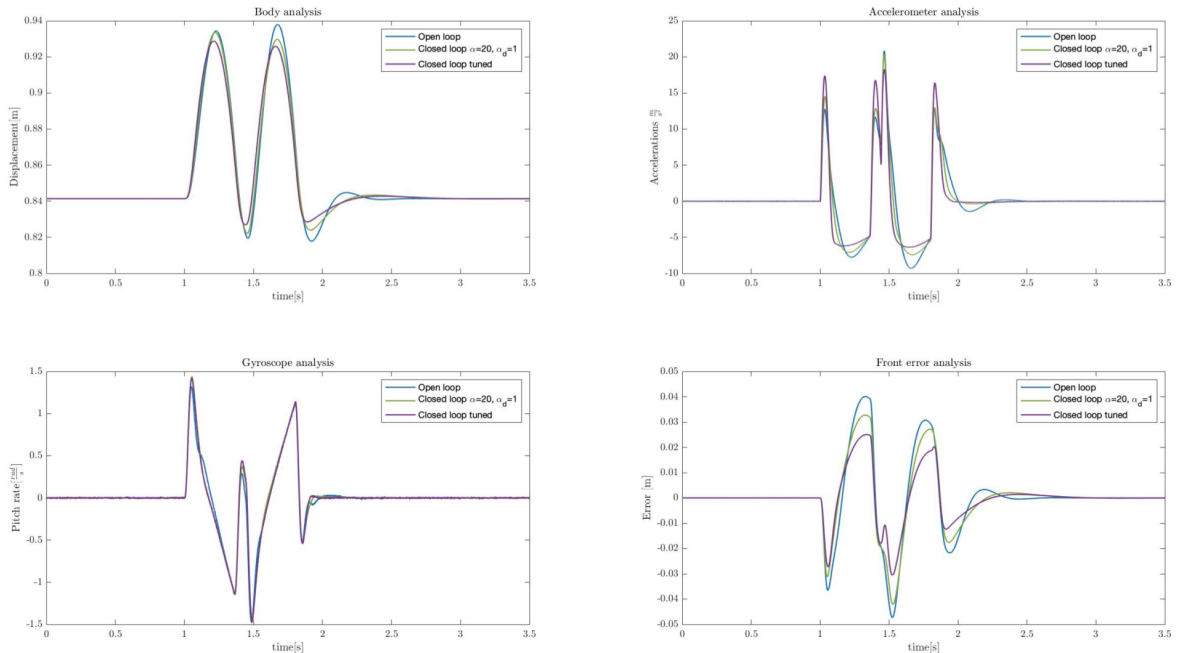


Figure 3.45: Race scenario system's response to speed-bump disturbance

Figure 3.45 shows how much the control is focused in keeping the bike as stable as possible by minimizing the error related to the suspension. At the same time, high importance is attributed to the pitch rate to avoid fast pitch movement that will destabilize the rider. The motorcycle body displacement is not too limited as can be seen in figure 3.46 but that it's what the driver request by choosing the driving scenario. Accelerations of the optimal closed loop system's response are higher than the open-loop's one but as for the body displacement that is part of the trade-off. Closed-loop system with intermediate α and α_d values works pretty good, but it's not optimal and this further shows how much work has been done on the tuning phase to let the system work at its best.

Similar considerations can be done for comfort scenario, indeed the objective of this scenario are: reduce accelerations and body motion. From figure 3.46 is evident that the body displacement has been highly restricted and the accelerations reduced, not as much as the open-loop plant, but that is part of the performance trade-off. What needs to be pointed out is that in such case accelerations are still very low in value so the ‘positive delta’ between optimal system and open-loop is not so relevant. Error in the suspension is reduced and this guarantees a stable and horizontal motorbike.

What can be already concluded from this test is that the desired performances has been achieved for both the comfort and the race scenario.

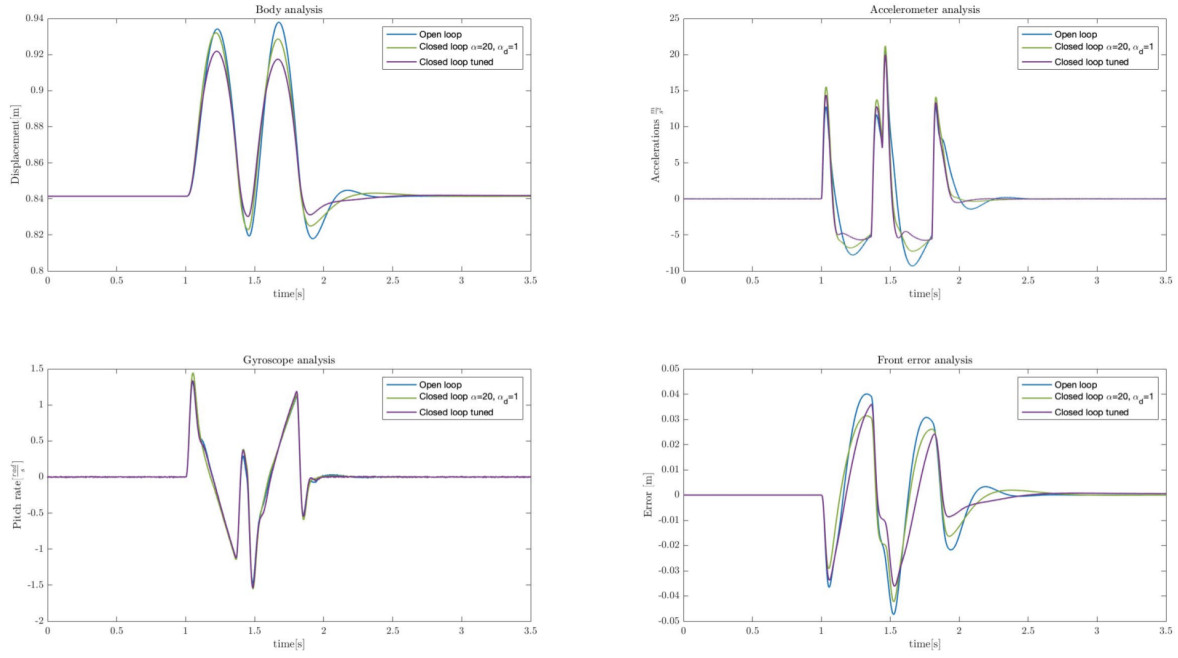


Figure 3.46: Comfort scenario system's response to speed-bump disturbance

Test 2 SAE road roughness level D.

Figure 3.47 shows that results obtained with the speed-bump as disturbance has been confirmed for road roughness. Indeed, race map drastically reduces the error between the reference point and the sensor's measured value of the suspension displacement letting the acceleration increase if compared to the open-loop one. The green line shows an intermediate response again, the accelerations and pitch rate are a bit worse than the others but still has better body control than the open loop. Comfort scenario results shows that body displacement has been controlled very well, unlike accelerations that tends to increase a bit over the road roughness. This is perfectly fine because their value is still very low.

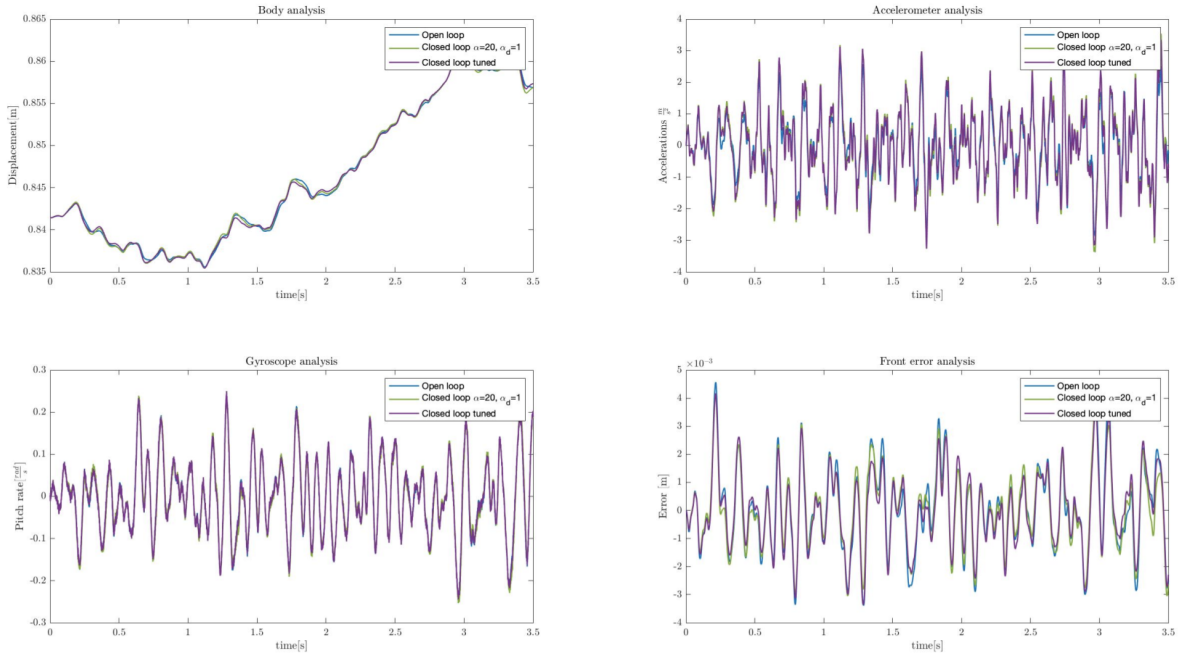


Figure 3.48: Comfort scenario system's response to road roughness disturbance

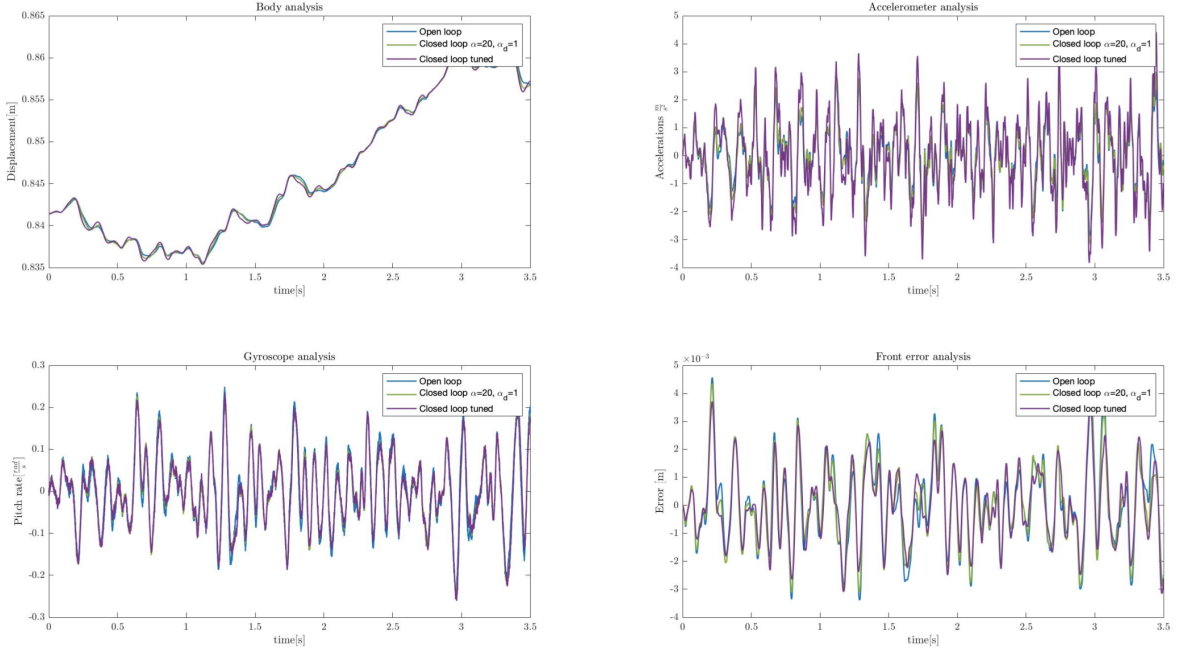


Figure 3.47: Race scenario system's response to road roughness disturbance

The last two tests remaining aims at analyzing the state coordinates of open-loop system and fully optimized one, but considering even the system made by the '*first tentative values*'. This is necessary to show the original values obtained by the non-optimized system.

Test 3 State analysis in race scenario over standard speed-bump.

In analogy to what have been showed before, figure 3.49 shows the capabilities for the control on keeping the motorcycle stable. In all the four plots is evident how strong the control is on avoiding bounces of the motorbike by "straightening" all the possible oscillations and stabilizing the vehicle.

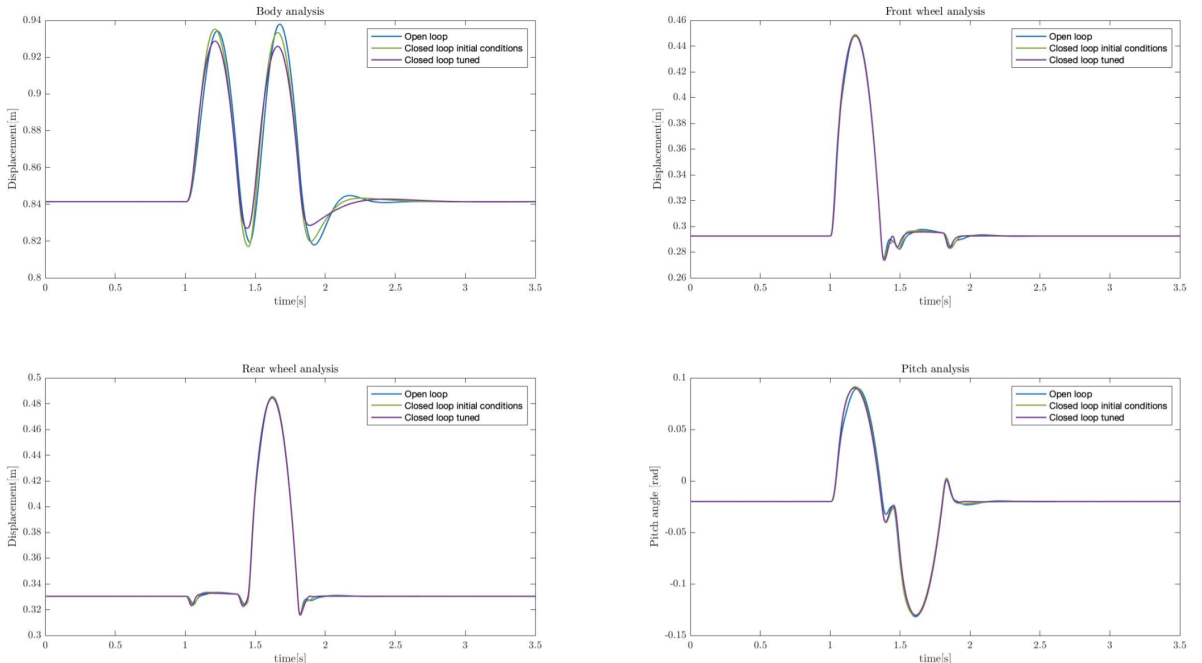


Figure 3.49: State space coordinates x_1, x_3, x_5, x_7 in Race scenario

Test 4 State analysis in race scenario over level D SAE road roughness.

Figure 3.50 highlights how well the race scenario could handle such kind of disturbance by minimizing the error of the suspension, keeping the motorcycle horizontal and reducing the pitch angle.

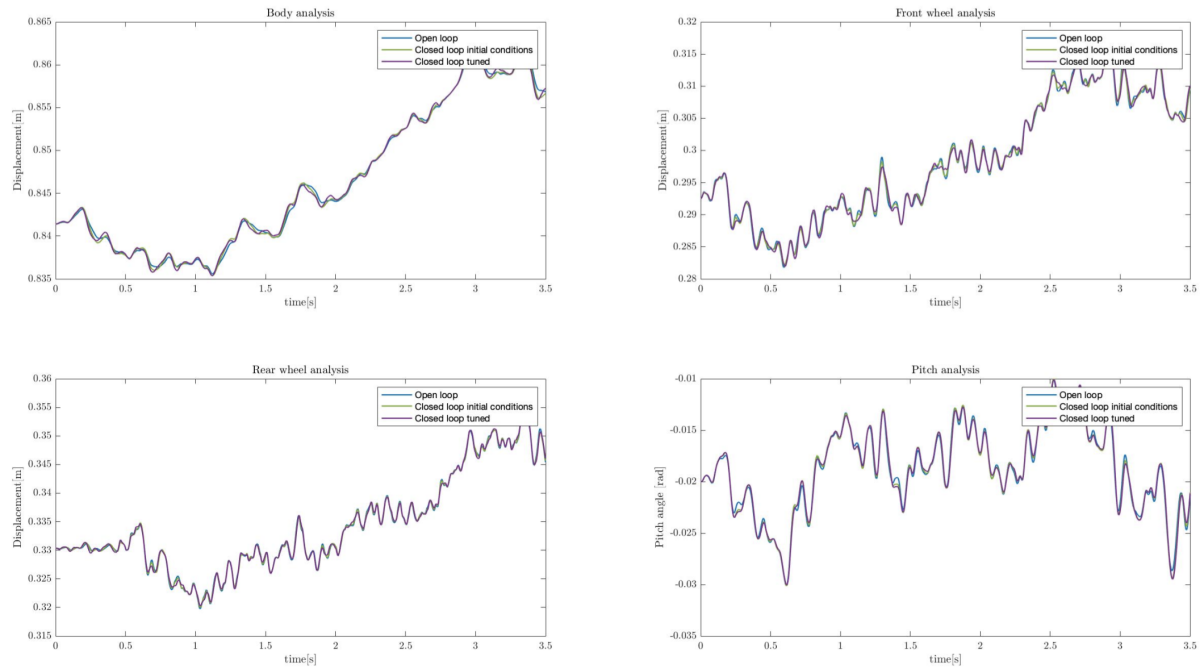


Figure 3.50: Comfort scenario system's response to road roughness disturbance

After the analysis of all the system's performances it is possible to conclude that the system tuning has been completed successfully.

Chapter 4

Conclusions and further investigations

The system proposed is effective and it provides proper trade-off between performance, cost and complexity. The resulting performances has always been better than the non-active counterpart, performing well in various scenarios. In particular, the system enabled higher safety and velocity in track condition or achieving a greater comfort.

Beginning with the fully active air suspension system, its performances has been studied in order to create a semi-active suspension model capable of providing quite good performances if related to the field of application. Afterwards, the semi-active system and its parameters have been investigated and all the dependencies have been shown; the main optimization parameters have been analysed by creating some functions which relate them to performance. The parameters have been optimized individually, then a unique cost function has been created to allow simultaneously the optimization of the most important parameters required to satisfy the performance request.

The fully optimized system has been deeply analysed and then compared to other possible solution, then through some tests, the objectification of the parameters have been confirmed, that means that the cost function problem was well posed and coherent to the system.

The results obtained in the various tests have been split into the two different scenarios proposed: *comfort* (standard commuting and slow speed city usage) and *race* (high speed track usage, strong acceleration and deceleration). The first scenario needs a reduction of the vertical accelerations and of the body pitch rate; the second one needs to keep the motorcycle as stable as possible by reducing the body pitch and the integrated error generated by the difference between the reference and the actual suspension deflection.

Even though two maps can cover approximately all the scenarios in which a sport bike could be used, it is possible to introduce more maps to further increase the performance in other cases.

Future development of the system are the following:

- Increasing the maximum pressure allowed by the suspension and investigate the further optimization needed to make the system effective in such conditions;
- Increase the cross section area of the suspension and investigate the further optimization needed to make the system effective in such conditions;
- Investigate the possibility to use different fluids than air inside the suspension, varying the equivalent stiffness produced at the same pressure. For example, the patent CarbonAirTM has been deposited on air-suspension which uses a mix of air and carbon particles to achieve a more linear response of the suspension;
- Introduce more scenarios such as mountain road, highway or some map related to the kind of asphalt that the driver has been riding on, to increase the control precision;
- Introduce equations which take into account the aerodynamic forces acting on the bike while riding;
- Improve the model by introducing a variable velocity system;

- Implement a function capable of taking into account all the parameters subjected to optimization to find an ‘optimal’ compromise value that simultaneously minimises the control action and guarantees performance and stability;
- Implement a function capable of taking into account the possible detachment of tyres from the found and that acts consequently;
- Implement a consistent solution to keep the suspension travel always inside the boundaries (for example by introducing a strong non linearity on the stiffness that simulates a bump-stop);
- Introduce the thermodynamic equations that considers the behaviour of the fluid inside the air spring.

Some of the proposed future developments need to take into account the energy consumption of the system. For example, increasing the maximum pressure of the suspension can requires to couple the system with a more powerful compressor; however this has multiple disadvantages (such as weight). It would be possible to further investigate the performance of the suspension based on the hybrid suspension system like the one proposed by AirtenderTM, visible in figure 4.1.

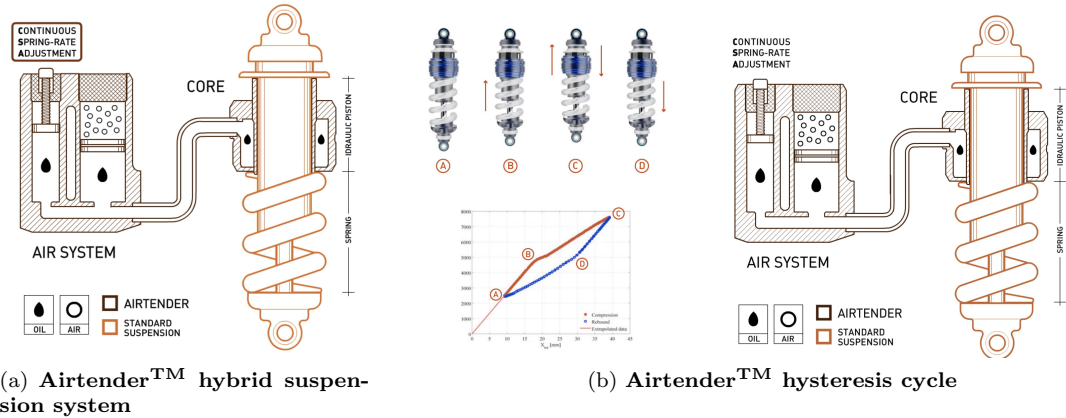


Figure 4.1: Future possible suspension implementation

Bibliography

- [1] W. Bauer. *Hydropneumatic Suspension Systems*. VDI-Buch. Springer Berlin Heidelberg, 2010. ISBN: 9783642151477. URL: <https://books.google.it/books?id=YVB80K3KnLIC>.
- [2] V. Cossalter. *Motorcycle Dynamics*. Vittore Cossalter, 2006. ISBN: 9781430308614. URL: <https://books.google.it/books?id=rJTQxITnkbGc>.
- [3] Hrovat D. “Optimal passive vehicle suspensions [Ph.D. thesis]”. In: *Vehicle System Suspensions* (2011).
- [4] D. García-Pozuelo et al. “Bump Modeling and Vehicle Vertical Dynamics Prediction”. In: *Advances in Mechanical Engineering* 6 (Feb. 2014), pp. 736576–736576. DOI: [10.1155/2014/736576](https://doi.org/10.1155/2014/736576).
- [5] Mouad Garziad and Abdelmjid Saka. “Modelling and Control of a Semi-active Suspension System of Motorcycle”. In: *2018 International Conference on Electronics, Control, Optimization and Computer Science (ICECOCS)*. 2018, pp. 1–8. DOI: [10.1109/ICECOCS.2018.8610635](https://doi.org/10.1109/ICECOCS.2018.8610635).
- [6] Smith RE Goran MB Bachrach BI. “The design and development of a broad bandwidth active suspension concept car”. In: *Total Vehicle Dynamics* 2 (1992).
- [7] S. Lee. “Development and analysis of an air spring model”. In: *International Journal of Automotive Technology* 11 (Aug. 2010), pp. 471–479. DOI: [10.1007/s12239-010-0058-5](https://doi.org/10.1007/s12239-010-0058-5).
- [8] Hua Li et al. “Simulation of Semi-Active Air Suspension Based on Neural Network-Adaptive Control Algorithm”. In: *2009 Second International Conference on Intelligent Computation Technology and Automation*. Vol. 2. 2009, pp. 236–239. DOI: [10.1109/ICICTA.2009.294](https://doi.org/10.1109/ICICTA.2009.294).
- [9] Zhongxing Li, Wenhao Yu, and Xiaoli Cui. “Online Classification of Road Roughness Conditions with Vehicle Unsprung Mass Acceleration by Sliding Time Window”. In: *Shock and Vibration* 2018 (Oct. 2018), pp. 1–13. DOI: [10.1155/2018/5131434](https://doi.org/10.1155/2018/5131434).
- [10] Consolatina Liguori et al. “Characterization of motorcycle suspension systems: Comfort and handling performance evaluation”. In: *2013 IEEE International Instrumentation and Measurement Technology Conference (I2MTC)*. 2013, pp. 444–449. DOI: [10.1109/I2MTC.2013.6555457](https://doi.org/10.1109/I2MTC.2013.6555457).
- [11] Charles Poussot-Vassal et al. “Survey and performance evaluation on some automotive semi-active suspension control methods: A comparative study on a single-corner model”. In: *Annual Reviews in Control* 36.1 (Apr. 2012), pp. 148–160. DOI: [10.1016/j.arcontrol.2012.03.011](https://doi.org/10.1016/j.arcontrol.2012.03.011). URL: <https://hal.archives-ouvertes.fr/hal-00733261>.
- [12] Sergio M Savaresi et al. *Semi-active suspension control design for vehicles*. Elsevier, 2010.
- [13] Sergio M. Savaresi et al. “Semi-Active Control Strategies for High-Performance Motorcycle”. In: *IFAC Proceedings Volumes* 41.2 (2008). 17th IFAC World Congress, pp. 4689–4694. ISSN: 1474-6670. DOI: <https://doi.org/10.3182/20080706-5-KR-1001.00789>. URL: <https://www.sciencedirect.com/science/article/pii/S1474667016396847>.
- [14] H. Eric Tseng and Davor Hrovat. “State of the art survey: active and semi-active suspension control”. In: *Vehicle System Dynamics* 53.7 (2015), pp. 1034–1062. URL: <https://doi.org/10.1080/00423114.2015.1037313>.
- [15] Long Wu, Yunlu Cao, and Hualing Chen. “Hierarchical Modeling Control of a Motorcycle Semi-Active Suspension with Six Degree-Freedoms”. In: *2008 IEEE/ASME International Conference on Advanced Intelligent Mechatronics*. 2008, pp. 1400–1405. DOI: [10.1109/AIM.2008.4601867](https://doi.org/10.1109/AIM.2008.4601867).